الجمهورية الديمقراطية الشعبية الجزائرية

République Algérienne Démocratique et Populaire

Ministère de l'Enseignement Supérieur
et de la Recherche Scientifique
Ecole Supérieure des Sciences Appliquées
d'Alger

وزارة التعليم العالي والبحث العلمي

المدرسة العليا في العلوم التطبيقية بالجزائر

Département du second cycle

Mémoire de Fin d'Etudes

En vue de l'obtention du diplôme d'ingéniorat d'état

Filière : **Electrotechnique**

Spécialité : **Traction électrique**

Thème :

Processor in the Loop Based Rotor Fault Diagnosis of an Induction Machine

Présenté par : Ait mouloud Louiza

Encadré (e) par : Deboucha Abdelhakim

Co-encadré(e) par : Baderdine Ouannas

Soutenu publiquement, le : 08/10/2020,

Devant le Jury composé de :

Dr Hamache Amar	Président
Dr Deboucha Abdelhakim	Encadreur
Prof Hadji Seddik	Examinateur

Monôme N° : 28/PFE. / 2020

Abstract

Induction machines (IM) are asynchronous/electromechanical machines usually used as motors where they have many advantages as they are rugged, less expensive, and require less maintenance. These advantages make them the most used machines in the industry nowadays. However, induction machines can be found mostly in hazardous environments where they are exposed to harsh conditions resulting in failures that lead eventually to the machine downtimes, therefore, production shutdowns, financial losses, and waste of raw materials. Hence, to prevent such catastrophic consequences, online detection and diagnosis of such faults becomes of interest.

In this study, the induction machine model has been developed along with faulty cases when the squirrel cage bars/end ring are cracked. Using MATLAB software, the model is simulated for healthy and faulty cases along with Fast Fourier Transform analysis. Three faulty cases were taken into consideration; where, two adjacent, two separated broken bars and the end ring cracking are simulated. Moreover, and as a preliminary to real time diagnosis, the FFT is implemented on the STM32 as a processor in the loop (PIL) to quickly detect the failure in the IM.

Simulation results show that time domain analysis could only categorize whether the IM is healthy or faulty. Whereas, spectral analysis would give more insight on the failure by detecting the number of broken bars.

On the other hand, the FFT implementation on the STM32 board raises promises to give initial real diagnosis failures that existed on the induction machine.

Résumé

Les machines à induction (IM) sont des machines asynchrones / électromécaniques généralement utilisées comme moteurs. Elles présentent de nombreux avantages : robustesse, moins coûteuses et nécessitent moins d'entretien. Ces avantages en font aujourd'hui les machines les plus utilisées dans l'industrie. Cependant, les machines à induction se trouvent principalement dans des environnements dangereux où elles sont exposées à des conditions difficiles entraînant des pannes qui entraînent éventuellement des temps d'arrêt de la machine, par conséquent des arrêts de production, des pertes financières et un gaspillage de matières premières. Par conséquent, pour éviter de telles conséquences catastrophiques, la détection et le diagnostic en ligne de tels défauts deviennent intéressants.

Dans cette étude, le modèle de la machine à induction a été développé avec des cas défectueux lorsque les barres de la cage d'écureuil / la bague d'extrémité sont fissurées. À l'aide du logiciel MATLAB, le modèle est simulé pour les cas sains et défectueux avec une analyse de transformation de Fourier rapide. Trois cas défectueux ont été pris en considération ; où, deux barres cassées adjacentes, séparées et la fissuration de l'anneau d'extrémité sont simulées. De plus, et comme préalable au diagnostic en temps réel, la FFT est implémentée sur le STM32 pour détecter rapidement la panne dans le MA.

Les résultats de la simulation montrent que l'analyse du domaine temporel ne pouvait que catégoriser si la messagerie instantanée est saine ou défectueuse. Alors que l'analyse spectrale donnerait plus d'informations sur l'échec en détectant le nombre de barres cassées.

En revanche, l'implémentation FFT sur la carte STM32 promet de donner un diagnostic initial de véritables échecs qui existaient sur la machine à induction.

ملخص

آلات الحث (IM) هي آلات غير متزامنة / كهروميكانيكية تستخدم عادة كمحركات حيث تتمتع بالعديد من المزايا حيث أنها متينة وأقل تكلفة وتتطلب صيانة أقل. هذه المزايا تجعلها أكثر الآلات استخدامًا في الصناعة في الوقت الحاضر. ومع ذلك ، يمكن العثور على آلات الحث في الغالب في بيئات خطرة حيث تتعرض لظروف قاسية تؤدي إلى أعطال تؤدي في النهاية إلى تعطل الماكينة ، وبالتالي ، إيقاف الإنتاج ، والخسائر المالية ، وإهدار المواد الخام. ومن ثم ، لمنع مثل هذه العواقب الكارثية ، اصبح اكتشاف هذه الأخطاء وتشخيصها ميدانيا أمرًا مهمًا.

في هذه الدراسة ، تم تطوير نموذج آلة الحث مع الحالات المعيبة عندما يتم تصدع قضبان قفص السنجاب / حلقة النهاية. باستخدام برنامج MATLAB ، تمت محاكاة النموذج للحالات الصحية والعيوب جنبًا إلى جنب مع تحليل تحويل فوريه السريع. تم أخذ ثلاث حالات معيبة في الاعتبار ؛ حيث يتم محاكاة قضيبين متجاورين ، وقضبان مكسورة منفصلة وتكسير حلقة النهاية. علاوة على ذلك ، وكتمهيد للتشخيص في الوقت الفعلي ، يتم تنفيذ FFT على STM32 لاكتشاف الفشل في IM بسرعة.

تظهر نتائج المحاكاة أن تحليل المجال الزمني يمكن أن يصنف فقط ما إذا كانت الرسائل الفورية صحية أو معيبة. في حين أن التحليل الطيفي من شأنه أن يعطي مزيدًا من المعلومات حول الفشل من خلال الكشف عن عدد الأشرطة المكسورة.

من ناحية أخرى ، فإن تطبيق FFT على لوحة STM32 يثير وعودًا بإعطاء تشخيص أولي حقيقي لفشل كان موجودًا في آلة الحث.

Acknowledgment

Praises be to Allah for providing me the time, good health and strength to work in completing this study.

High appreciation and deepest gratitude are given to my Advisor Dr. DEBOUCHA for his invaluable guidance, encouragement, generous assistance, patience and strong support throughout this study, and also for his trust on my ability to produce the case study.

Acknowledgements are not completed without thanking all my lecturers at ESSA-Alger.

Finally, I gratefully acknowledge my family and my friends for their support and constant advice.

TABLE OF CONTENTS

LIST OF FIGURES

LIST OF SYMBOLS

N_s	Number of turns in the stator winding.
nb	Number of rotor bars
K	Natural number
K_0	Friction coefficient
P	Number of pair poles
μ_0	Permeability factor of the air gap
g	Air gap between the stator and the rotor
r_d	The average radius of the air gap[m]
θ_r	The rotor angular position[rad]
r	Mean diameter of the machine;
l	Length of the slots in the stator.
J	Moment of Inertia [$kg.m^2$]
T_L	Load torque [N.m]
T_e	Electromagnetic torque[N.m]
W_{co}	Co-energy
F_a	The winding function for phase “a”
B_a	The magnetic flux in the air gap [T]
Φ_{sa}	The magnetic flux for phase “a” [Wb]
Φ	The magnetic flux [Wb]

Φ_{rjrj}	The rotor loop self-magnetic flux [Wb]
Φ_{rja}	The magnetic flux in the rotor loop j[Wb]
Φ_s	The stator flux vector[Wb]
Φ_r	The rotor flux vector [Wb]
L_{am}	The magnetizing inductance of the phase “a” [H]
L_{sl}	Leakage inductance [H]
ls	The total inductance of phase “a” [H]
L_{mrj}	The magnetizing inductance of the loop j[H]
L_{rjj}	The total rotor inductance of the k^{th} mesh[H]
L_{rja}	The mutual inductances between the k^{th} rotor loop and phase “a” [H]
L_{rjb}	The mutual inductances between the k^{th} rotor loop and phase “b” [H]
L_{rjc}	The mutual inductances between the k^{th} rotor loop and phase “c” [H]
L_s	Stator inductance [H]
$L_{r(j+1)j}$	The mutual inductances between rotor loops [H]
L_{rkj}	The mutual inductances between rotor loops [H]
$L_{r(j-1)j}$	The mutual inductances between rotor loops [H]
L_{sr}	The mutual inductance between the rotor loop and the stator winding[H]
L_b	Rotor bar inductance[H]
L_e	Rotor end ring inductance[H]
L_r	Rotor inductance[H]

M_s	Mutual Stator inductance
r_s	Stator winding resistance [Ω]
R_s	Total Stator resistance[Ω]
R_r	Total Rotor resistance [Ω]
R_{bk}	Rotor bar resistance[Ω]
R_e	End ring resistance[Ω]
V_s	Stator voltage vector [V]
V_{as}	Stator voltage vector of phase “a” [V]
V_{bs}	Stator voltage vector of phase “b” [V]
V_{cs}	Stator voltage vector of phase “c” [V]
V_{rk}	Rotor loop voltage [V]
V_{re}	Rotor end ring voltage [V]
I_s	Stator current vector[A]
I_{as}	Stator current vector of phase “a” [A]
I_{bs}	Stator current vector of phase “b” [A]
I_{cs}	Stator current vector of phase “c” [A]
I_r	Rotor loop current vector [A]
I_{rk}	Rotor loop current [A]
I_{re}	Rotor end ring current [A]

CHAPTER 1

INTRODUCTION

1.1 Background

Induction motors (IM) are complex electro-mechanical machinery and are the workhorse of the modern industries as they exist in many applications such as manufacturing, processing, energy, transportation, etc. Such motors are robust, highly reliable, require low maintenance, and have relatively high efficiency. However, their use in hazardous industrial plants (petrochemical and natural gas plants) and severe environments (grain elevators, shredders, and equipment for coal plants) make them susceptible to many types of faults, according to (Thomson and Fenger, 2001) statistics as shown in figure 1.1.

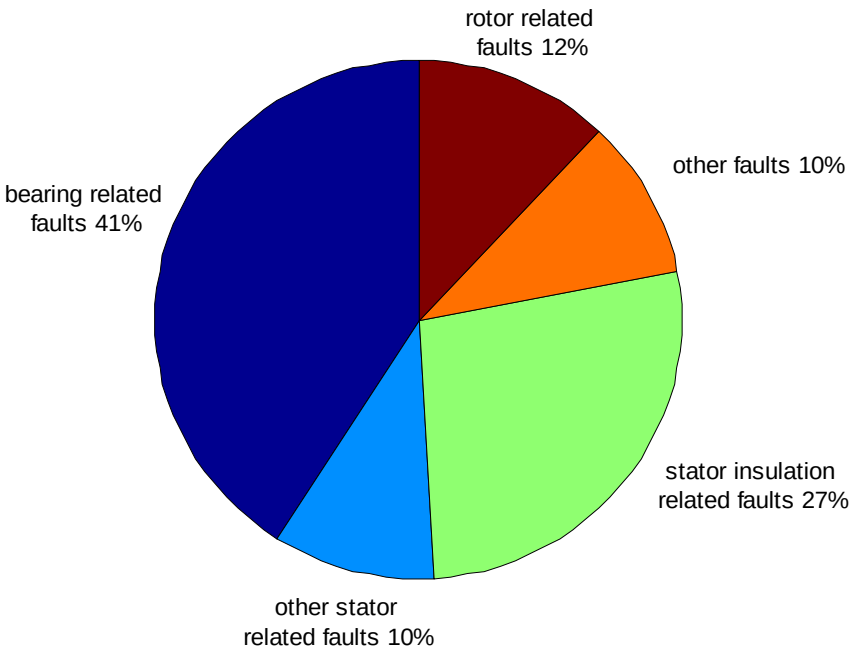

Figure 1.1: Different failure mode of the induction motor

Condition monitoring and fault diagnosis plays a great role in improving reliability and preventing the machinery downtime. Thus, there are many monitoring techniques for accessing the health conditions of motors, which might be represented in: vibration, acoustic, current, partial discharge, magnetic flux, gas and chemical analysis, instantaneous power, and temperature. The latter is processed to detect and diagnose faults using different signal processing techniques such as root mean square (RMS), frequency domain analysis such as Fast Fourier Transform(FFT), and time-frequency domain analysis such as wavelet technique (Jigyasu, et al, 2018).

In this study, motor's stator current signature analysis (MCSA) is selected for rotor fault diagnosis of the IM. It consists of decomposing the spectral of the steady-state stator currents which can be acquired with simple measurement equipment and under normal operation of the machine. It has several advantages since it is a non-invasive, on-line monitoring technique that avoids the use of extra sensors, therefore, simplifying its implementation in industrial environments (M.seera et al, 2012); (Benbouzid et al, 2003).

1.2 Aim and objectives of the study

The main aim of this study is to diagnose and detect induction motor failures namely broken bar and broken end ring faults. For this purpose, several steps must be followed:

- ❖ Modelling the squirrel cage induction motor on MATLAB software,
- ❖ Applying different faults to the model (breaking bars and end rings),
- ❖ Applying signal processing method (FFT) on different signals,

  (current, torque, speed, …) that reveals abnormalities related to faults.
- ❖ Implement the FFT along with Hanning window algorithm for the stator current on the STM32 board that indicates whether the motor is healthy or faulty.

1.3 Format of the dissertation

The dissertation is divided into six chapters: Chapter two introduces the induction motor machine, its different failure modes and condition monitoring techniques to detect these failures. Chapter three concentrates on the different modelling methods of the machine, in which the winding function method is the adopted method in this study. The chapter also covers different faults modelling related to the rotor (bar and end ring breakage). Chapter four covers the time-domain simulation results of the induction motor model. Chapter 5 discusses the frequency domain simulation results obtained from spectral analysis based on Fast Fourier transform. Chapter 6 contains the conclusion and recommendations for further research.

CHAPTER 2

NOTIONS AND RELATED STUDIES

2.1 Induction motor construction

Although an induction motor has several parts as shown in Figure. 2.2, it is essentially composed of a rotor and a wound stator.

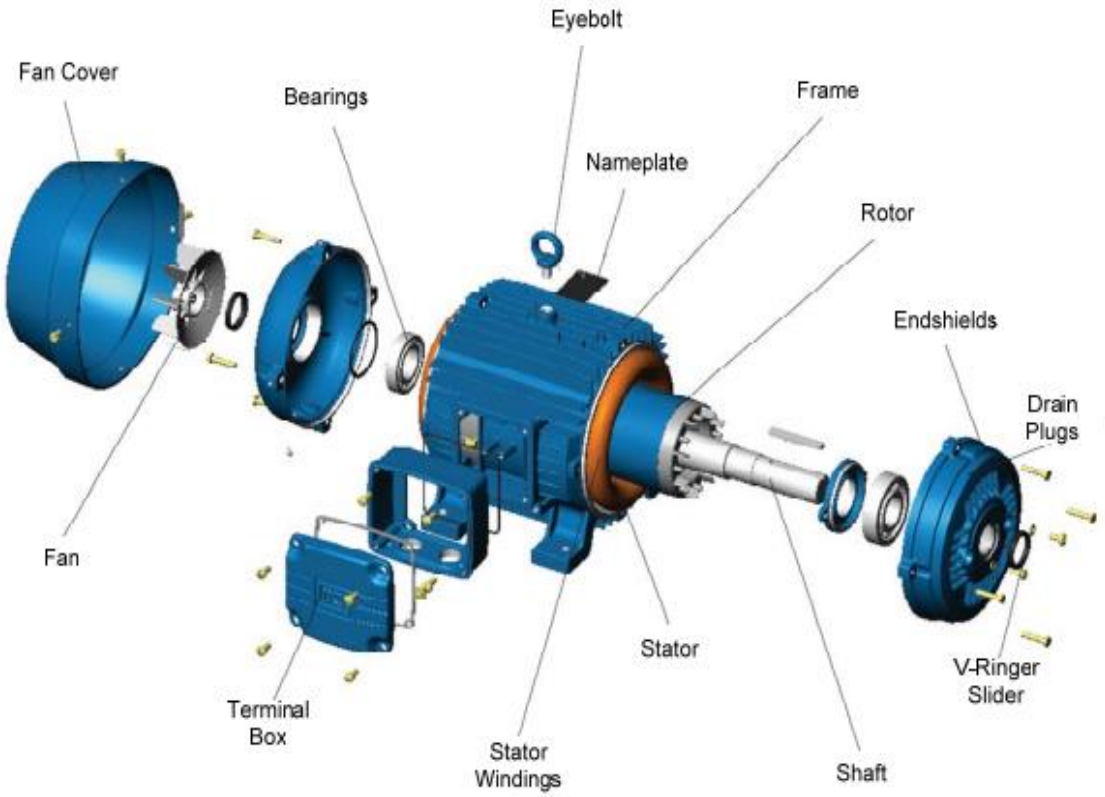

Figure 2.1: A typical 3-phase induction motor (Courtesy of Electro-motors WEG SA, Brazil)

2.1.1 The stator

The stator part has a cylindrical annulus magnetic core formed by stacking thin electrical steel laminations with uniformly spaced slots stamped in the inner

circumference to accommodate the stator windings which are coils of copper conductors insulated from each other by polish and from the slots by special paper.

2.2.2 The rotor

There are two types of induction motor rotors known as" wound rotor "and "squirrel cage rotor."

2.2.2.1 Wound rotor

A wound rotor consists of windings that are mirror images of the windings on the stator. It is usually Wey(Y) connected and the ends of these latter are shorted through brushes riding on the slip rings in which extra resistance can be inserted to modify the torque-speed characteristic of the motor (Stephen J. Chapman, 2005).

2.2.2.2 Squirrel cage rotor

A squirrel cage rotor is cylindrical in shape and has slots on its periphery, they are not made parallel to each other but they are rather bit skewed as the skewing prevents magnetic locking(cogging) of the stator and rotor teeth and makes the working of the motor smoother and quieter. The squirrel cage rotor consists of aluminum, brass, or copper bars these last ones are called rotor conductors and are placed in slots on the periphery of the rotor. In order to provide mechanical strength, these rotor conductors are braced to end ring and hence form a complete closed circuit resembling like a cage and hence got its name as "squirrel cage induction motor" (Stephen J. Chapman, 2005).

2.3 Working principle of the induction motor

A machine with only amortisseur (damper) windings is called an induction machine (Stephen J. Chapman, 2005). When the stator windings of the induction motor are supplied with three phase currents, a flux will be produced within the air gap and will cut the rotor bars(windings) in order to induce an electromotive force and since the bars (windings in case of wound rotor) are short circuited, a sinusoidal current will also be produced. The current in each bar will exert a force on the bar which will produce a torque and cause the rotor to rotate at a specific speed less than the synchronous speed of the stator winding. The difference between these speeds is called the slip which is the relative motion of the rotor and the magnetic fields.

2.4 Failure modes of the induction motor

Failures in induction machine could be classified into two categories; one is known as mechanical failures and the other is electrical failures.

2.4.2 Mechanical failure mode

Mechanical failures are most common failures in induction motors. They are mainly due to harsh working conditions in which the machine operates such as the presence of foreign materials, dirt, water, acid, and humidity that cause deterioration to its rotary parts (Önel et.al, 2008).

2.4.2.1 Bearing failure

According to the study given by the Electric Power Research Institute (EPRI), 41% to 42% of induction motor failure is due to faults in the bearing (Choug et al, 2019). This can be affected whether locally (pitted, spalled or cracked) on the ball inner raceway or outer raceway; or in a distributed way (waviness, misaligned races, and surface roughness). Many condition monitoring methods reveal bearing failures as follows:

Additional harmonics in the stator current spectrum (Schoen.et all,1995): $f_{bg} = |f_s \pm m f_v|$

where, f_s is the supply frequency, f_v is one of the characteristic vibration frequencies calculated based on bearing dimensions and m=1,2,3 ...

Additional harmonics in vibration signals as addressed in (Fabio et al, 2013).

Outer race frequency:

$$f_o = \left(\frac{n f_r}{2}\right)\left(1 - \left(\frac{D_b}{D_p}\right)\cos\varphi\right)$$

Inner race defect frequency:

$$f_{st} = \left(k \pm \frac{n(1-s)}{p}\right) f_s$$

Ball defect frequency:

$$f_b = \left(\frac{D_b}{D_p} f_r\right)\left(1 - \left(\frac{D_b}{D_p}\right)^2 \cos\varphi^2\right)$$

where f_r is the rotor speed, D_p is the pitch diameter of the bearing, D_b is the ball diameter, φ is the contact angle and n is the number of balls.

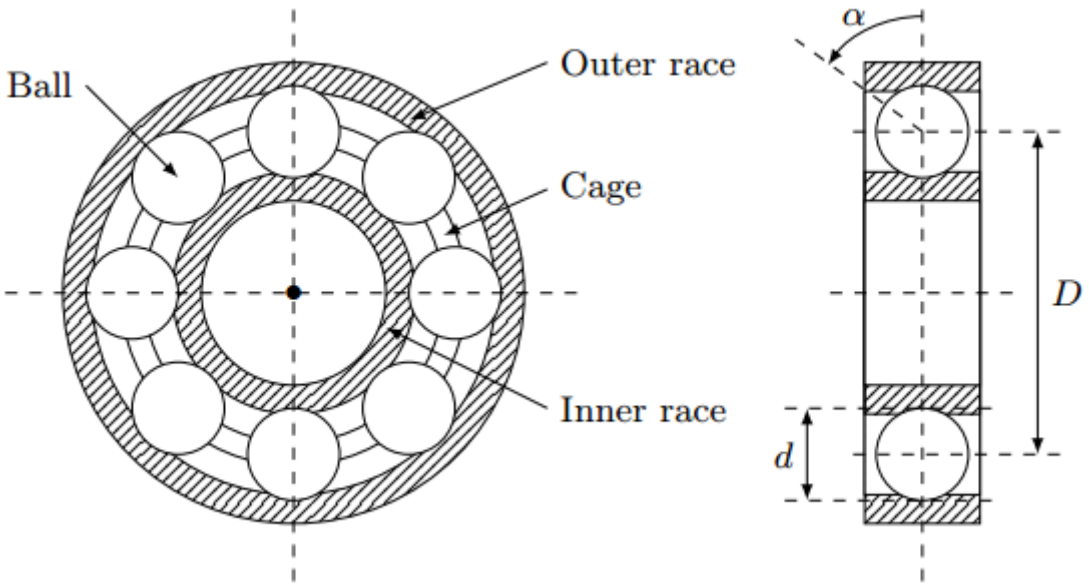

Figure 2.2: Bearing structure with mean dimensions (El Bouchikhi et al, 2015)

2.4.1.1.1 Causes and consequences of bearing failure

Bearing usually operates in a rough environment in which hard materials, humidity, dirt, acid and water are commonly present and cause mainly major deterioration factors namely corrosion and contamination which leads to a rough running of the bearing as the balls are unable to rotate properly causing excessive heat and eventually grease breakdown that reduces lubrication and accelerates the bearing failure. Another factor for bearing failure is improper assembly which causes damage in raceways in the form of brinelling or false brinelling; it can also result in misalignment. An ultimate bearing failure can be caused by fatigue failure, indirect failures such as unacceptable operating conditions (transport, storage and handling), other machine's part failures such as shaft vibration. The latter are a consequence of typical damage symptoms for instance vibration (T.Harris et al ,2001) (R.F.Schiferl et al ,2004) (Izzet et al ,2008).

2.4.2.2 Eccentricity Related Fault

Eccentricity can be identified by the frequency component in stator current spectrum (Bellini,et al, 2002), (Sahraoui, et al., 2008)

$$f_{ec} = f_s \left[\frac{(kN_r \pm n_d)(1-s)}{p \pm v} \right]$$

where k is an integer, N_r is the number of rotor slots, s is the slip, p is the number of pole pairs, f_s is the fundamental frequency, n_d is an integer representing the eccentricity order, $n_d = 0$ represents the static eccentricity (SE) and $n_d = 1,\ 2,\ 3$ represents the dynamic eccentricity (DE), v is the stator time harmonics. Moreover, if the SE and DE simultaneously occur, specific harmonic can be observed around fundamental frequency given by (Faiz.et al, 2015):

$$f_{mix} = f_s \pm m f_r$$

$$f_r = \left(1 - \frac{s}{p}\right) f_s$$

where m = 1, 2, 3 ....

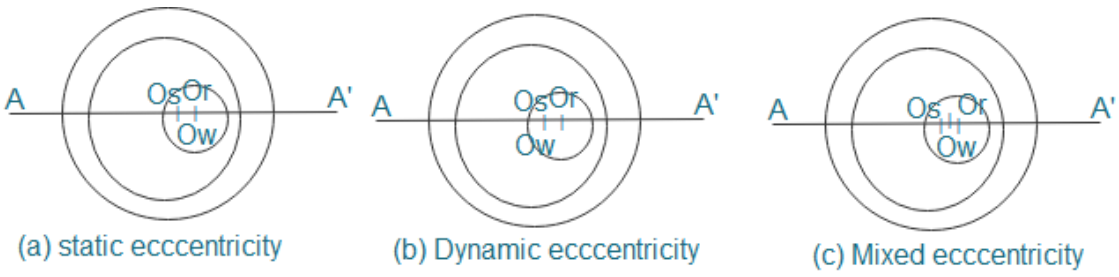

Figure 2.3: cross-section of motor for three types of eccentricity:(a) static eccentricity;(b) dynamic eccentricity;(c) mixed eccentricity.

2.4.2.1.1 Types of eccentricity

Static air-gap eccentricity: the rotor is displaced from the stator center, but it rotates around its center this may lead to unequal air-gap between the stator and rotor. Moreover, irregularities in the circular shape of the stator core.

Dynamic air gap eccentricity: the rotor is also displaced from the stator center, but it rotates around the center of the stator center causing bent in the rotor shaft, bearing wear, misalignment, mechanical resonance at critical speed, and unbalanced magnetic pulls due to static eccentricity.

Mixed air gap eccentricity: the center of the stator, the center of the rotor and the rotation axis are displaced with respect to each other, in other words, static and dynamic eccentricity occurring simultaneously. The letters eccentricities may eventually result Bearing failure and Stator to rotor rubs.

2.4.1.3 Misalignment Fault

Misalignment considered to be the second mechanical fault in the induction machine after unbalance fault. It may occur in different forms:(a) Angular misalignment occurs when the motor is set at an angle to the driven equipment. The angle of mismatch can be to the left or the right, or above or below. If the centerlines of the motor and the driven equipment shafts were to be extended, they would cross each other, rather than superimpose or run along a common centerline. (b) Parallel misalignment occurs when the two shaft centerlines are parallel, but not in the same line. They are offset horizontally or vertically (or both), displaced to the left or right, or positioned at different elevations. (c) Combination misalignment occurs when the motor shaft suffers from angular misalignment in addition to parallel misalignment.

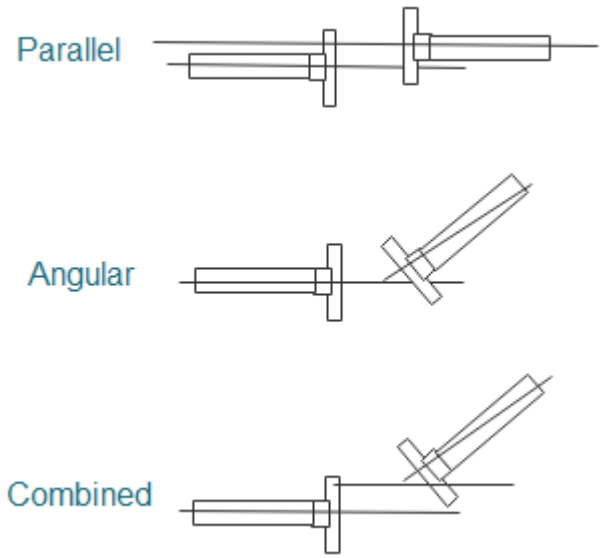

Figure 2.4: Types of misalignment

2.4.1.3.1 Causes and consequences of misalignment fault

Misalignment is one of the most frequent faults observed in rotating machinery, this fault is caused mainly by improper assembly of machines, unequal settlement of the foundation, and, asymmetry in applied loads. It leads to undesirable consequences such as decrease in the efficiency and unnecessary vibration, gives stresses on motor and bearings and also the danger of short-circuiting in stator and rotor winding (E.Ayaz, 2014).

2.4.3 Electrical failure mode

Failures in induction machines could be classified into two categories, one is known as the mechanical failure and the other are electrical failures

2.4.3.1 Rotor Broken Bar Fault(BRB)

The presence of BRB fault prevents the current flow through the broken rotor bar and results in an unbalanced rotor flux. The Unbalanced rotor flux can also be considered as

a combination of positive- and negative sequence components, rotating in opposite directions at the slip frequency. This may result in the appearance of distinguishing characteristic frequencies (sideband frequencies around the supply frequency) that are given by Alwadia.et.al (2012), Kliman.et.al (1992).

$f_b = (1 \pm 2ks) f_s$, k=1,2,3, ...

The per unit slip is calculated as:

$$s = \frac{f_{slip}}{f_{sync}} = \frac{\frac{2f_s}{p - f_r}}{\frac{2f_s}{p}}$$

where f_s is the supply frequency, f_r is the frequency of rotor currents and p is the number of poles. The upper sideband $f_s(1+2ks)$ is due to consequent speed oscillation, while the lower sideband $f_s(1-2ks)$ is specifically due to broken rotor bars. The amplitude of the lower sideband frequency is proportional to the number of the broken rotor bars as follows (R. Hirvonen,1994):

$$\frac{I_{rbr}}{I_s} = \frac{\sin(\alpha)}{2p(2\pi - \alpha)}$$

where I_s is the stator current fundamental frequency component, I_{rbr} is the amplitude of the frequency component $f_s(1+2ks)$ and $\alpha = \frac{2R_b p\pi}{R}$ where R_b is the number of broken bars. However this frequency component may not exist for some cases such as the case in which the broken bars are electrically $\frac{\pi}{2}$ radians from each other (Benbouzid et. al,2014), moreover, some experiments showed that both skewing and non-insulation of rotor bars lead to reduce the broken rotor bar harmonic components and if this latter is

smaller than the fundamental frequency component amplitude, the rotor may be considered as healthy (R. Hirvonen,1994).

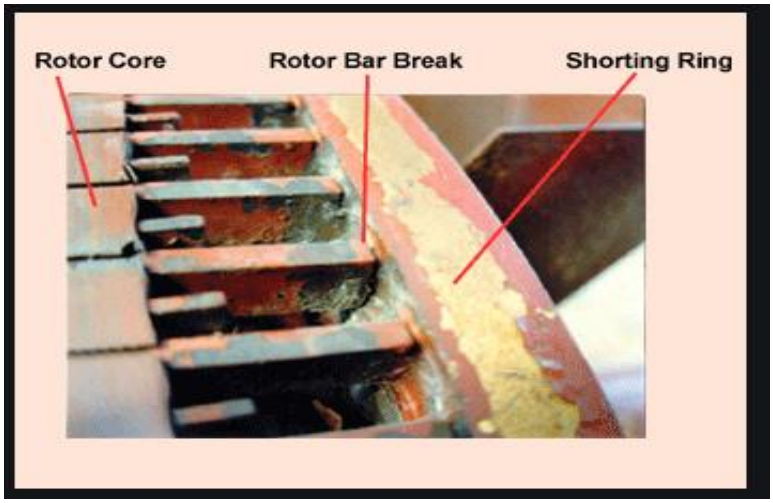

Figure 2.5: Induction motor broken rotor bar (Jivajee et al,2004)

2.3.2.1.1 Causes and effects of broken bar fault

Several factors may cause the bar breakage, among them, hot spots, sparking and thermal unbalance, chemical contamination, moisture abrasion of the rotor materials, manufacturing defects, thermal stresses due to high induced current as well as high ambient operating temperature, and/or mechanical stress caused by bearing faults and metal fatigue. The breakage of the rotor bar may lead to undesirable consequences, such as a decrease in the efficiency of the motor and increase harmonics in slip torque characteristic.

2.4.1.3 Stator Faults

There are three sorts of faults that can be occurred on the stator: stator winding fault, winding laminations fault, and the frame of the stator fault. As per the study by Electric Power Research Institute (EPRI), faults occur in the stator winding of IM are 36% and

28% respectively this later can be classified into a turn to turn, coil to ground faults, coil to coil, phase to phase fault in which a turn-to-turn fault or shorted turn is due to insulation failure between two adjacent turns in a coil. The frequency component on the axial flux, and thus stator current due to turn fault is given by (Mpendulo.al,2013)

$$f_{st} = \left(k \pm \frac{n(1-s)}{p} \right) f_s$$

Where p is the number of poles, f_s is the supply frequency, n=1,2,3,...(2p-1), k=1,3,5,..,and s is the slip.

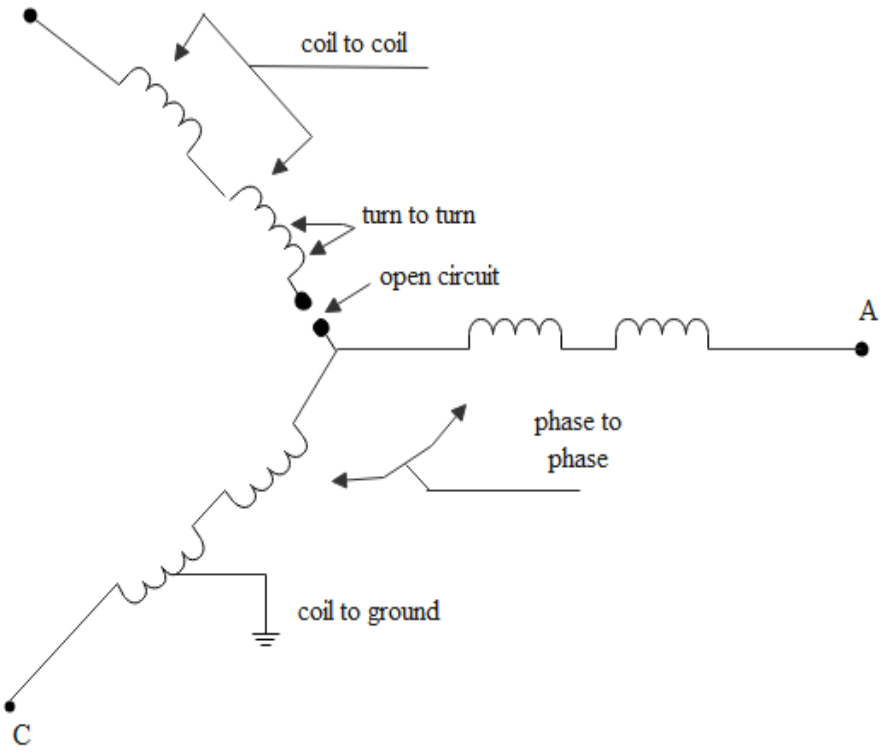

Figure 2.6: Different types of stator winding fault

2.4.1.3.1 Causes and consequences of the stator faults

Stator is the main area of the induction motor that mostly get defected, and the major causes of this defection are long thermal ageing that results in deterioration of the

winding insulation, voltage transients, open fuse, contactor or breaker failure, connection failure, or power supply failure, phase loss which is caused by an unbalanced voltage that is caused by an unbalanced load in the power line and bad connection of the motor terminals, or bad connections in the power circuits. The stator faults may lead to premature bearing failures due to extra heating that will cause unbalanced magnetic field which results in excessive vibration and eventually bearing failure.

2.5 Condition monitoring techniques

Condition monitoring is an essential process in detecting failures in electric machines. Therefore, improving productivity, efficiency, and reduction of financial losses. With growing technologies machinery, downtime can be even prevented using condition monitoring based artificial intelligence techniques. There are numerous condition monitoring techniques in which some of them are discussed in this section.

2.5.1 Vibration Monitoring

In the operating environment, the induction machine generates vibrations which are the effects of electromagnetic force on the motor parts i.e. stator and rotor (Donnellan P et al,2000). The vibration signals captured by piezoelectric sensors, are weak in healthy case, however, ones the fault occurs on the rotating components, their amplitude become larger, as well as the frequency component of their spectrum changes, compared to the reference spectrum (Bhowmik et al, 2013); (Choudhary et al,2018). Therefore. this technique is useful for failure detection in induction motors.

2.5.2 Acoustic Emission Monitoring

Acoustic Emission monitoring is a popular method for fault diagnosis in induction motors failures. It consists of recording acoustic signals using a digital voice recorder or in case of online monitoring, low-cost capacity microphone with a computer is used. The later signal is processed further to detect incipient fault in the machine. Acoustic-based fault diagnosis technique has many advantages, which are: non-invasive technique, low cost and instant measurement of acoustic signals (Glowacz, 2018).

2.5.3 Air-Gap Torque Monitoring

Air-gap torque monitoring is non-expensive non-complex monitoring technique used for fault detection in induction motor. The technique consists of spotting any changes in the air gap which is mainly dependent of flux linkages and currents in both the stator and the rotor. The later can be acquired in a short time using simple measurements: data-acquisition facility and personal computer that has a sufficient high-memory capacity.

2.5.4 Motor Current Signature Analysis

Motor current signature analysis is a non-invasive method for detecting failures in an induction motor. This method consists of acquiring stator current using a current sensor (probe), the later current is processed further to extract current harmonics with frequencies related to a certain type of fault. The major faults of IM that can be detected with MCSA technique are: Stator faults, bearing fault, broken rotor bar, Misalignment, Abnormal stator winding connections and irregularities in static or dynamic air-gap (Choudhary et al,2018).

2.5.5 Infrared Thermography

Infrared thermography is a well-known technique in condition monitoring of electric machines. It is based on measuring superficial temperatures using infrared cameras that work on converting infrared radiation measurements into temperature measurements. Thus motor faults usually lead to temperature rises that may be detected via infrared data analysis (Lopez-Perez et al, 2016).

2.6 Machine learning techniques for condition monitoring of rotary machinery

Automation and smart manufacturing are aspects of industry 4.0, although, it integrates the most recent technologies such as Internet of Things, Cyber-Physical Systems, Digital Twins, Cloud Computing or Big Data Analytics. These technologies serve in predictive maintenance and intelligent condition monitoring of rotary machinery. Thus nowadays machines are equipped with wireless multi-sensors that collect a huge amount of data to be processed and analyzed using machine learning tools such as k-Nearest neighbor, Naive Bayes classifier, and few most common techniques including Artificial Neural Network (ANN), Support Vector Machine (SVM), Deep Learning(DP), approaches are discussed in this section.

2.6.2 Artificial Neural network(ANN)

Artificial Neural Network is a technique that mimics the way the biological human nervous system works and process information, it consists of computation element called neurons which emulates the neurons of the biological brain these latter are connected with weights and associated bias and organized in three different sorts of layers: the input layer,

the hidden layer and the output layer. Two types of learning are used: supervised learning in which the outputs are set as desired, backpropagation is an example for supervised algorithm while the unsupervised learning is unlike supervised learning the input data does not contain information about the desired output, Hopfield Nets is an example for such an algorithm. A simple structure of ANN is described in the following formula (Kumar et al, 2020):

$$y = A(w^T x) = A(\sum_{i=1} w_i x_i + b)$$

where A is an activation function (can be sigmoid, logsig, purelin etc.), W is a weight matrix, b is a bias (scalar). Initially, weights (W) are initialized randomly and then optimized by an iterative training procedure, based on relationship between input-output patterns. ANN is a powerful and more accurate tool to estimate and predict the remaining useful life of electrical rotating machinery (Gindy et al, 1997).

2.6.2 Support Vector Machine(SVM)

Support vector machine is a supervised machine learning algorithm introduced in 1994 by Vapnik, it is used for less samples classification and regression challenges, it consists of constructing a hyperplane for separating different clusters or classes, the larger the margin between the hyperplane and the nearest data in the clusters the more the algorithm is robust. SVM is an excellent technique for modelling linear and nonlinear relationships thus a Kernel function is used for solving non-linear classification problems. Besides SVM is popular in the area of machine fault detection due to its attractive features and good empirical performance, it has two main advantages which are: computationally faster compared with nonparametric techniques such as ANN and works effectively even when the training data is imperatively limited.

2.6.3 Decision Tree and Random Forest

The decision tree is a popular supervised, learning method used mostly in solving classification and regression problems, as its name indicates this method has a tree-like structure and graphical representation which makes it easy to understand, besides DT, is a non-parametric method which means that decision trees have no assumptions about the spatial distribution and the classifier structure, moreover this method can handle both linear and non-linear relationships, despite its many advantages DT suffers from several limitations such as inaccuracy, overfitting and instability as a small change in data lead to a huge change in the decision making, for overcoming such deficiencies, Tin Kam Ho developed a new algorithm called Random Forest, which consists of a multitude of decision trees known for its feature randomness , which provides a better accuracy than a signal decision tree. The possible solute ions to a given problem emerge as the leaves of a tree, each node representing a point of deliberation and decision. (Niklaus Wirth, 1934).

2.6.4 K-Nearest Neighbor

K-nearest neighbor is a simplest supervised machine learning algorithm, mostly used for classification, this algorithm is known as a lazy learner, though, it is used for small, labelled and free noise data, it consists on storing all available cases and classifies new cases based on similarity measures which are determined using Euclidean distance calculation between a test sample and the specified training samples. For better accuracy, the k parameter has to be chosen properly, not too small to avoid noisy data, not too big to prevent difficulties.

2.6.5 Naive Bayes classifier (NBC)

Naive Bayes is the simplest machine learning method used for small and medium data size. The algorithm is trained mainly for the classification problems, it is most suitable for continuous, discrete, and categorical features data sets, thus Naive Bayes classifier also called independent Bayes that's because the values of features in the class are independent from each other, given the class variable. Despite the naive nature of the algorithm. NB is known for its quick and effective computation of unknown class from high dimensional datasets (Pandarakone et al, 2018), in addition, it is capable of performing the classification of both supervised and unsupervised data.

NBC is based on the probability concept namely Bayes' theorem**,** that describes the probability of an event, based on prior knowledge of conditions that might be related to the event, in other words, it is a combination of prior and likelihood probability to form a posterior probability like stated in the following equation : $P(A \mid B) = \frac{P(B \mid A)P(A)}{P(B)}$

where A and B are events and $P(B) \neq 0$

$P(A \mid B)$: is a conditional probability in which, the likelihood of event A occurring given that B is true.

$P(B \mid A)$:is also a conditional probability in which, the likelihood of event B occurring given that A is true.

$P(A)$ and $P(B)$ are the probabilities of observing A and B respectively; they are known as the marginal probabilities.

2.6.6 Deep Learning

Deep learning or deep neural network is an advanced technique for induction machine fault monitoring. It is based on adding multiple hidden layers to the artificial neural network to create a deep architecture capable of learning features automatically at multiple levels of abstraction, allowing to learn complex input-to-output functions directly from data, without depending on feature extractors, which can be of great benefit for industrial rotating machinery fault diagnosis **(**Liu et al, 2018).

CHAPTER 3

INDUCTION MACHINE MODELLING

3.1 Introduction

Modelling is an important element in diagnosing and predicting machinery behavior as it is a mathematical representation of the physical phenomena's, associated with the machine measured parameters, thus the failure in electric machines namely induction machines is the result of the change of the later parameters (Singh et al, 2016). With the help and growth of computational capacities, many software offers an interactive environment for machinery modelling and MATLAB is the most used software among engineers and scientists.

3.2 Modelling methods

The models are categorized as multiple coupled circuit models, *DQ* models, magnetic equivalent circuit models and finite element models.

3.2.1 Finite Element Method(FEM)

Finite Elements Method (FEM) is a numerical technique used to obtain an accurate and complete model for the electric machines as it provides detailed information of the machine nonlinear effects (W. Zaabi et al,2014). Therefore, it is used for diagnosis and analysis of changes in electric, magnetic and mechanic behavior of the machine due to any fault. FEM works on breaking down the machine into many small elements than apply Maxwell's equations which are based on solving the magnetic field non-linear

Partial Differential Equation (PDE) which are strongly coupled with mechanical motional equations and electric circuits equations. (Arkkio et al, 1987).

3.2.2 Permeance Network Method

Permeances network is a numerical nonlinear modelling technique consists of representing the machine as flux tubes characterized by their magnetic permeances that depends mainly on the machine geometry (Y. Amara et.al,2001). This technique known also as a Magnetic equivalent circuit model, thus the stator and rotor slot can be modelled as a simplified magnetic equivalent circuit comprising closed-loop paths containing a magnetic flux, magnetic reluctance and magneto-motive forces (Singh et al,2016).

The model has two important advantages over finite element method which are :1) taking into account the local magnetic saturation and 2) the simulation time is relatively less.

3.2.3 Winding Function Method

In this dissertation, a winding function approach is used to model the induction motor, this approach consists of representing the machine in terms of coupled magnetic circuits (inductances and resistances) rather than magnetic fields (Lipo, 2008) which is computationally effective for obtaining different operating characteristics (Carrera et .al, 2018).

This multiple coupled circuit is defined in the aim of approaching the real structure of the rotor cage. The method supposes that the squirrel cage rotor is composed of n_b bars and two end rings, each bar is represented by an inductance (L_b) and resistance (R_b), related to another bar by means of a segment of an end ring which is also represented by

resistance namely(R_e) and an inductance(L_e). The current in each mesh of the rotor cage is an independent variable (Houdouinet.al,2003); as shown in Figure 2.1 and Figure 2.2

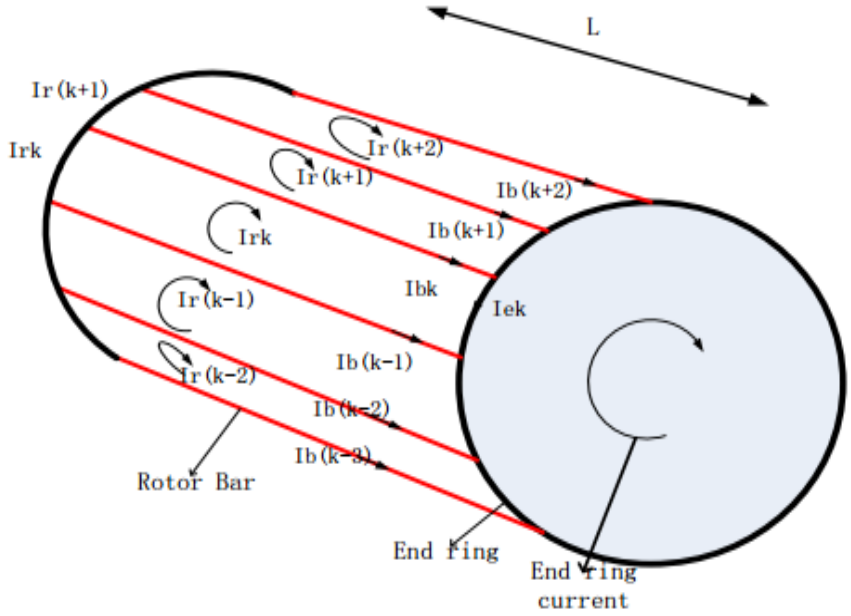

Figure 3.1: Elementary rotor loops and current definitions (Shi et al,2013).

.

Figure 3.2: The equivalent circuit of the rotor squirrel cage (Shi et al,2013).

3.2.3.1 Inductance determination by Winding Functions

Initially few assumptions must be considered; the machine is symmetric (stator winding with axes of symmetry and uniformly distributed rotor cage bars), air-gap is uniform and smooth i.e. neglecting the existence of stator and rotor slots, the rotor bars are insulated from the rotor and there is no inter-bar current flows through the laminations, the permeability of machine armatures is assumed infinite, eddy current, friction and windage losses (power losses caused by air resistance to the rotor) are neglected, and negligible saturation. (Priteem et.al,2016) (Ye et al,2001) (Shi et.al,2013). With these assumptions, the mutual inductance between any two circuits can be determined from motor geometry and dimensions by Winding Function Method which provides a more accurate calculation to the latter (Ibrahim et al. (2010):

$$L_{ij}(\theta_r) = \frac{r_d\, l \mu_0}{g} \int_0^{2\pi} N_i(\theta_r, \varphi) N_j(\theta_r, \varphi) d\varphi \qquad 3.1$$

where, $\mu_0 = 4\pi.10^{-7}$is the permeability factor of the air gap, $\theta_r$is the rotor angular position, r_d is the average radius of the air gap, l is the active stack length of the motor, φ is angular position, and Ni(θ,φ), Nj(θ,φ) is called the winding function of circuit i and j and represents the magneto motive force (MMF) distribution along the air gap. For a sinusoidal distributed stator windings, the winding function for phase"a" is

$$F_a(\varphi) = \frac{2\, N_s}{\pi\, p}\, i_{sa} \cos(p\, \varphi) \qquad 3.2$$

and, the magnetic flux density in the air gap isgiven by:

$$B_a(\varphi) = \frac{2\mu_0\, N_s}{\pi g p} i_{sa} \cos(p\varphi) \qquad 3.3$$

the magnetic flux in(2.4) is a result of (2.3) integration:

$$\phi = BS = \int_0^l dz \int_{\frac{-\pi}{2p}}^{\frac{\pi}{2p}} B_a(\varphi)\, r\, d\varphi \qquad 3.4$$

therefore,

$$\phi = \frac{4 N_s\, r\, l \mu_0}{\pi g p^2} i_{sa} \qquad 3.5$$

where, the magnetic flux in phase "a" is defined as follows

$$\phi_{sa} = \phi N_s = \frac{4\mu_0 N_s^2\, r\, l}{\pi g p^2} i_{sa} \qquad 3.6$$

The magnetizing inductance of the phase "a" is:

$$L_{am} = \frac{\varphi_{sa}}{i_{sa}} = \frac{4\mu_0 N_s^2 r\, l}{\pi g p^2} \qquad 3.7$$

The total inductance of phase "a" is the sum of the leakage inductance and the magnetizing inductance as follows:

$$l_s = L_{am} + L_{sl} \qquad 3.8$$

The mutual stator inductance is:

$$M_s = L_{am} \cos\left(\frac{2\pi}{3}\right) = \frac{-L_{am}}{2} \qquad 3.9$$

Since the stator windings are symmetric, the mutual and the self-inductances of all phases are equal.

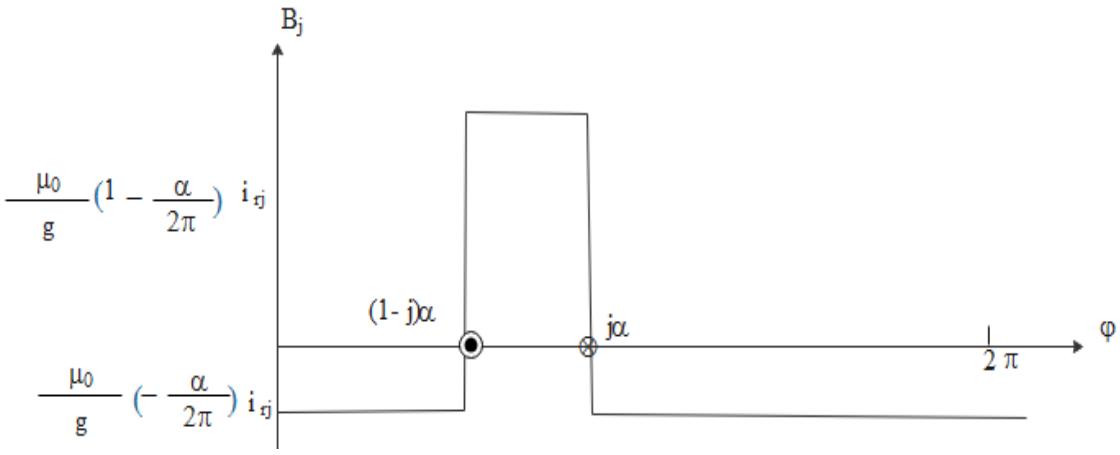

Figure 4.3: The magnetic flux density of the rotor loop

The rotor loops self-magnetic flux is given as follows

$$\varphi_{rjrj} = \int_0^l dz \int_{(j-1)\alpha}^{j\alpha} \frac{\mu_0 r}{g}\left(1 - \frac{\alpha}{2\pi}\right) i_{rj}\, d(\varphi') \qquad 3.10$$

After integration, we have:

$$\varphi_{rkrj} = \frac{\mu_0 r l}{g}\left(-\frac{\alpha}{2\pi}\right)\alpha i_{rj} \qquad 3.11$$

The magnetizing inductance of the loop j is:

$$L_{mrj} = \frac{\varphi_{rjrj}}{i_{rj}} = \frac{2\pi\mu_0(n_b - 1) r l}{g\, n_b^2} \qquad 3.12$$

The total rotor inductance of the j^{th}mesh is:

$$L_{rjj} = L_{mrj} + 2L_{bj} + L_{b(j+1)} + 2L_e \qquad 3.13$$

The mutual inductances between rotor loops:

$$L_{r(j+1)j} = \frac{\varphi_{r(j+1)rj}}{i_{rj}} - L_{b(j+1)} = -\frac{2\pi\mu_0 r l}{g\, n_b^2} - L_{b(j+1)} \qquad 3.14$$

$$L_{rkj} = \frac{\varphi_{rkrj}}{i_{rj}} = -\frac{2\pi\mu_0 r l}{g\, n_b^2} \qquad 3.15$$

$$L_{r(j-1)j} = \frac{\varphi_{r(j-1)rj}}{i_{rj}} - L_{bj} = -\frac{2\pi\mu_0 r l}{g\, n_b^2} - L_{bj} \qquad 3.16$$

The magnetic flux density in the rotor reference frame is:

$$B_a(\varphi') = \frac{2\mu_0 N_s}{\pi g p} i_{sa} \cos\left[p(\varphi' + \omega_r t)\right] \qquad 3.17$$

and,

$$\varphi = \varphi' + \omega_r t \qquad 3.18$$

The magnetic flux in the rotor loop j is:

$$\phi_{rja} = \int_0^l dz \int_{(j-1)\alpha}^{j\alpha} B_a(\varphi') r \, d\varphi' \qquad 3.19$$

After integration we have:

$$\phi_{rja} = M i_{sa} \cos\left[p\left(\frac{(2j-1)\pi}{n_b} + \omega_r t \right) \right] \qquad 3.20$$

and,

$$M = \frac{4\mu_0 N_S r l}{\pi g p^2} \sin\left(\frac{\pi p}{n_b}\right) \qquad 3.21$$

The mutual inductances between the j^{th} rotor loop and phase "a", "b", and, "c" respectively are:

$$L_{rja} = \frac{\phi_{rja}}{i_{sa}} = M \cos\left[p\left(\frac{(2j-1)\pi}{n_b} + \omega_r t \right) \right] \qquad 3.22$$

$$L_{rjb} = \frac{\phi_{rjb}}{i_{sb}} = M \cos\left[p\left(\frac{(2j-1)\pi}{n_b} + \omega_r t \right) - \frac{2\pi}{3} \right] \qquad 3.23$$

$$L_{rjc} = \frac{\phi_{rjc}}{i_{sc}} = M \cos\left[p\left(\frac{(2j-1)\pi}{n_b} + \omega_r t \right) + \frac{2\pi}{3} \right] \qquad 3.24$$

3.3 Coupled circuit model of the induction machine

The induction motor model can be described using stator and rotor differential equations.

3.3.1 Stator voltage equations:

$$\left[V_s\right]=\left[R_s\right]\left[I_s\right]+\frac{d\left[\phi_s\right]}{dt} \qquad 3.25$$

where,

$$\left[\phi_s\right]=\left[L_s\right]\left[I_s\right]+\left[L_{sr}\right]\left[I_r\right] \qquad 3.26$$

Then, substituting 3.26 into 3.25 gave the following

$$\left[V_s\right]=\left[R_s\right]\left[I_s\right]+\frac{d\left(\left[L_s\right]\left[I_s\right]\right)}{dt}+\frac{d\left(\left[L_{sr}\right]\left[I_r\right]\right)}{dt} \qquad 3.27$$

Since $\left[L_s\right]$ is constant, we have,

$$\left[V_s\right]=\left[R_s\right]\left[I_s\right]+\left[L_s\right]\frac{d\left(\left[I_s\right]\right)}{dt}+\left[L_{sr}\right]\frac{d\left(\left[I_r\right]\right)}{dt}+\left[I_r\right]\frac{d\left(\left[L_{sr}\right]\right)}{dt} \qquad 3.28$$

and,

$$\frac{d\left(\left[L_{sr}\right]\right)}{dt}=\frac{d\left(\left[L_{sr}\right]\right)}{d\theta_r}\frac{d\theta_r}{dt}=\frac{d\left(\left[L_{sr}\right]\right)}{d\theta_r}\omega_r \qquad 3.29$$

Therefore,

$$\left[V_s\right]=\left[R_s\right]\left[I_s\right]+\left[L_s\right]\frac{d\left(\left[I_s\right]\right)}{dt}+\left[L_{sr}\right]\frac{d\left(\left[I_r\right]\right)}{dt}+\left[I_r\right]\frac{d\left(\left[L_{sr}\right]\right)}{d\theta_r}\omega_r \qquad 3.30$$

where,

$$[V_s] = [V_{as}\ V_{bs}\ V_{cs}]^T \tag{3.31}$$

$$[I_s] = [I_{as}\ I_{bs}\ I_{cs}]^T \tag{3.32}$$

$$[I_r] = [I_{r1}\ I_{r2}\ I_{r3}....I_{mb}\ I_{re}]^T \tag{3. 33}$$

with,

$[V_s]$: is the terminal stator voltage vector;

$[\phi_s]$: is the stator flux vector;

$[I_s]$:is stator current vector;

$[I_r]$: is the rotor loop current vector;

$[L_s]$is symmetric 3x3 matrix represents the stator inductance:

$$[L_s] = \begin{bmatrix} L_{am}+L_{sl} & M_s & M_s \\ M_s & L_{bm}+L_{sl} & M_s \\ M_s & M_s & L_{cm}+L_{sl} \end{bmatrix} \tag{3.34}$$

$[R_s]$is symmetric 3x3 matrix represents the stator resistance:

$$[R_s] = \begin{bmatrix} r_s & 0 & 0 \\ 0 & r_s & 0 \\ 0 & 0 & r_s \end{bmatrix} \tag{3.35}$$

where r_s is the resistance of the stator winding which depends on the conductance of the material and the dimensions of the windings.

3.3.2 Rotor voltage equations

Figure 3.4 represent the *j* , *j*-1 and *j*+1 meshes of the squirrel cage motor.

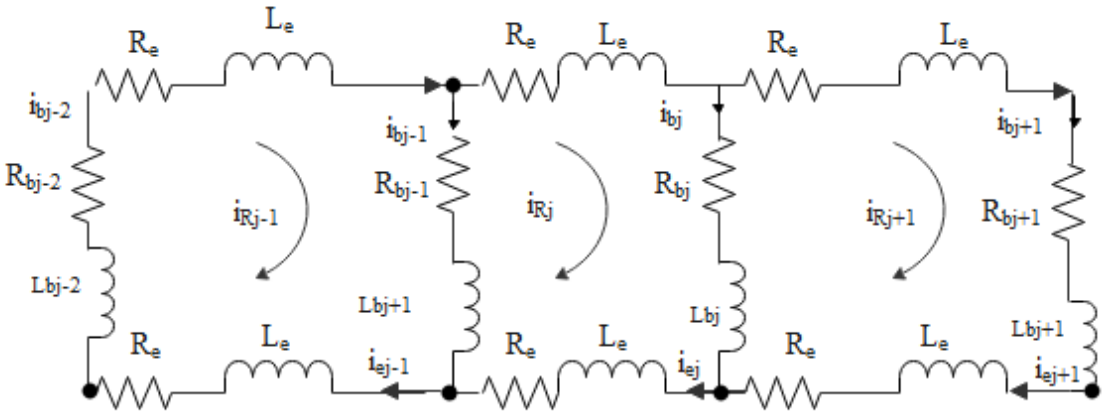

Figure 3.4: Equivalent circuit of three meshes of the rotor squirrel cage

Applying Kirchoff law to the kth mesh we have:

$$2(R_b+R_e)i_j - R_b i_{j+1} - R_b i_{j-1} - R_e i_e + \frac{d}{dt}\left[\begin{array}{l}(L_{r\,j\,r\,j}) + 2(L_b+L_e)i_j + (L_{r\,j\,r\,j+1} - l_b)i_{j+1} \\ +(L_{r\,j\,r\,j-1} - l_b)i_{j-1} + \cdots - L_e i_e + L_{r\,j\,s1} i_{s1} + \cdots + L_{r\,j\,sm}\end{array}\right] = 0 \qquad 3.36$$

After applying Kirchoff law to the whole meshes, this leads to:

$$[V_r] = [R_r][I_r] + \frac{d[\phi_r]}{dt} \qquad 3.37$$

where,

$$[\phi_r] = [L_r][I_r] + [L_{rs}][I_s] \qquad 3.38$$

Then,

$$\left[V_r\right]=\left[R_r\right]\left[I_r\right]+\frac{d(\left[L_r\right]\left[I_r\right])}{dt}+\frac{d(\left[L_{rs}\right]\left[I_s\right])}{dt} \quad 3.39$$

Since, $\left[L_r\right]$ is constant ,the equation 3.39 became:

$$\left[V_r\right]=\left[R_r\right]\left[I_r\right]+\left[L_r\right]\frac{d(\left[I_r\right])}{dt}+\left[L_{rs}\right]\frac{d(\left[I_s\right])}{dt}+\left[I_s\right]\frac{d(\left[L_{rs}\right])}{dt} \quad 3.40$$

with,

$$\frac{d(\left[L_{rs}\right])}{dt}=\frac{d(\left[L_{rs}\right])}{d\theta_r}\frac{d\theta_r}{dt}=\frac{d(\left[L_{rs}\right])}{d\theta_r}\omega_r \quad 3.41$$

Therefore,

$$\left[V_r\right]=\left[R_r\right]\left[I_r\right]+\left[L_r\right]\frac{d(\left[I_r\right])}{dt}+\left[L_{rs}\right]\frac{d(\left[I_s\right])}{dt}+\left[I_s\right]\frac{d(\left[L_{rs}\right])}{d\theta_r}\omega_r \quad 3.42$$

where,

$$\left[V_r\right]=\left[V_{r1}\ V_{r2}\ V_{r3}...V_{rnb}\ V_{re}\right]^T \quad 3.43$$

and,

$$\left[\phi_r\right]=\left[\phi_{r1}\ \phi_{r2}\ \phi_{r3}...\phi_{rnb}\ \phi_{re}\right]^T \quad 3.44$$

And,

$\left[V_r\right]$: is the terminal rotor voltage vector; in case of a cage rotor, the rotor end-ring voltage is $V_{re}=0$, and the rotor loop voltages are $V_{rk}=0$, (k=1,2…*nb*);

$\left[\phi_r\right]$: is the rotor flux vector;

$\left[R_r\right]$: is a symmetric (nb+1) x (nb+1) matrix represents the rotor resistance:

$$[R_r]=\begin{bmatrix} R_{bo}+R_{b(n_b-1)}+\frac{2R_e}{n_b} & -R_b & \dots & 0 & \dots & \dots & -R_{b(n_b-1)} & : & \frac{R_e}{n_b} \\ \dots & \dots & \dots & \dots & \dots & \dots & \dots & : & \dots \\ \dots & \dots & \dots & \dots & \dots & \dots & \dots & : & \dots \\ 0 & \dots & -R_{b(j-1)} & R_{bj}+R_{b(j-1)}+\frac{2R_e}{n_b} & -R_{bj} & \dots & 0 & : & \dots \\ \dots & \dots & \dots & \dots & \dots & \dots & \dots & : & \dots \\ \dots & \dots & \dots & \dots & \dots & \dots & \dots & : & \dots \\ -R_{b(n_b-1)} & \dots & 0 & \dots & \dots & -R_{b(n_b-1)} & R_{b(n_b-2)}+R_{b(n_b-1)}+\frac{2R_e}{n_b} & : & \frac{R_e}{n_b} \\ \dots & \dots & \dots & \dots & \dots & \dots & \dots & : & \dots \\ \frac{R_e}{n_b} & \dots & \dots & \dots & \dots & \dots & \frac{R_e}{n_b} & : & R_e \end{bmatrix} \quad 3.45$$

where, R_{bk} and R_e are the resistances of rotor bar and the end ring respectively, similarly to the stator resistance, it depends on the conductance of the material and the dimensions of the rotor loops and the end ring.

$[L_r]$ is a symmetric matrix (nb+1, nb+1) rotor inductance;

$$[L_r]=\begin{bmatrix} L_{am}+2L_b+\frac{2L_e}{n_b} & M_{rr}-L_b & \dots & \dots & M_{rr} & \dots & M_{rr}-L_b & : & \frac{-L_e}{n_b} \\ \dots & \dots & \dots & \dots & \dots & \dots & \dots & : & \dots \\ \dots & \dots & \dots & \dots & \dots & \dots & \dots & : & \dots \\ M_{rr}-L_b & \dots & M_{rr}-L_b & L_{am}+2L_b+\frac{2L_e}{n_b} & M_{rr}-L_b & M_{rr} & \dots & : & \dots \\ \dots & \dots & \dots & \dots & \dots & \dots & \dots & : & \dots \\ \dots & \dots & \dots & \dots & \dots & \dots & \dots & : & \dots \\ M_{rr}-L_b & \dots & M_{rr} & \dots & \dots & M_{rr}-L_b & L_{am}+2L_b+\frac{2L_e}{n_b} & : & \frac{-L_e}{n_b} \\ \dots & \dots & \dots & \dots & \dots & \dots & \dots & : & \dots \\ \frac{-L_e}{n_b} & \dots & \dots & \dots & \dots & \dots & \frac{-L_e}{n_b} & : & L_e \end{bmatrix} \quad 3.46$$

$[L_{sr}]$ is a $3x\,n_b$ matrix comprised of the mutual inductances between the stator coil and the rotor loops:

$$\left[L_{sr}\right]=\begin{bmatrix} L_{sr11} & L_{sr12} & \dots & L_{sr1n_b} & L_{sr1e} \\ L_{sr21} & L_{sr22} & \dots & L_{sr2n_b} & L_{sr2e} \\ L_{sr31} & L_{sr32} & \dots & L_{sr3n_b} & L_{sr3e} \end{bmatrix} \quad 3.47$$

$$\left[L_{rs}\right]=\left[L_{sr}\right]^{T}$$

3.3.3 Mechanical equation:

$$J\frac{d\omega_r}{dt}+T_r=T_e \quad 3.48$$

Where,

$$\frac{d\theta_r}{dt}=\omega_r \quad 3.49$$

The torque equation is deduced from co-energy computation as follows:

$$T_e=\left(\frac{\partial W_{co}}{\partial\theta_r}\right) \quad 3.50$$

where,

$$W_{co}=\frac{1}{2}\left[\left[I_s^T\right]\left[L_s\right]\left[I_s\right]+\left[I_s^T\right]\left[L_{sr}\right]\left[I_r\right]+\left[I_r^T\right]\left[L_{rs}\right]\left[I_s\right]+\left[I_r^T\right]\left[L_r\right]\left[I_r\right]\right] \quad 3.525$$

Then,

$$T_{e\,co}=\frac{1}{2}\left[\left[I_s^T\right]\left[\frac{\partial L_s}{\partial\theta_r}\right]\left[I_s\right]+\left[I_s^T\right]\left[\frac{\partial L_{sr}}{\partial\theta_r}\right]\left[I_r\right]+\left[I_r^T\right]\left[\frac{\partial L_{rs}}{\partial\theta_r}\right]\left[I_s\right]+\left[I_r^T\right]\left[\frac{\partial L_r}{\partial\theta_r}\right]\left[I_r\right]\right] \quad 3.52$$

Since, $\left[L_s\right],\left[L_r\right]$ are constants, we have:

$$T_{e\ co}=\frac{1}{2}\left[\left[I_s^T\right]\left[\frac{\partial L_{sr}}{\partial\theta_r}\right]\left[I_r\right]+\left[I_r^T\right]\left[\frac{\partial L_{rs}}{\partial\theta_r}\right]\left[I_s\right]\right] \quad 3.53$$

And $\left[L_{sr}\right],\left[L_{rs}\right]$ are equal, then:

$$T_e=\left[I_s^T\right]\left[\frac{\partial L_{sr}}{\partial\theta_r}\right]\left[I_r\right] \quad 3.54$$

3.5.4 Total voltage equation

$$\begin{bmatrix}[V_S]\\ [V_r]\end{bmatrix}=\begin{bmatrix}[R_s] & [0]\\ [0] & [R_r]\end{bmatrix}\begin{bmatrix}[I_s]\\ [I_r]\end{bmatrix}+\begin{bmatrix}[L_s] & [L_{sr}]\\ [L_{rs}] & [L_r]\end{bmatrix}\frac{d}{dt}\begin{bmatrix}[I_s]\\ [I_r]\end{bmatrix}+\omega_r\frac{d}{d\theta_r}\begin{bmatrix}[L_s] & [L_{sr}]\\ [L_{rs}] & [L_r]\end{bmatrix}\begin{bmatrix}[I_s]\\ [I_r]\end{bmatrix} \quad 3.55$$

3.3.4 Total model equation:

$$\begin{bmatrix}[V]\\ [T_e-T_r]\\ 0\end{bmatrix}=\begin{bmatrix}[R]+\frac{d[L]}{d\theta_r} & [0]\\ [0] & \begin{bmatrix}0 & 0\\ 1 & 0\end{bmatrix}\end{bmatrix}\begin{bmatrix}[I]\\ [\omega_r]\\ \theta_r\end{bmatrix}+\begin{bmatrix}[L] & [0]\\ [0] & \begin{bmatrix}J & 0\\ 1 & 0\end{bmatrix}\end{bmatrix}\frac{d}{dt}\begin{bmatrix}[I]\\ [\omega_r]\\ \theta_r\end{bmatrix} \quad 3.56$$

$$\frac{d}{dt}\begin{bmatrix}[I]\\ [\omega_r]\\ \theta_r\end{bmatrix}=\begin{bmatrix}[L] & [0]\\ [0] & \begin{bmatrix}J & 0\\ 1 & 0\end{bmatrix}\end{bmatrix}^{-1}\left(\begin{bmatrix}[V]\\ [T_e-T_r]\\ 0\end{bmatrix}-\begin{bmatrix}[R]+\frac{d[L]}{d\theta_r} & [0]\\ [0] & \begin{bmatrix}0 & 0\\ 1 & 0\end{bmatrix}\end{bmatrix}\begin{bmatrix}[I]\\ [\omega_r]\\ \theta_r\end{bmatrix}\right) \quad 3.57$$

3.4 Modeling broken bar and end rings faults

Two methods for simulating broken bars and broken end rings can be used: the first method consists of eliminating the current in the broken bar. The inductance and

resistance matrices are modified in a way that if the bar breaks, the current Ibk will be cancelled therefore the current in mesh k will be equal to the current in mesh (k-1) (Ir (K-1) =Irk), this is modelled by adding two columns and two lines related to the currents Ir (K-1) and Irk in resistance and inductance matrices(Belhamedi et al,2005)(Sahraoui et al,2003). The second method consists of increasing the broken rotor bar resistance. This method of breaking the bars seems more correct as the current in the broken bar is not annulated due to the existence of inter-turn bar currents that flow from bar to bar through the rotor core. In the following section, the second method is adopted and the broken rotor bar resistance is taken as (RF=10 x Rb) as well as the end ring. The corresponding resistance matrices for broken bars and end ring are presented in Appendix B

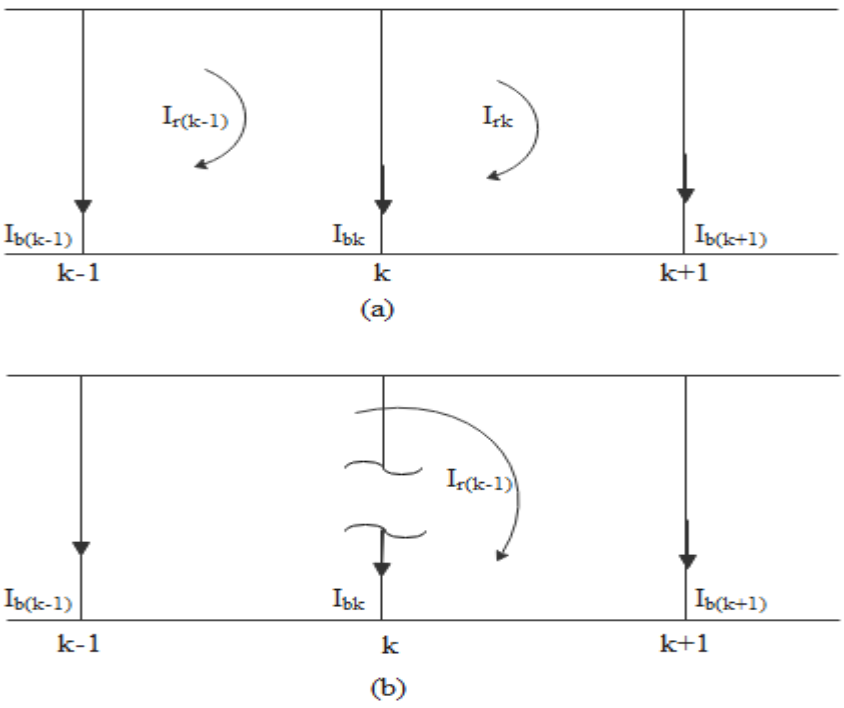

Figure 3.5: Equivalent circuit for the rotor cage (healthy case and broken bar case respectively)

3.5 Chapter summary

The chapter highlights the importance of the electric machine modelling in diagnosing induction motor failures, it also summarizes different modelling techniques (Pearmeance Network, Finite Element and Winding function) and provides a detailed mathematical description for the coupled magnetic circuit technique which is the one adopted in this thesis to simulate broken bars and end rings faults.

CHAPTER 4

SIMULATION RESULTS AND DISCUSSION

4.1 Introduction

In this chapter, time-domain simulation for both healthy and faulty induction machine is presented. Three main parameters of the machine were simulated including the torque, speed and currents for both the stator and the rotor.

4.2 Induction motor model simulation

MATLAB is a numerical computing environment developed by MathWorks in late 1984s, as its name stands for *matrix laboratory*. MATLAB allows matrix manipulations, plotting data, implementation of algorithms, creation of user interfaces, and interfacing with programs written in other languages.

In this thesis, MATLAB is used for induction motor modelling using difference equations, as well as performing spectral analysis using Fast Fourier Transform as will be mentioned in the following chapter (Chapter 5). The simulation is performed based on the selected induction machine parameters given in the appendix B (Table B.1).

4.3 Simulation results

In this section, a summary of the simulation results for an induction motor model are presented. The results include: stator current; rotor bar currents; electromagnetic torque; rotor speed and the RMS value of the rotor bar currents. The simulation is performed in both cases healthy and faulty (two separated broken bars, two adjacent broken bars and crack of a portion of an end ring). The simulation results are for the aim to spot the bad effect of the rotor bar faults on the performance of the induction motor in term of speed and torque.

4.3.1 Healthy case

Under healthy operations, the motor is loaded with 3.5 N.m. at t=0.6s as shown the below figures. for the stator current; electromagnetic torque; rotor speed; rotor bar currents and bar chart for the root mean square(RMS) values for the rotor bar currents.

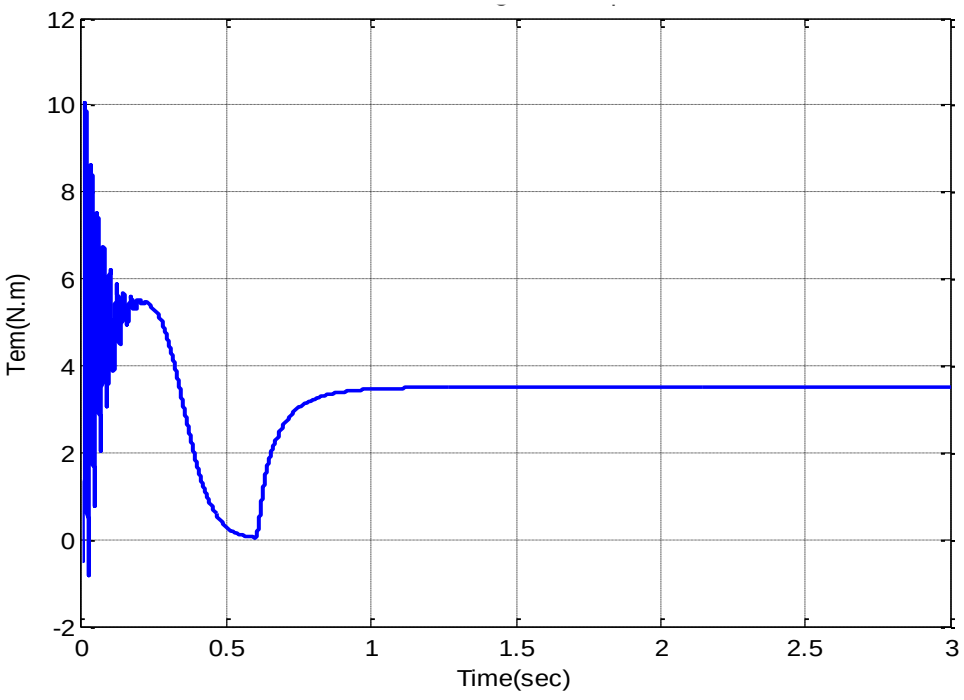

Figure 4.1: Electromagnetic Torque

Figure 4.1 illustrates the motor, developing an oscillatory torque during the transient event. The latter oscillations damped out to take a sufficient value 3.5 N.m at 0.6s.

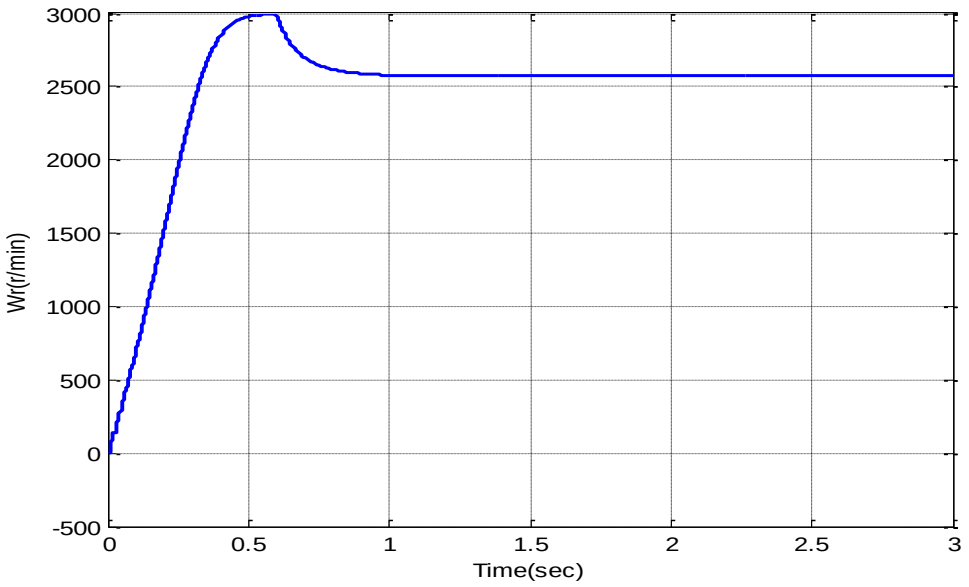

Figure 4.2: Rotor Speed

Figure 4.2 shows that the rotor speed increases to reach 3000 rpm at no load steady-state condition then it begins decreasing at the time the mechanical load is injected (0.6s) to reach about 2570 rpm as a final value.

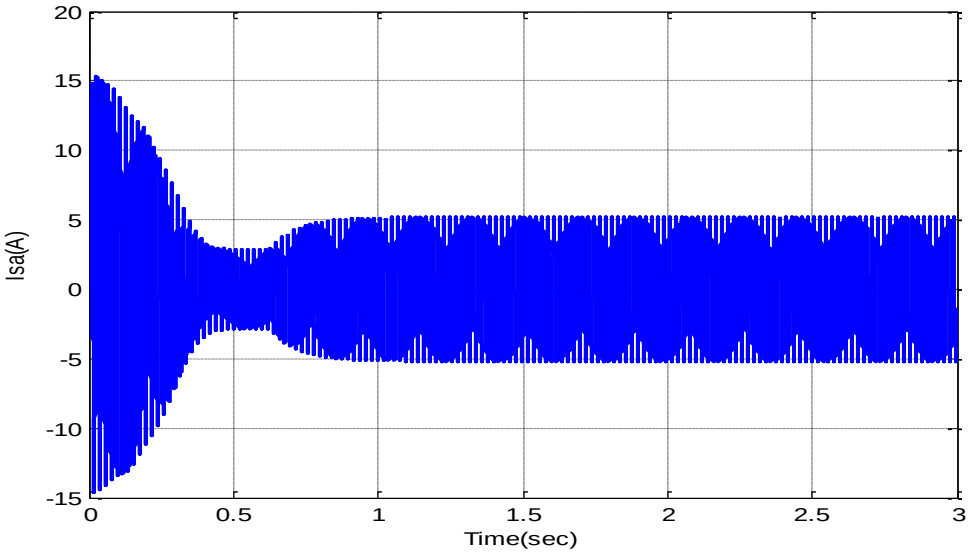

Figure 4.3: Stator current of phase “a”

From figure 4.3, it is noticeable that the start-up duration of the induction motor is about 0.4s. During this transient event the machine draws large currents of about 15 A which is about five times its steady-state current (2.8A). The steady-state current increases to (5.2 A) as the load introduced at 0.6s.

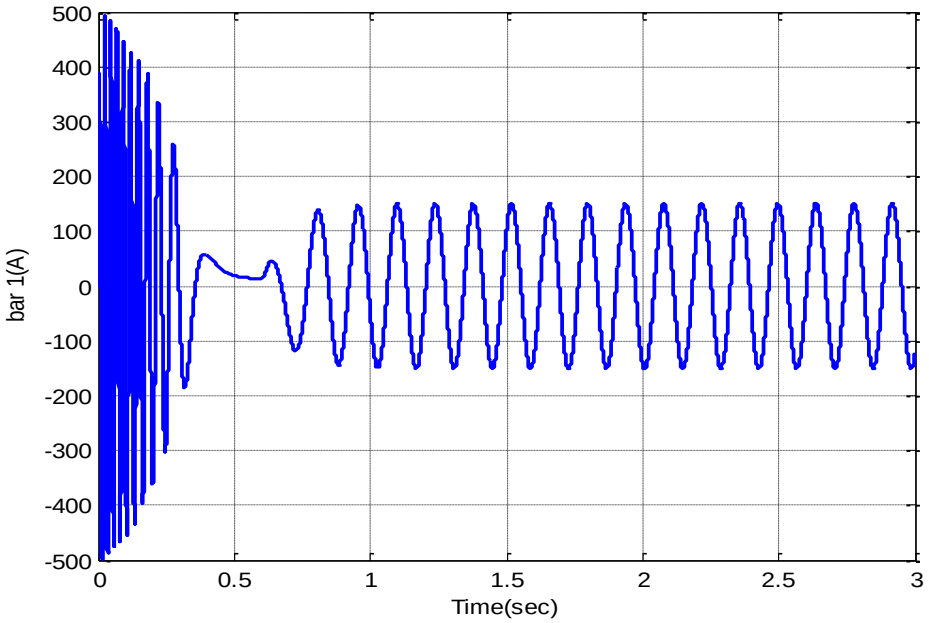

Figure 4.4: Rotor bar 1 current

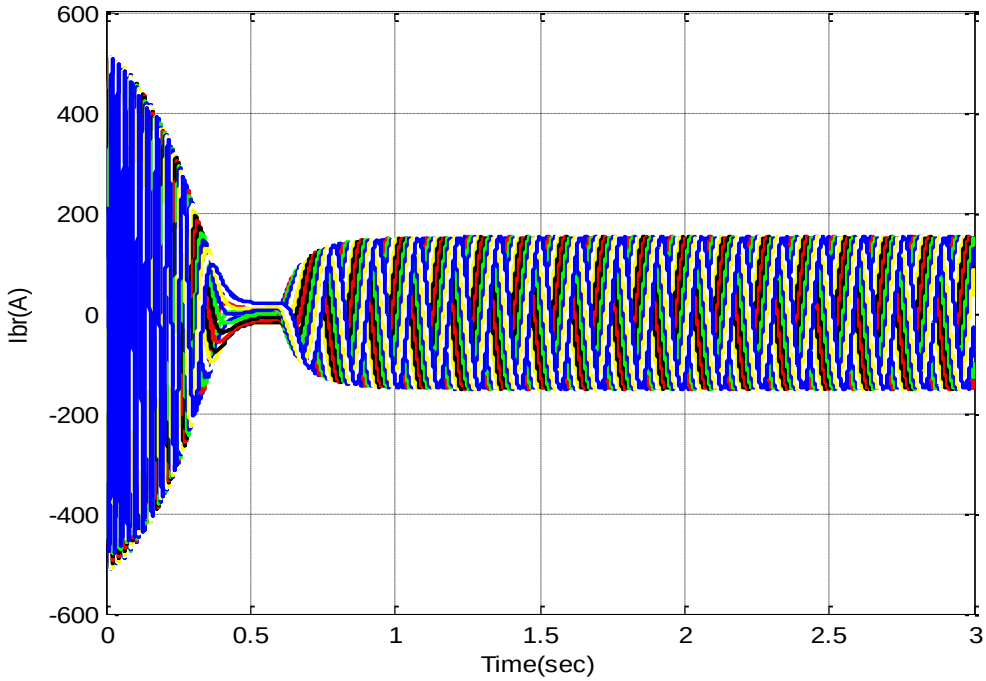

Figure 4.5: Rotor bars current

In figures 4.4 and 4.5, it is also observed that all the induced currents in 16 bars are equal to about 151.2 A at steady state after the load is applied.

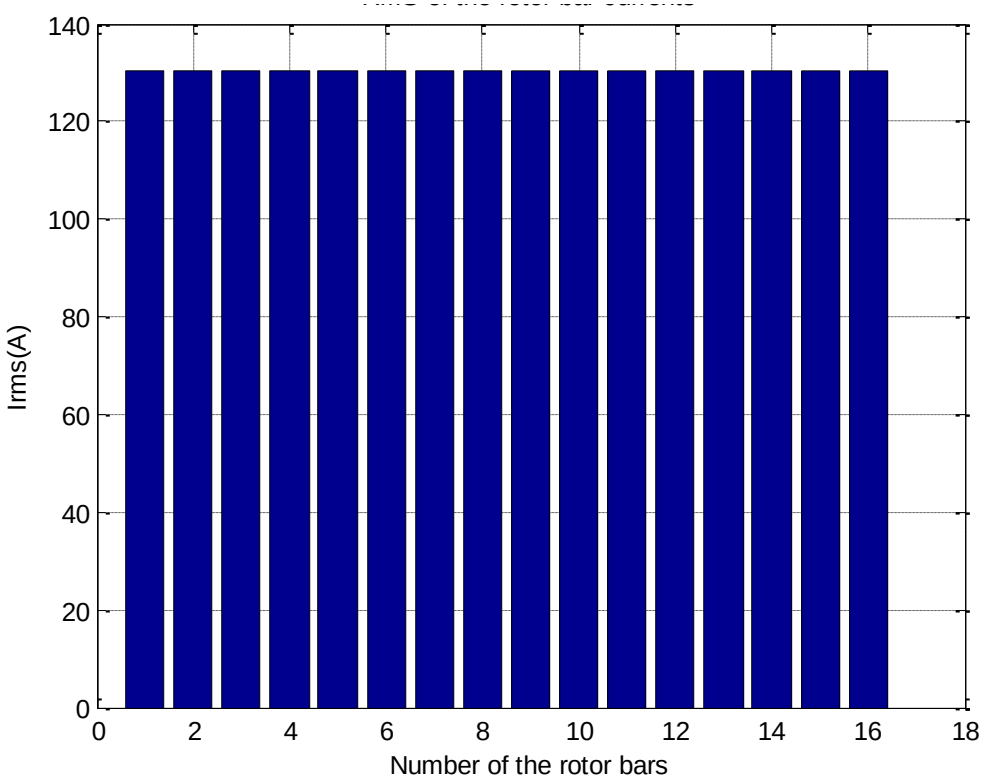

Figure 4.6: RMS of the rotor bar currents

The above bar chart shows the RMS currents of rotor bars while healthy which are approximately (130.4 A).

4.3.2 Faulty case

In this section, the simulation results while the IM is faulty are shown. Three cases were taken into consideration; the first case a model of two adjacent broken bars are simulated while the second case a model of two separated broken bars are simulated. In the third case, the cracking of the end ring is simulated. The bar's resistance when broken is taken 11 times the actual resistance of the bar.

4.3.2.1 Two adjacent broken bars

Under 3.5 N.m load, the rotor bar 1 breaks at t=1s, then the rotor bar 2 breaks at t=2s.

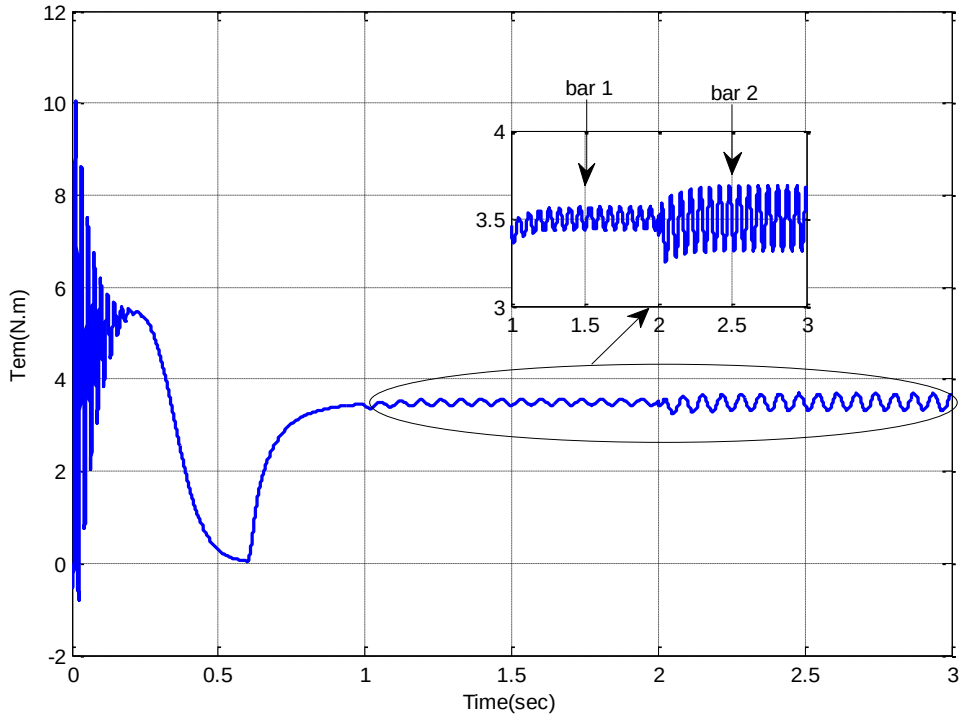

Figure 4.7: Electromagnetic Torque

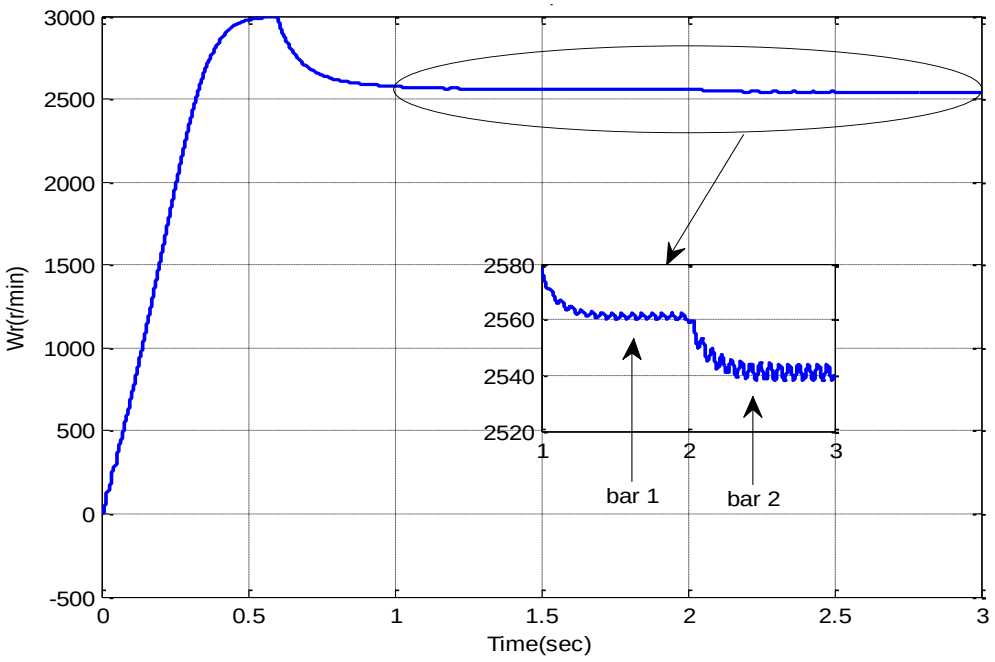

Figure 4.8: Rotor Speed

The simulation results in figures 4.7 and 4.8 show ripples in the torque and the rotor speed after the breakage of bar 1 at t=1s. however, the ripples even increase more as the 2nd bar breaks at t=2s.

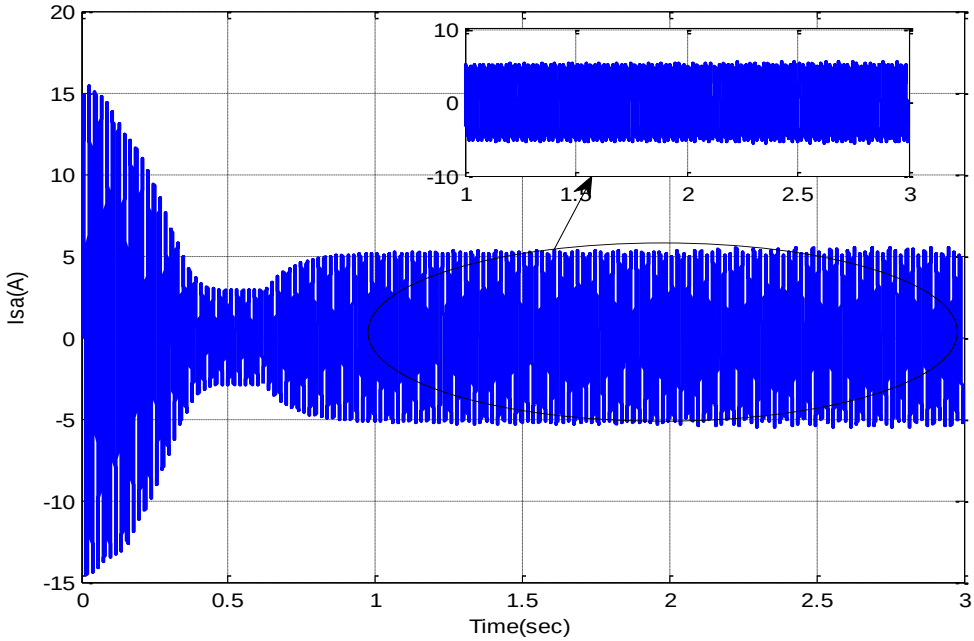

Figure 4.9: Stator current of phase "a"

Figure 4.9 also show the increase of the stator current envelope modulation, as more the bars break the more the modulation increases.

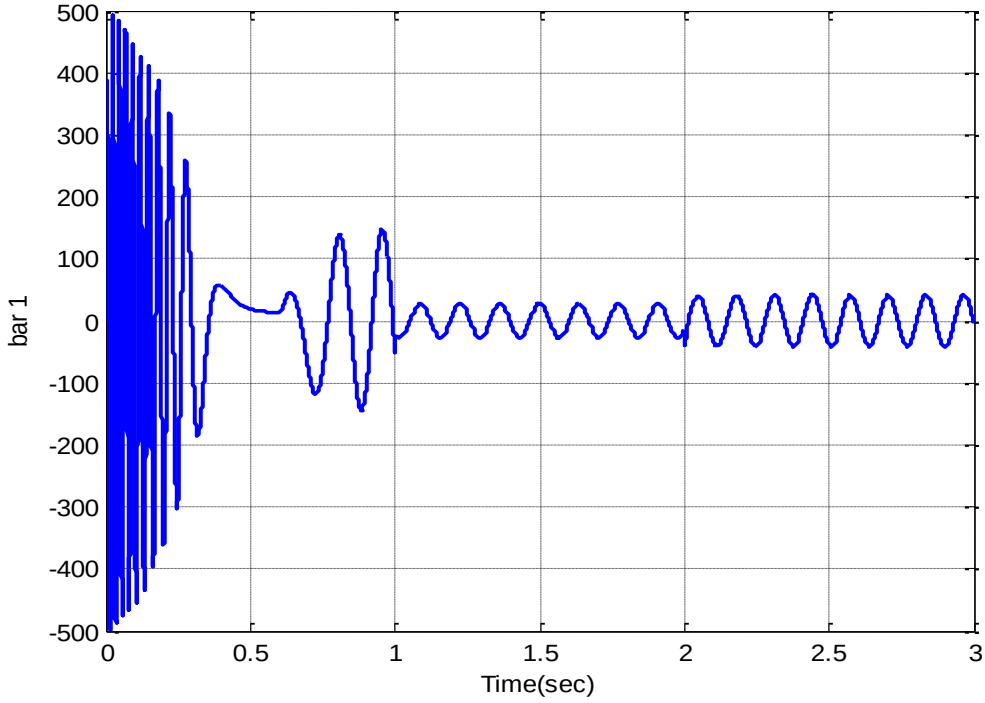

Figure 4.10: Rotor's 1st bar current

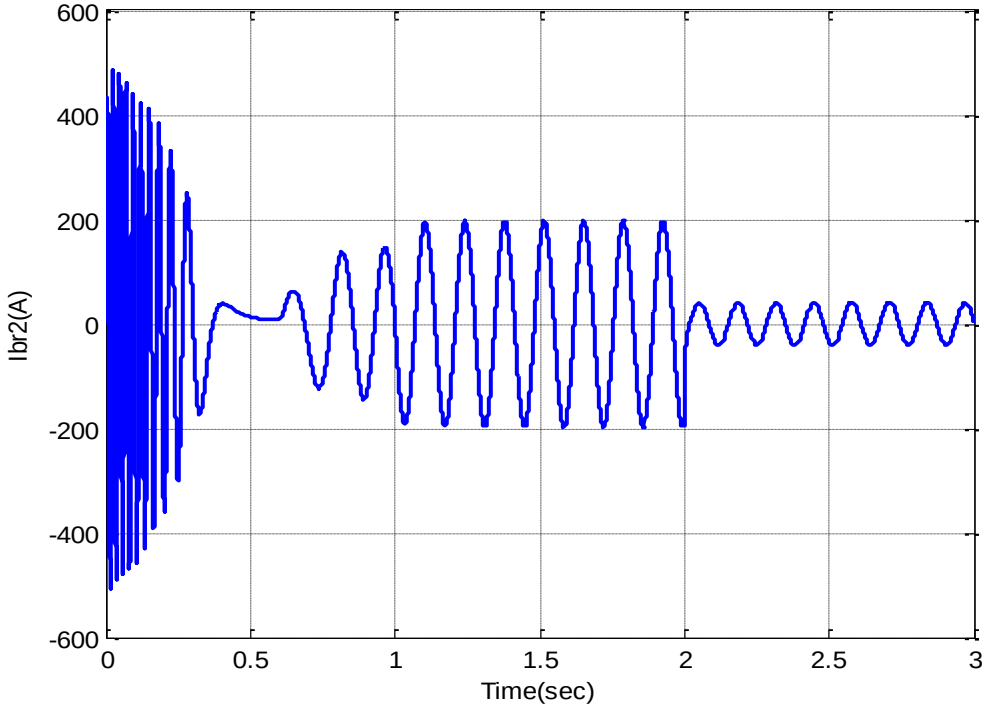

Figure 3.11: Rotor's 2nd bar current

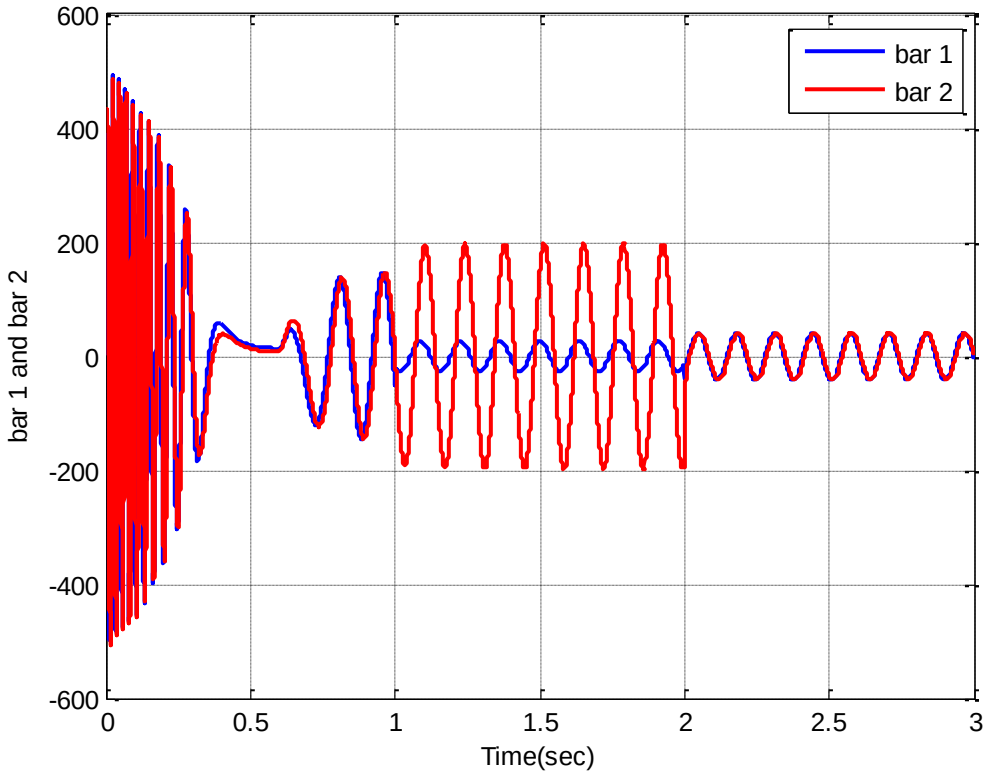

Figure 3.12: Rotor's 1st bar and 2nd bar currents

From figures 3.10, 3.11 and 3.12, it is clear that there is a decrease in the amplitude of the rotor bar currents after their breakage, as the current in the 1st bar decreases to around 27.8 A after t=1s while the 2nd bar current decreases to around 41.3 A at t=2s.

.

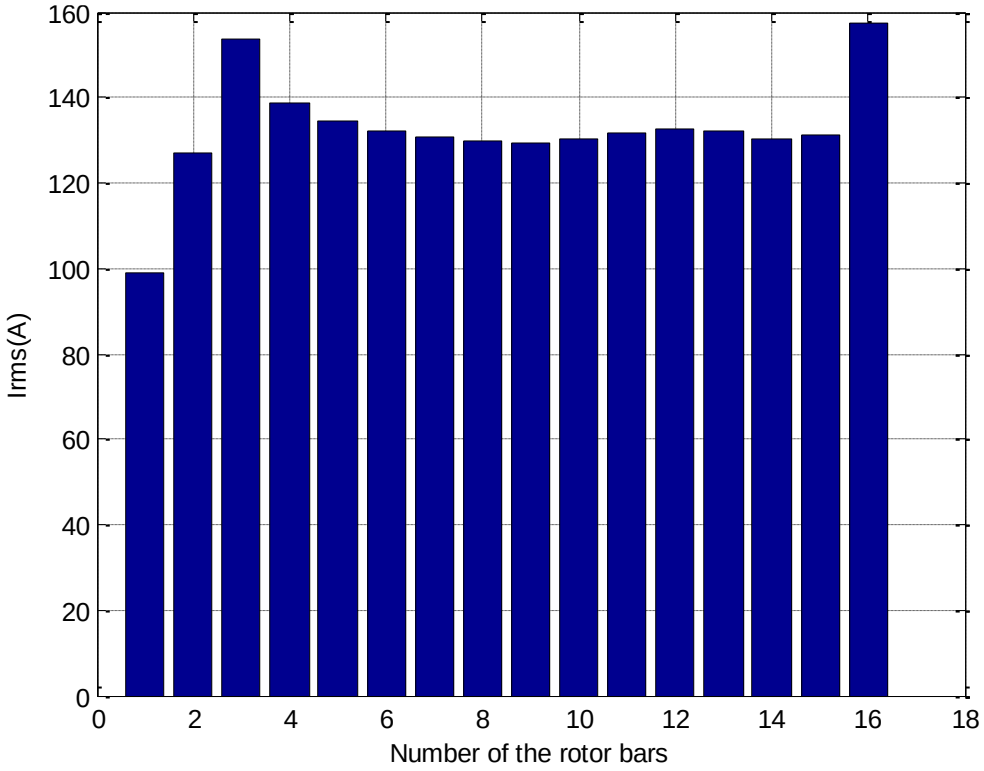

Figure 4.13: RMS of the rotor bar currents

The bar chart in figure 4.13 supports the previous results, as it shows clearly that the RMS value of the currents that correspond to the broken bars are decreased compared to the currents in other bars, and the currents of the adjacent broken bars are increased compared to the other bars. This may be caused by the current leakage of the broken bars to their following adjacent bars.

4.3.2.2 Two separated broken bars

Within the same conditions, the simulation take place by breaking the 1st bar at t =1s and the 8th bar in the rotor at t=2s.

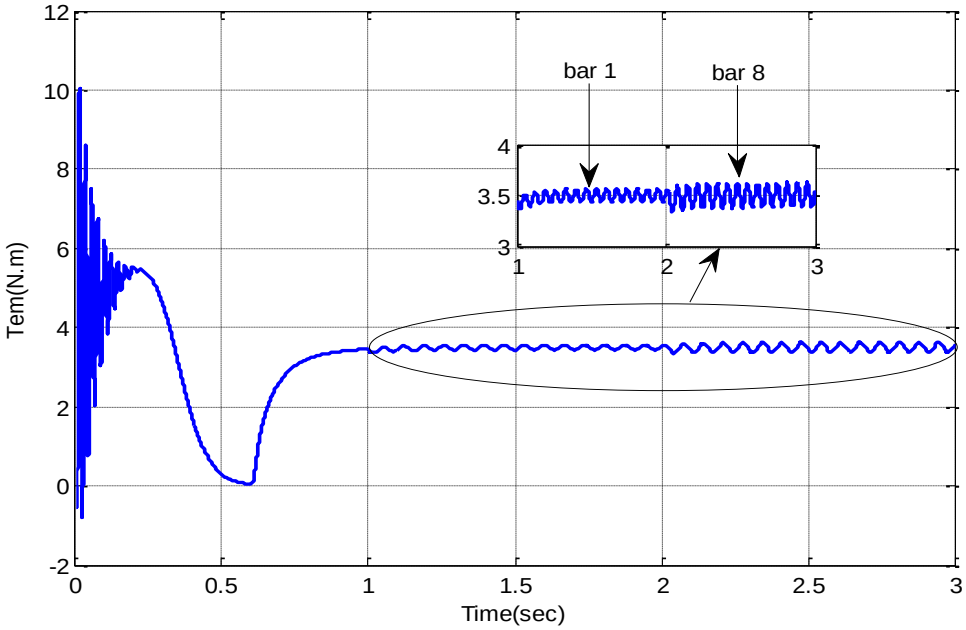

Figure 4.14: Electromagnetic Torque

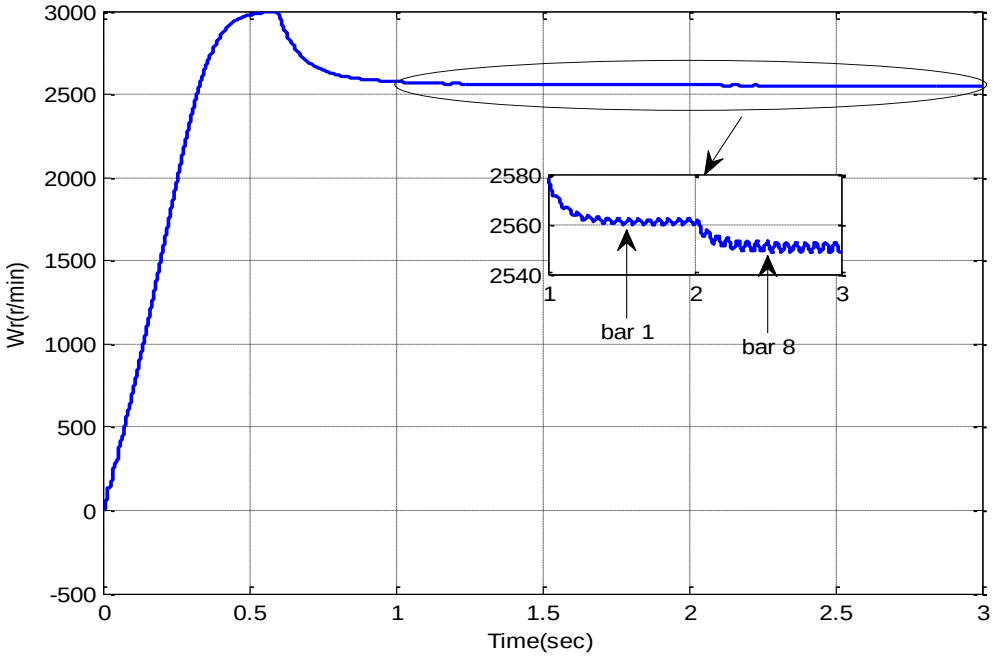

Figure 4.15: Rotor Speed

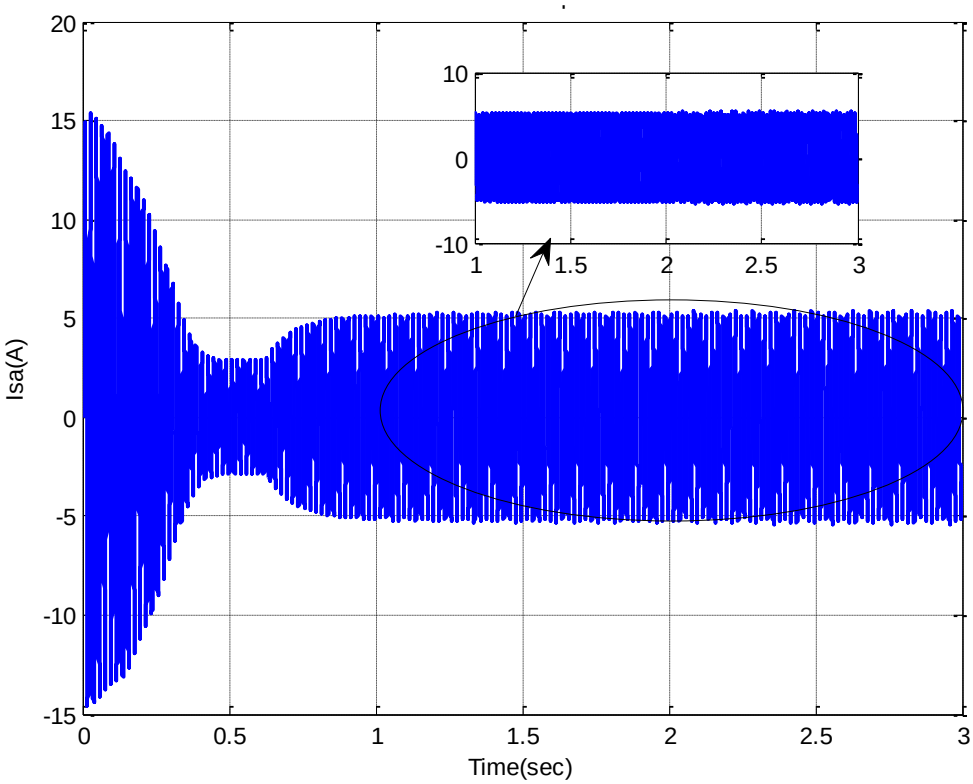

Figure 4.16: Stator current for phase "a"

The simulation results from the above Figures 4.14, 4.15, and 4.16 show that the more the number of broken bars increases the more the amplitude of the stator current modulates and the more the ripples in torque and speed appears, which leads eventually to the decrease of the average value of the rotor speed and the decrease of the torque. However, it is noticeable that the ripples in this case are less intense compared with the previous case (breakage of two adjacent bars) as it is known electrically symmetrical non-adjacent bars can hardly be detected by commercial electrical test methods.

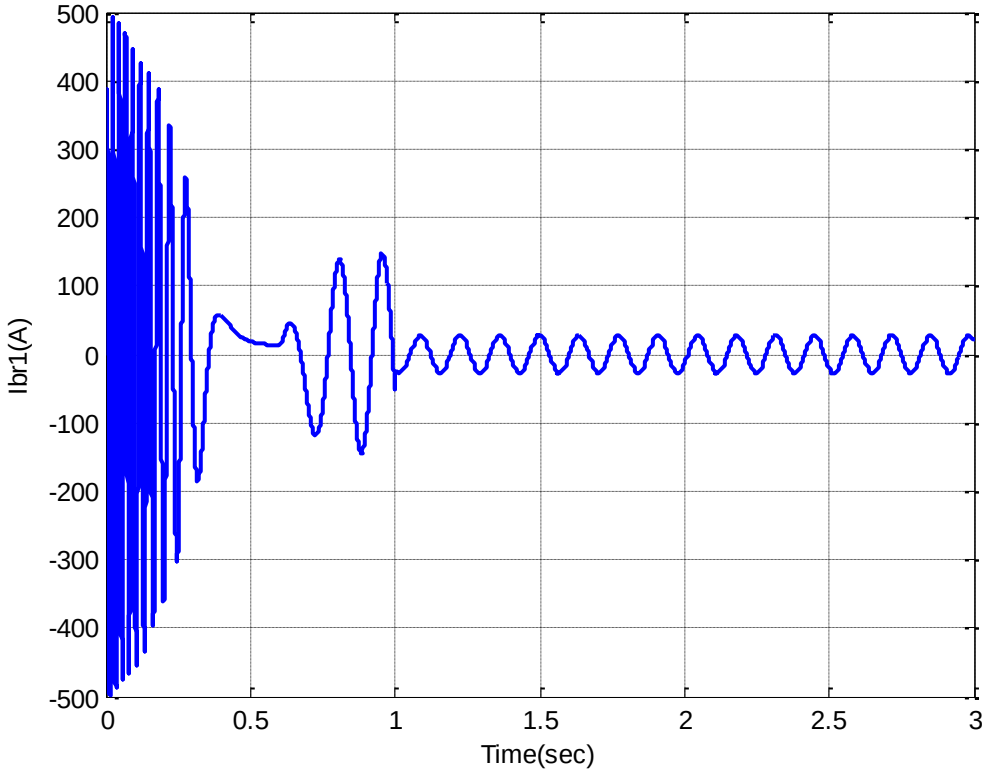

Figure 4.17: Rotor's 1st bar current

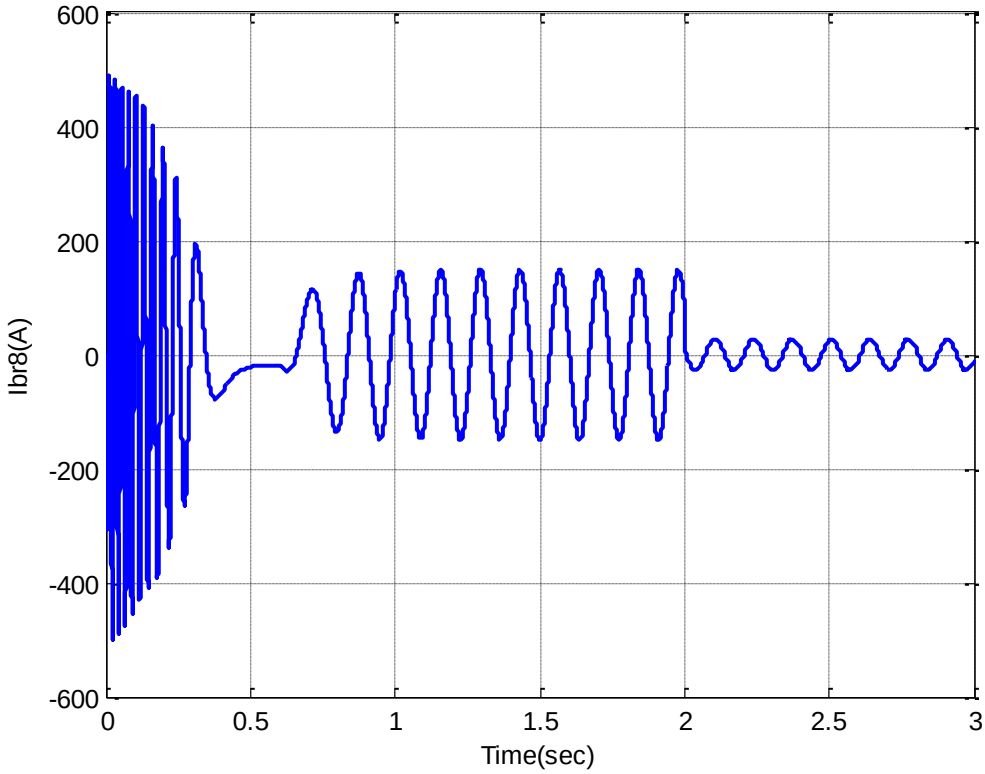

Figure 4.18: Rotor's 8th bar current

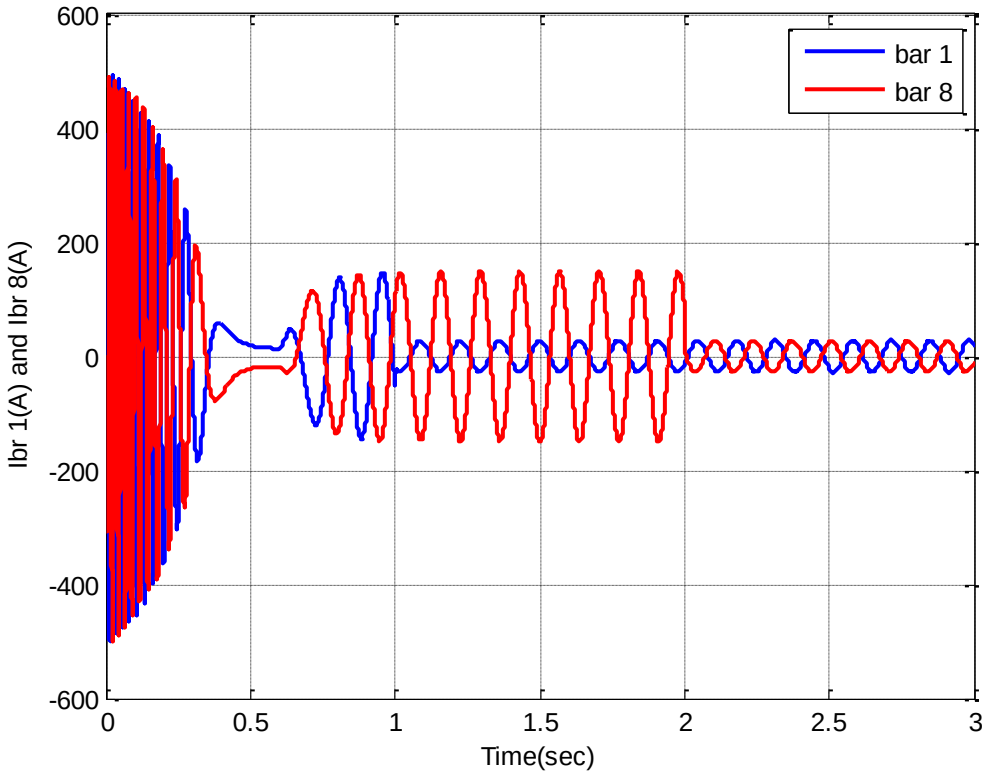

Figure 4.19: Rotor's 1st and 8th bars currents

From the above figures (figure 3.17, figure 3.18 and figure 3.19), it is noticeable that the currents in both 1st and 8 bars are minimum (around 28.1 A and 27.8 A, respectively) compared to the other bars.

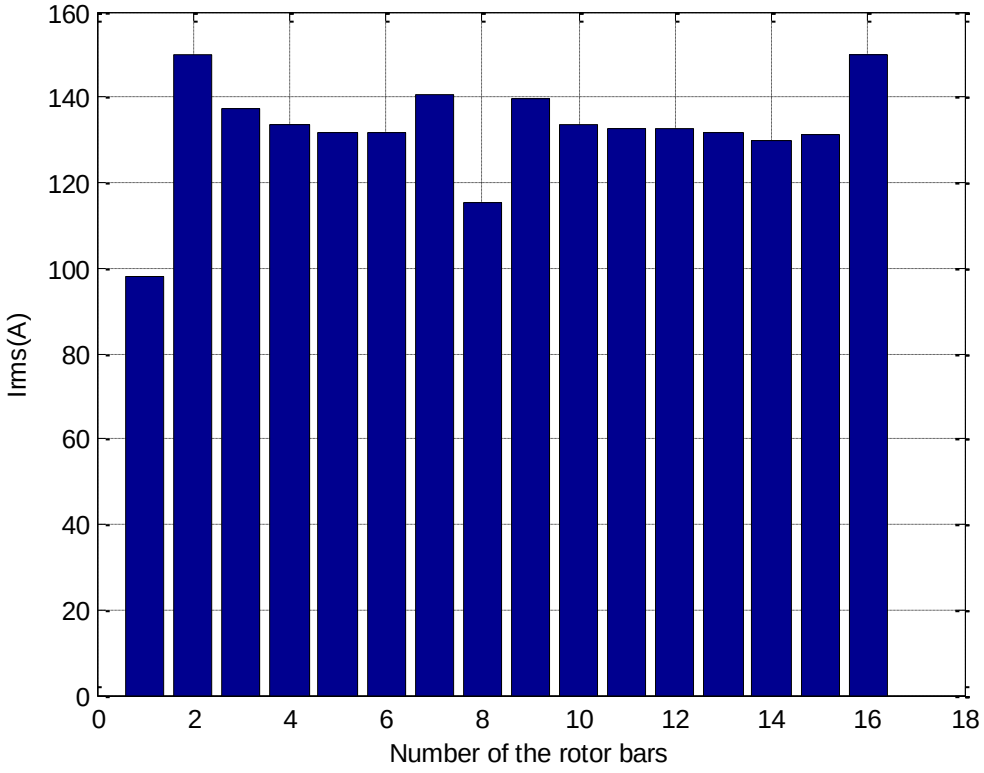

Figure 4.20: RMS of the rotor bar currents

Again, from the above chart illustrated in figure 4.20, results show that the Root Mean Squares (RMS) currents of 1st and 8th bars are less than 116 A while in the adjacent bars exceed 140A. This means the effect of two adjacent broken bars is higher than two separated broken bars on the IM.

4.3.2.3 Crack of the end ring

Under the same conditions (loading the motor at t=0.6s with TL=3.5N.m), a portion of an end ring that is between bar 1 and bar 16 cracks at t=1s, and the simulation results for this case is not very different from the previous cases.

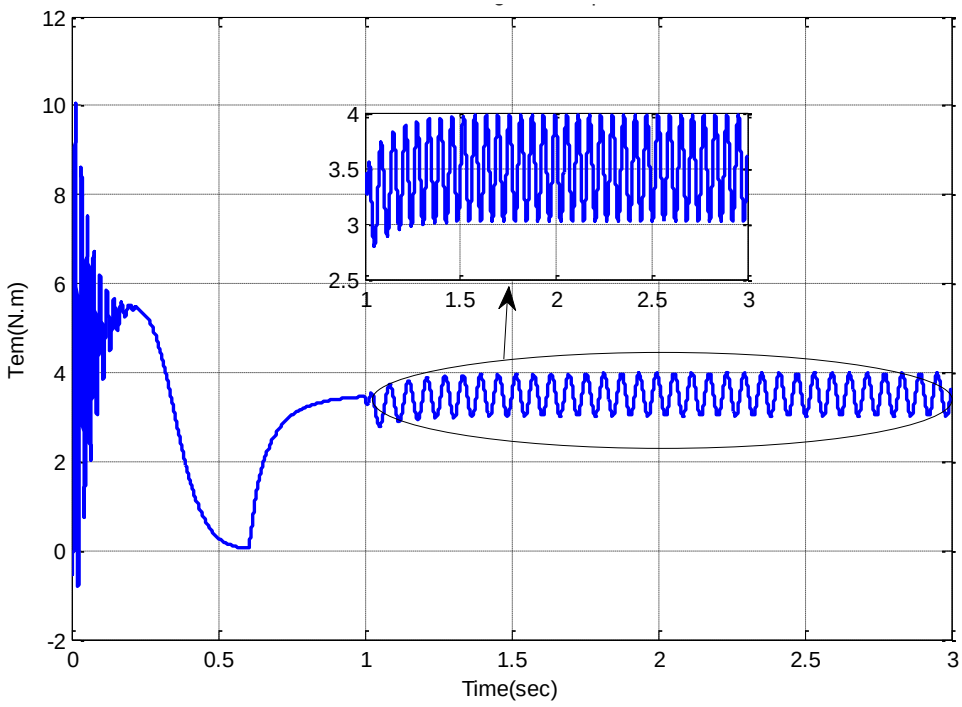

Figure 4.21: Electromagnetic Torque

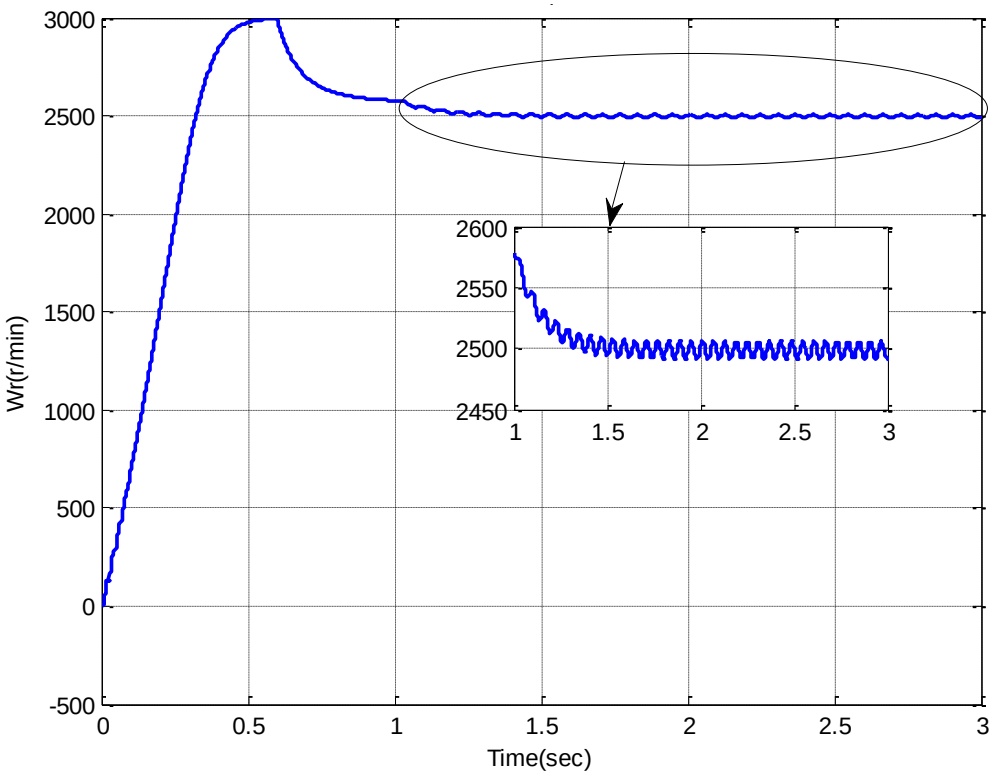

Figure 4.22: Rotor Speed

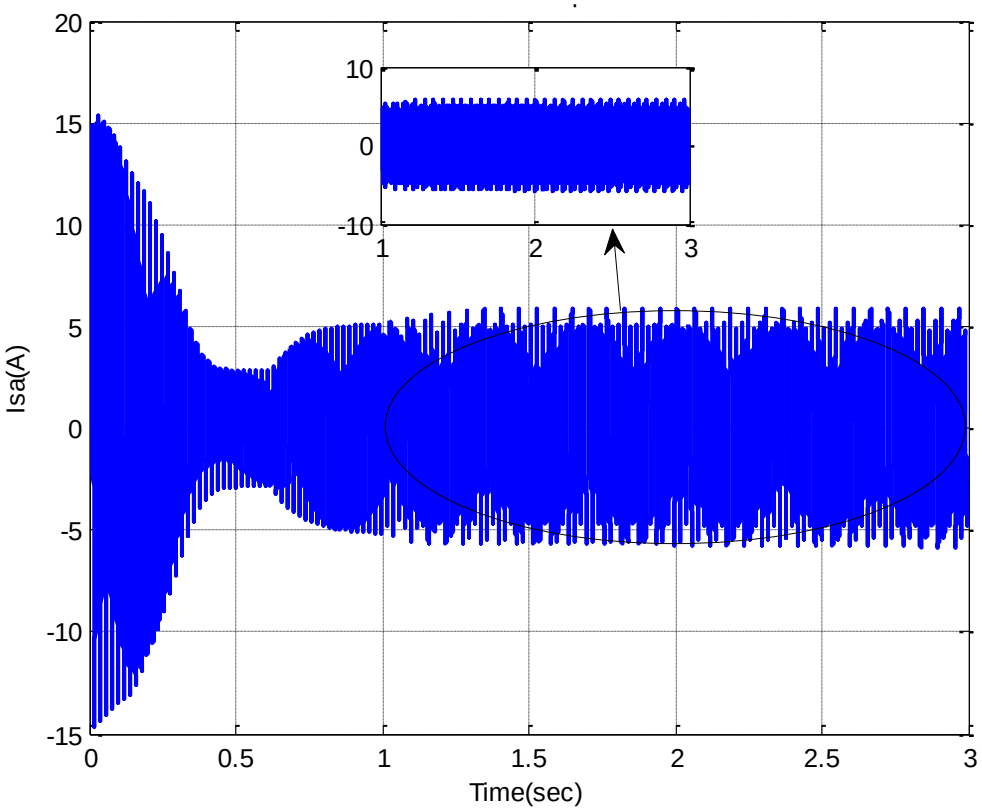

Figure 4.23: Stator current for phase" a"

The above Figures 4.21 and 4.22 show the appearance of ripples in both torque and speed, where the torque ripples are more condensed than the speed ones. From figure 4.23 it is also shown that the stator current envelope modulation increases starting from the moment of the crack. It is also noticed that the intensity of both ripples and modulation increases in case of breakage of two adjacent bar compared to the breakage of separated bars.

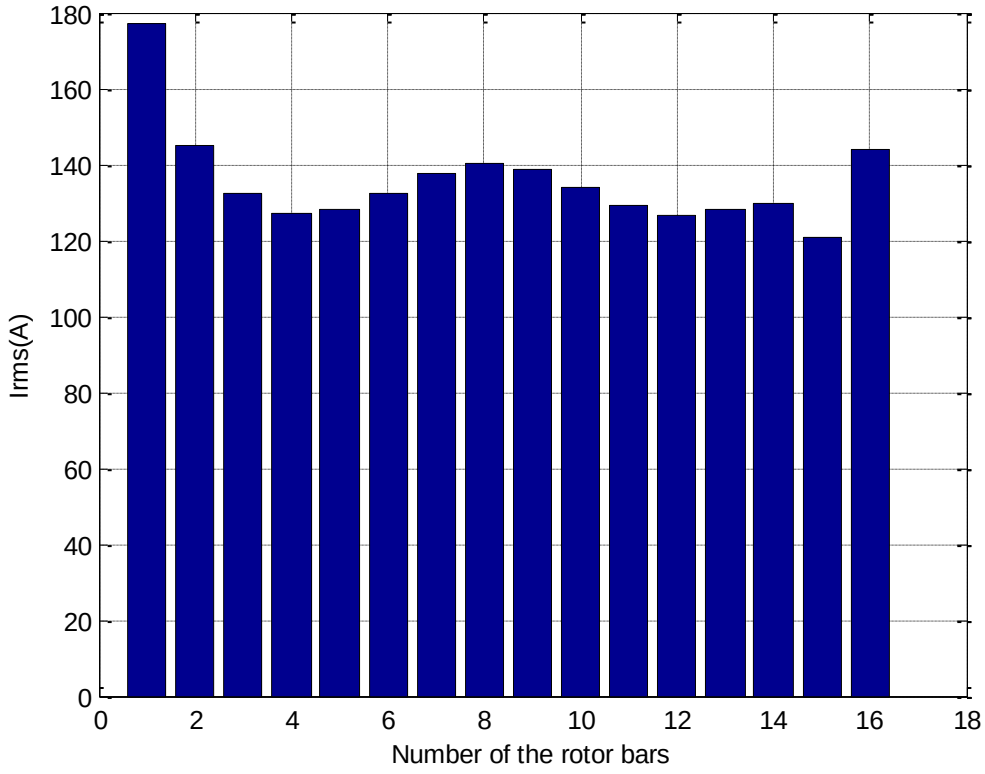

Figure 4.24: RMS of the rotor bar currents

From figure 4.24, it can be seen that currents in the 1st bar and the 16th bar are higher compared to their counterparts. It is also seen from the bar chart that current in the 2nd bar is effected as well, that's because it is close to 1st bar.

4.4 Chapter summary

This chapter presents the simulation results for the induction motor model. Throughout the results it can be concluded that the bars breakage and end ring fault manifest on the machine signals (current, torque and speed). As a consequence, the more faults are severe, the ripples in the latter signals get more inconsistent. Time domain methods are low fault sensitivity, for instance, it is difficult to detect faults in noisy environments.

CHAPTER 5

SPECTRAL ANALYSIS RESULTS AND DISCUSSION

5.1 Introduction

Signal processing techniques play an important role in electric machinery fault diagnostic. Once one of those techniques applied to one of the induction motor's signals such as vibration or current signals, it identifies the motor fault's severity. In this study, the machine signals (current, speed, electromagnetic torque) are processed using Fast Fourier Transform along with Hanning window to identify the number of broken bars based on the frequency spectrum that shows abnormal frequencies related to faults.

5.2. Fast Fourier Transform

Fast Fourier transform(FFT) is a frequency domain operation that decomposes a time-domain signal into a frequency component. Fourier transform can be implemented at high speed using Fast Fourier Transform(FFT) which makes it suitable for digital signal processing systems.

5.3 Simulation results for spectral analysis based on Fast Fourier Transform

In this section, a summary of the simulation results for the spectral analysis applied for the stator current, electromagnetic torque and rotor speed are presented. The spectral analysis is performed using the Fast Fourier Transform algorithm which reveals frequency continent in the signals. Along with FFT, windowing is needed in order to have

good frequency resolution and reduce spectral leakage, in this thesis, Hanning window is chosen to be applied to the steady-state stator current.

5.3.1 Spectral analysis results of the healthy induction motor

From figure 5.1 the spectral analysis of the stator current for a healthy motor reveals smooth graph with the fundamental frequency and very low amplitude sideband frequencies which are maybe due to asymmetries in motor construction caused by ellipticity and shaft misalignment.

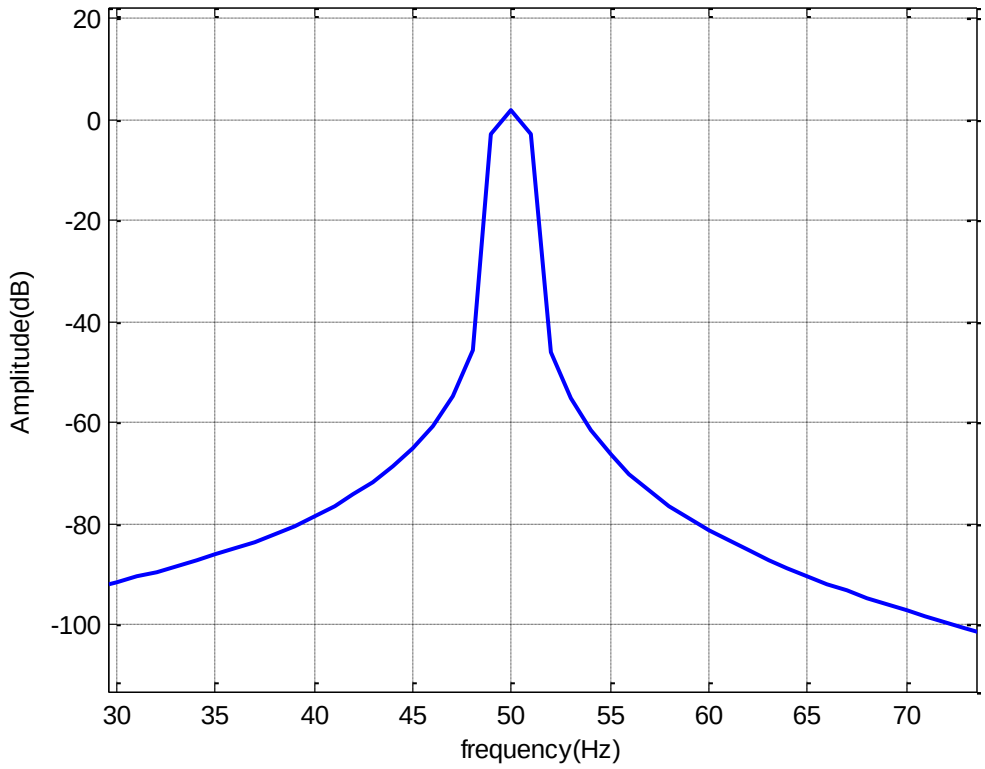

Figure 5.1: Stator Current Spectrum (healthy case)

Figures 5.2 and 5.3 illustrate spectral analysis results for both rotor speed and electromagnetic torque respectively, the graphs in the figures appear smooth with no abnormal frequencies of any kind.

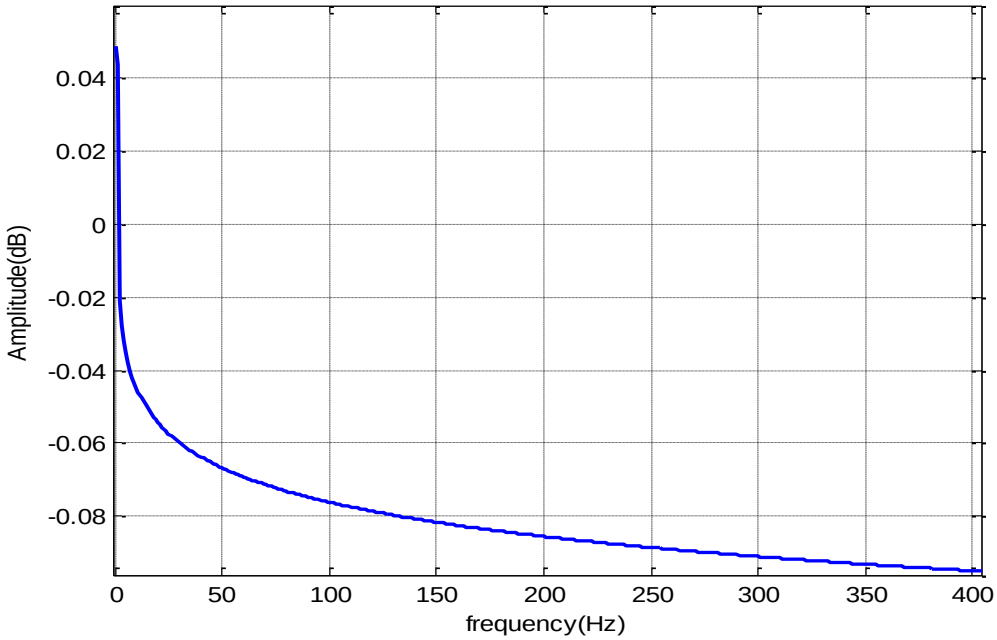

Figure 5.2: Rotor Speed Spectrum (healthy case)

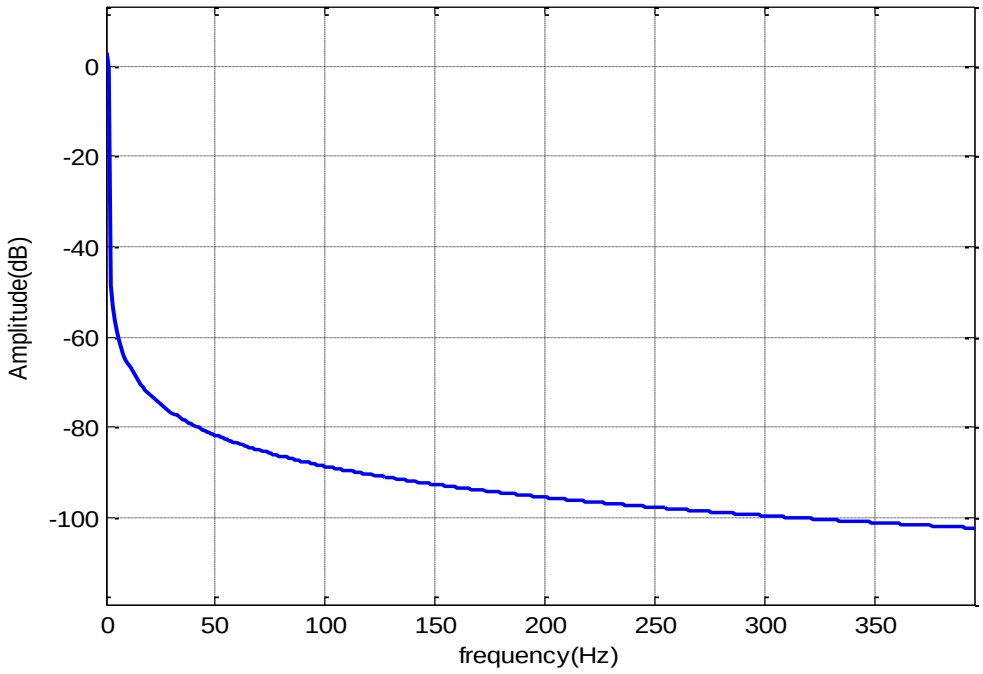

Figure 5.3: Electromagnetic Torque Spectrum (healthy case)

5.3.2 Spectral analysis results of the induction motor with one broken bar

Figures 5.4, 5.5, illustrate the results of spectral analysis applied to the motor with one broken bar. The results clearly show sideband frequencies around stator current those

frequencies have the following values (20,35,65,80) [Hz] with the following amplitudes respectively (-65.5, -26.5,-93,-46.93)[dB] in case of the faulted resistance that equals eleven times the rotor bar resistance and in case of the faulted resistance that equals thirty times the rotor bar resistance, the amplitudes are slightly increased. The sideband frequencies are of type $f_b = (1 \pm 2ks) f_s$ in which lower frequencies $f_b = (1 - 2ks) f_s$ are due to rotor faults and upper frequencies $f_b = (1 + 2ks) f_s$ are due to speed oscillations.

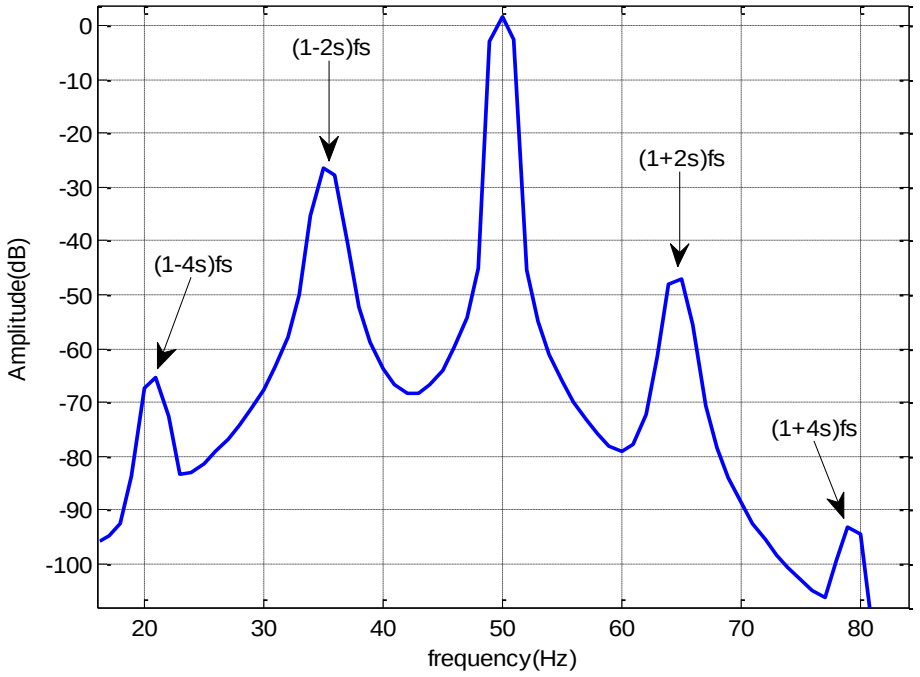

Figure 5.4: Spectral analysis of the stator current (RF=10 x Rb)

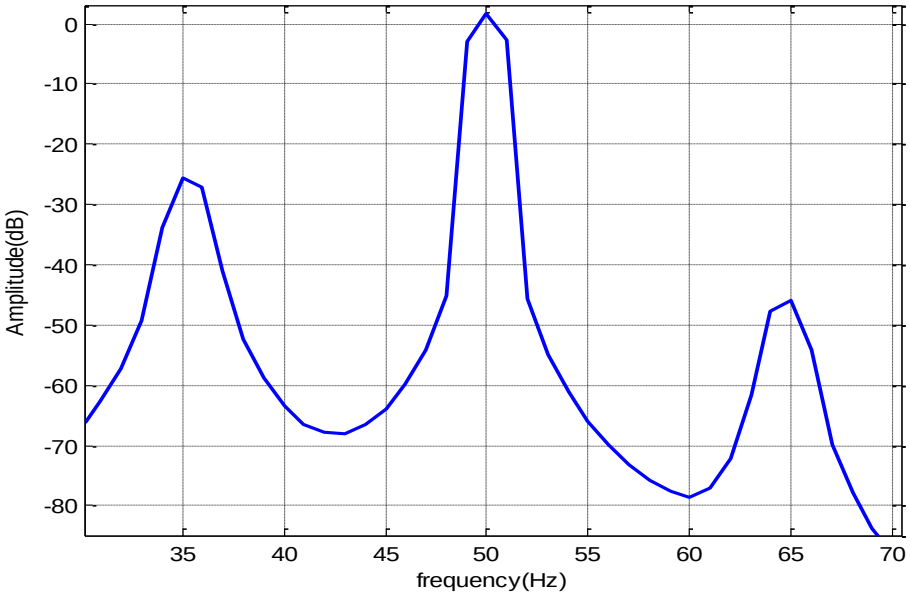

Figure 5.5: Spectral analysis of the stator current (RF=30 x Rb)

Figures 5.6 and 5.7 show extra frequencies in the electromagnetic torque Spectral. Those frequencies which are under 50 Hz with the approximated amplitudes (-20 dB and-50 dB) respectively are due to broken bar fault. And more the breakage is severed the more the amplitudes of the latter frequencies increase.

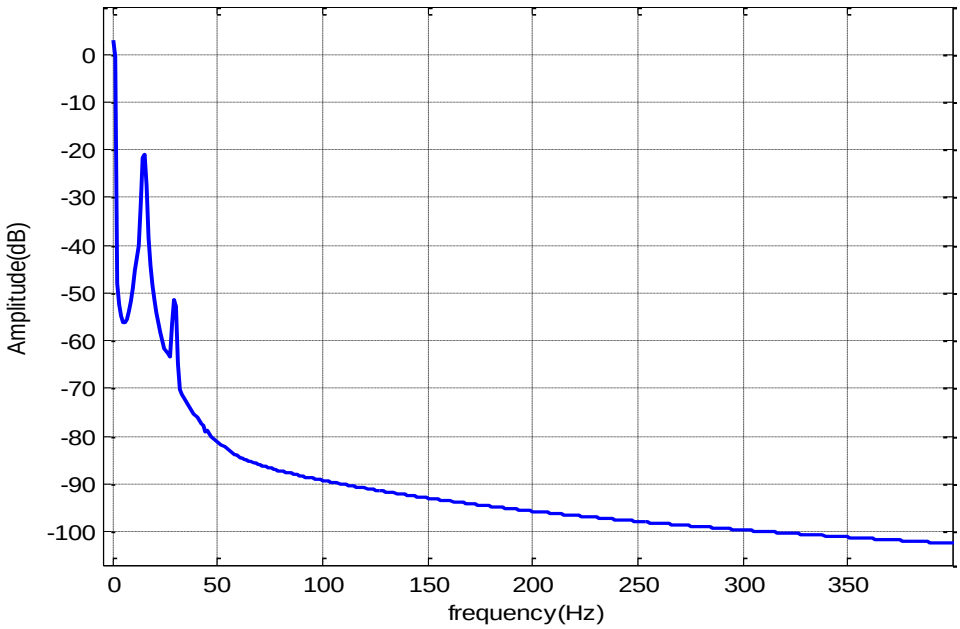

Figure 5.6: Spectral analysis of the electromagnetic torque (RF=11 x Rb)

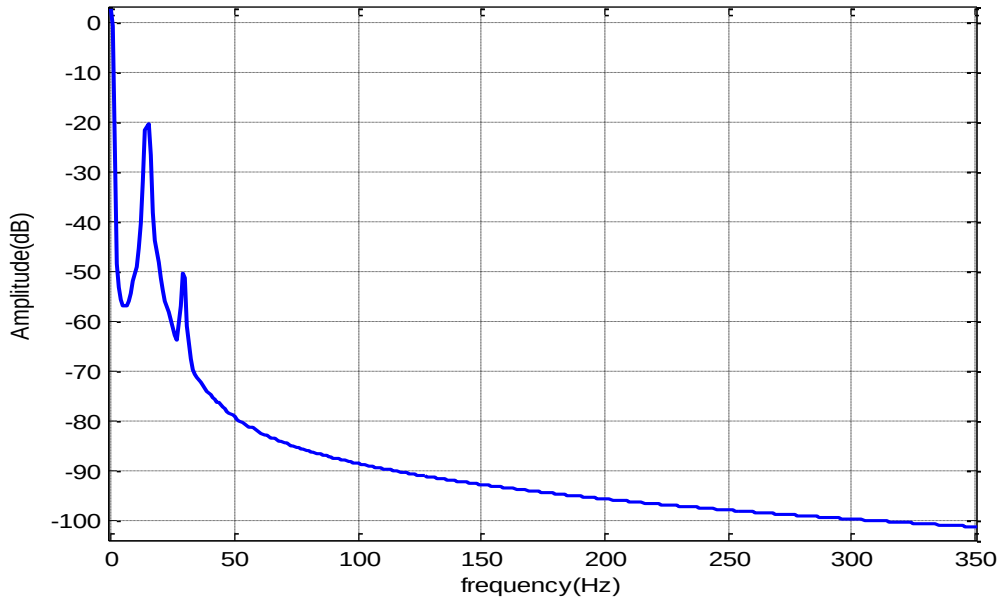

Figure 5.7: Spectral analysis of the electromagnetic torque (RF=30 x Rb)

Figure 5.8 and 5.9 show two of abnormal frequencies in the rotor speed spectral. the amplitude of those frequencies reaches approximately -0.02 dB and -0.045 dB respectively and they increase when the resistance of the bar increased which represents, in reality, the severity of the crack.

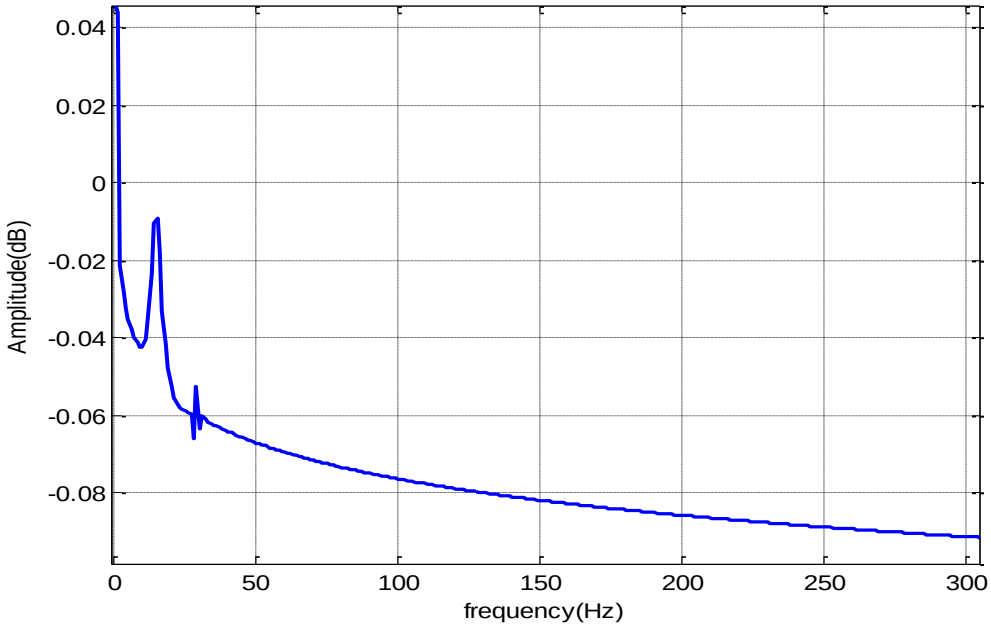

Figure 5.8: Spectral analysis of the rotor speed (RF=11 x Rb)

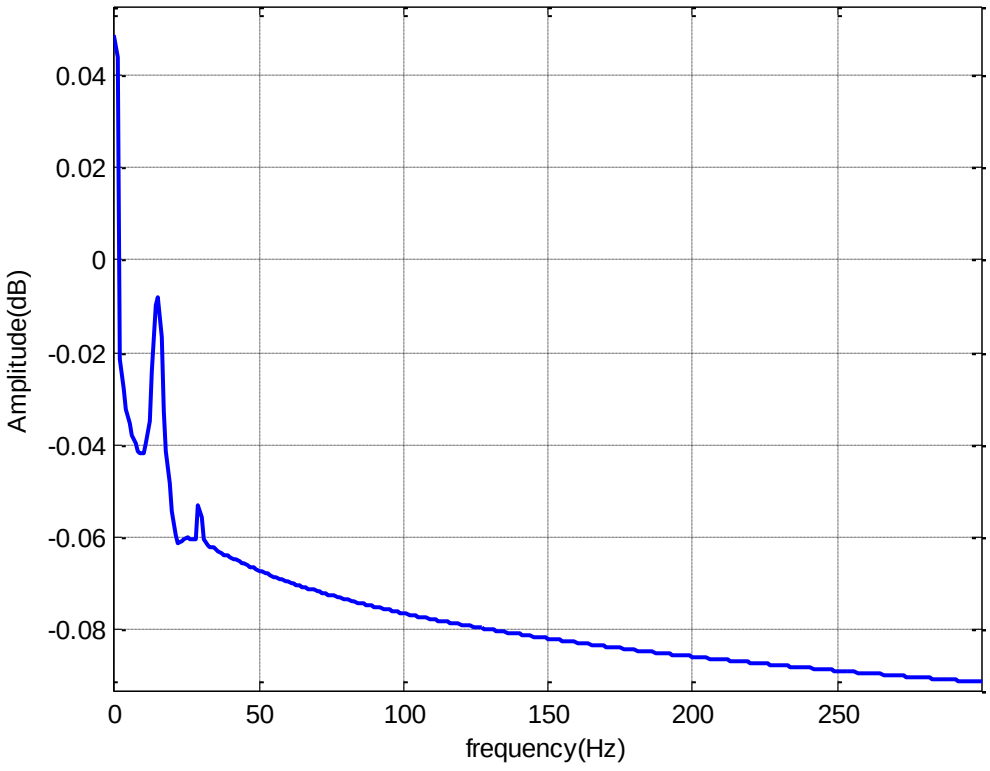

Figure 5.9: Spectral analysis of the rotor speed (RF=30 x Rb)

5.3.3 Spectral analysis results of the IM with two adjacent broken bars

Figures 4.10 and 4.11 illustrate almost the same results as previous except that in this case, two adjacent bars are broken which leads to the increase of the amplitudes of sideband frequencies that take the following values (-52.52, -19, -80.65,-40.2)[dB] respectively. Therefore, the more the number of broken bars increases the more the amplitudes of sideband frequencies are increased. It is also noticed that when (RF=30 x Rb), the amplitudes of the later frequencies are increased. As when the bars are highly cracked (RF=30 x Rd) the effect is major compared to when they are slightly cracked (RF=11 x Rd).

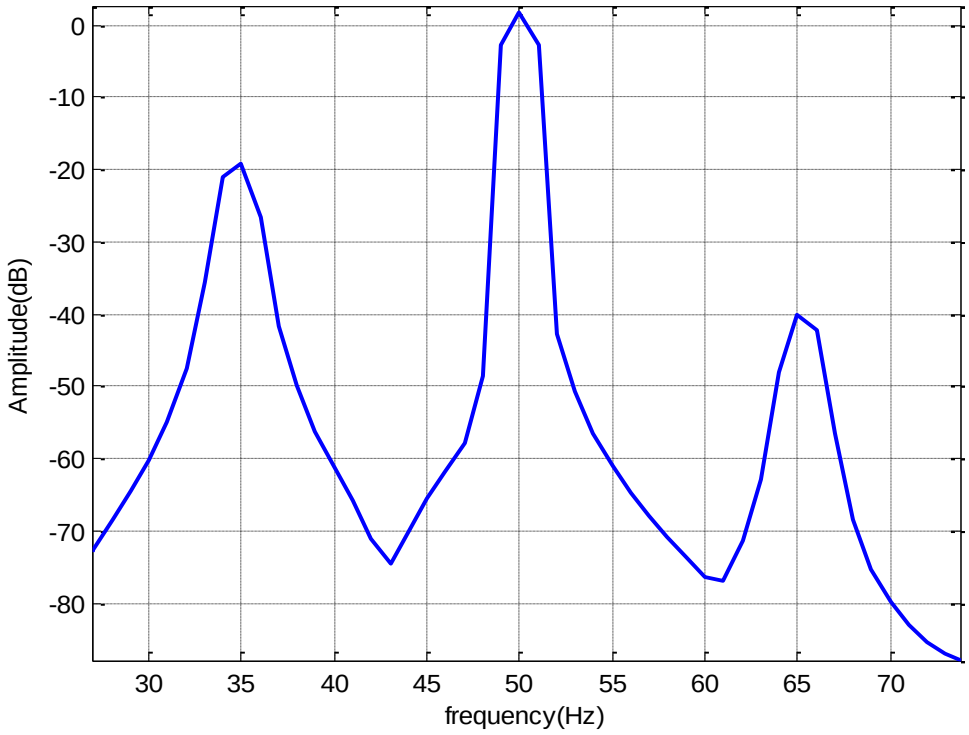

Figure 5.10: Spectral analysis of the stator current (RF=11 x Rb)

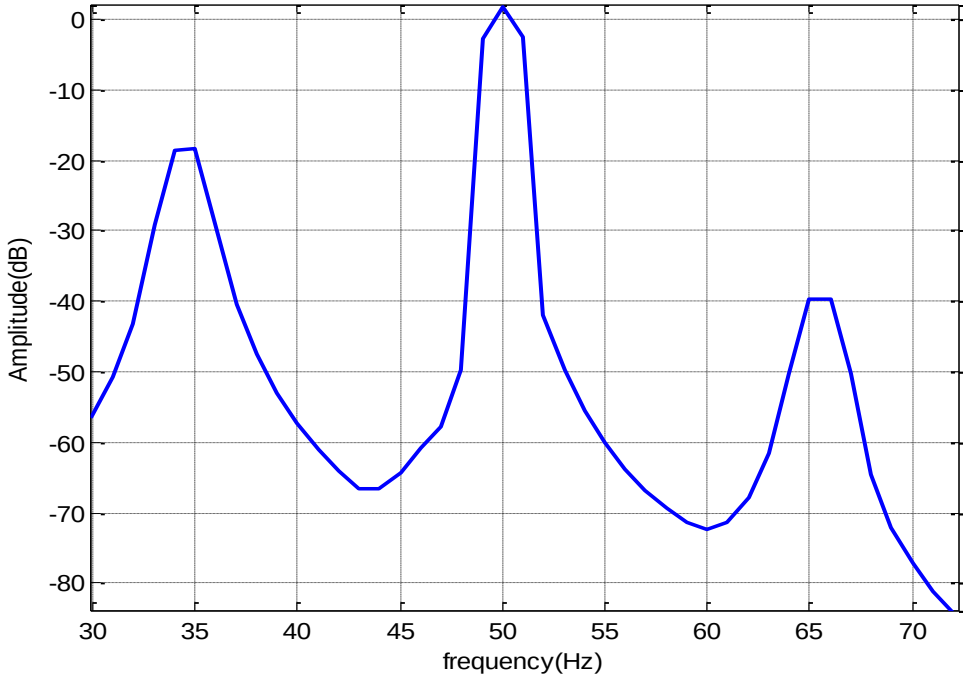

Figure 5.11: Spectral analysis of the stator current (RF=30 x Rb)

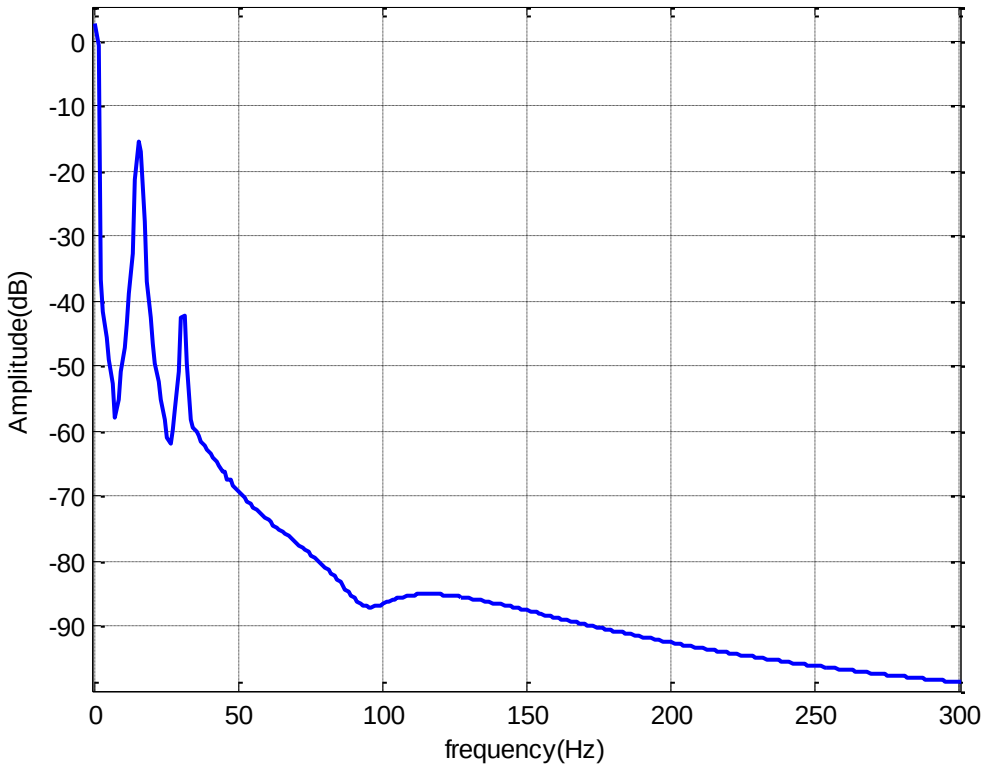

Figure 5.12: Spectral analysis of the electromagnetic torque (RF=11 x Rb)

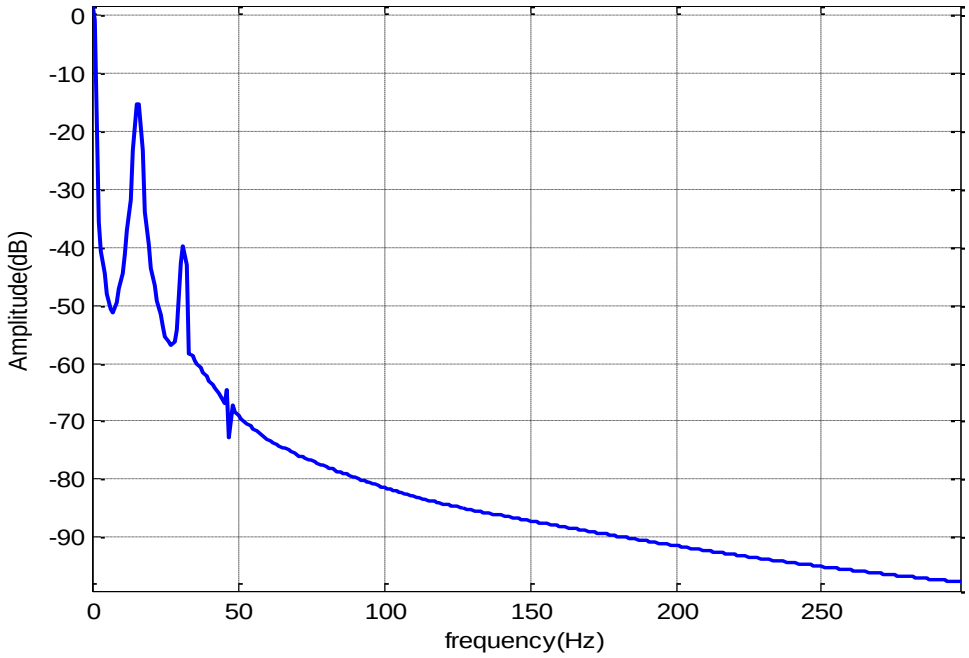

Figure 5.13: Spectral analysis of the electromagnetic torque (RF=30 x Rb)

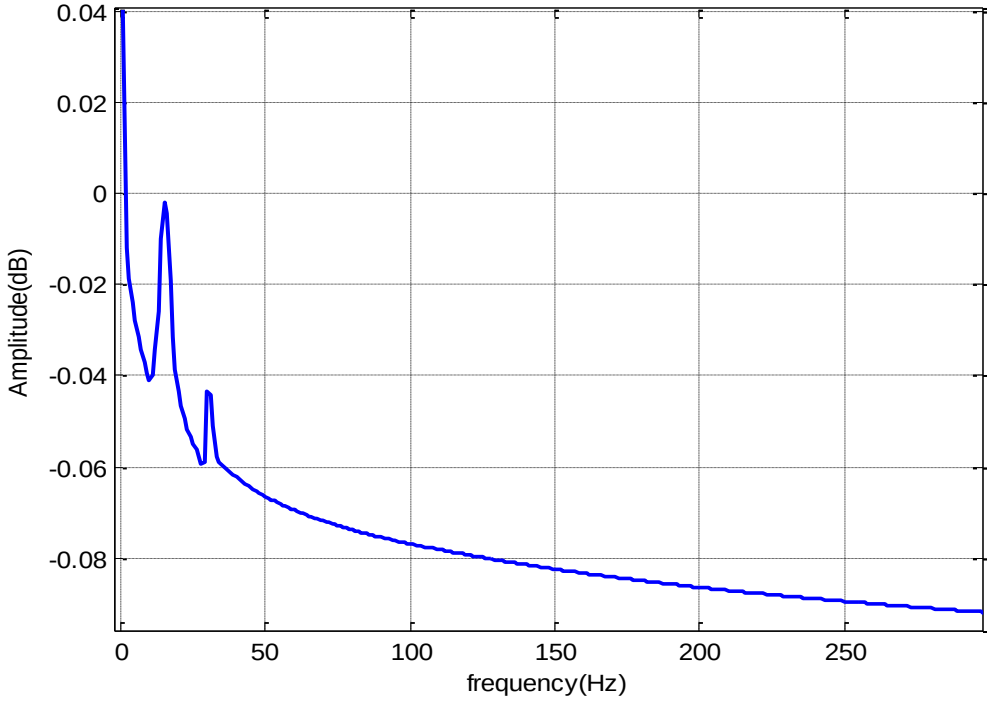

Figure 5.14: Spectral analysis of the rotor speed (RF=11 x Rb)

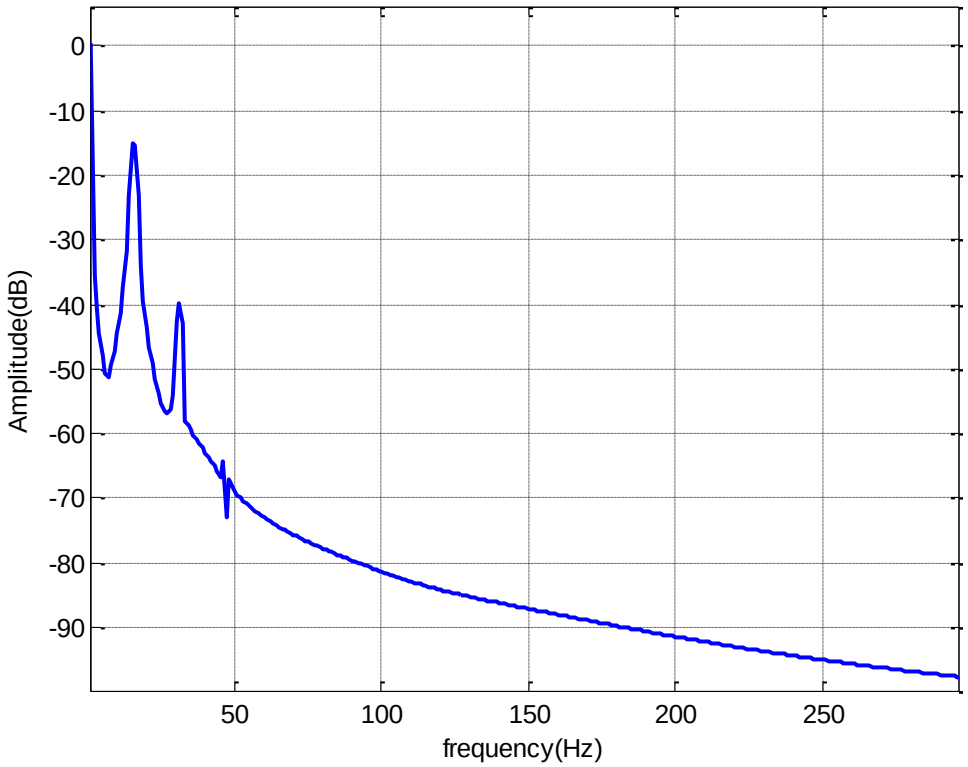

Figure 5.15: Spectral analysis of the rotor speed (RF=30 x Rb)

From the above figures, it is shown that the frequency content in both torque and speed, when two adjacent bars break didn't change compared to the case where only one bar is broken. However, the amplitudes of frequencies are increased when the number of bar breakage increases. It is also noticed that just like in the previous case the more the crack is severe the more the amplitudes of frequencies take higher values.

5.3.4 Spectral analysis results of the induction motor with two separated broken bars

Figures 5.16 and 5.17 show results for separated broken bars, from this figure it is observed that the amplitude of sideband frequencies are of the following values (-57.4, -21.7, -84.97, -42.52). Compared with one broken bar case the amplitudes are increased. However, comparing with the two adjacent broken bar case the amplitudes are decreased. Therefore, broken adjacent bar faults is more severe that two separated bar fault. Moreover, as seen in case of one broken bar and two adjacent broken bars the amplitudes of the side band frequencies increase as the crack intensifies.

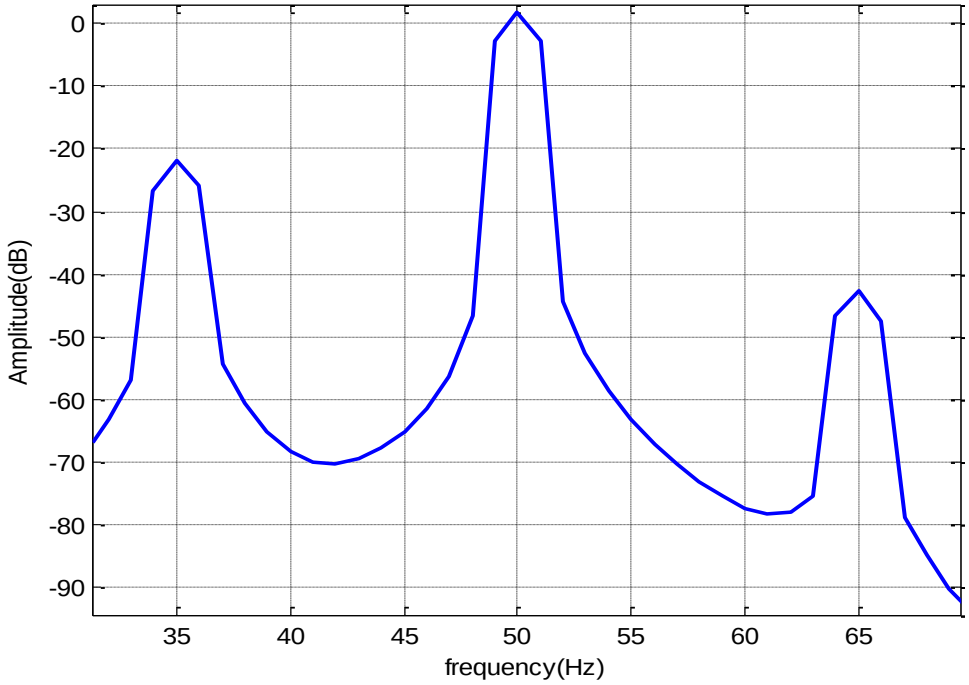

Figure 5.16: Spectral analysis of the stator current (RF=11 x Rb)

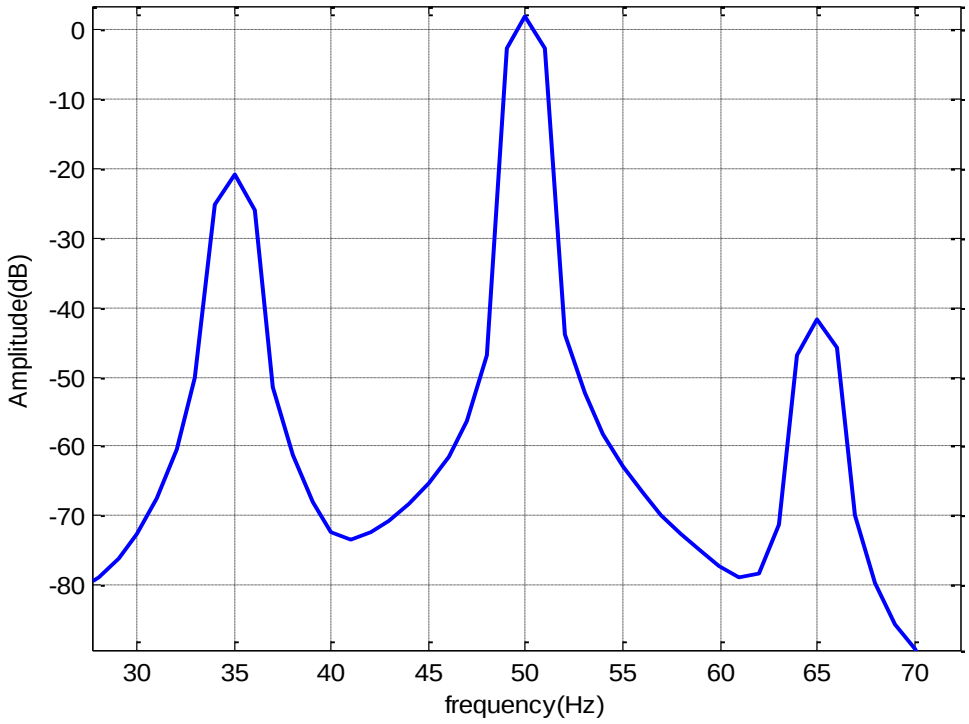

Figure 5.17: Spectral analysis of the stator current (RF=30 x Rb)

The results of spectral analysis for both Torque and speed in the above figures are not very much different from the results seen in the previous case, as they clearly show that the more the number of broken bars increases the more the amplitude of frequencies increases. However, the effect of breakage of two adjacent bars are more severe than separated bars, moreover, the more the resistance of the bar increases the more the amplitude of frequencies reaches higher values. As in reality the more the bar cracks the more the leakage of the current gets more inconsistent.

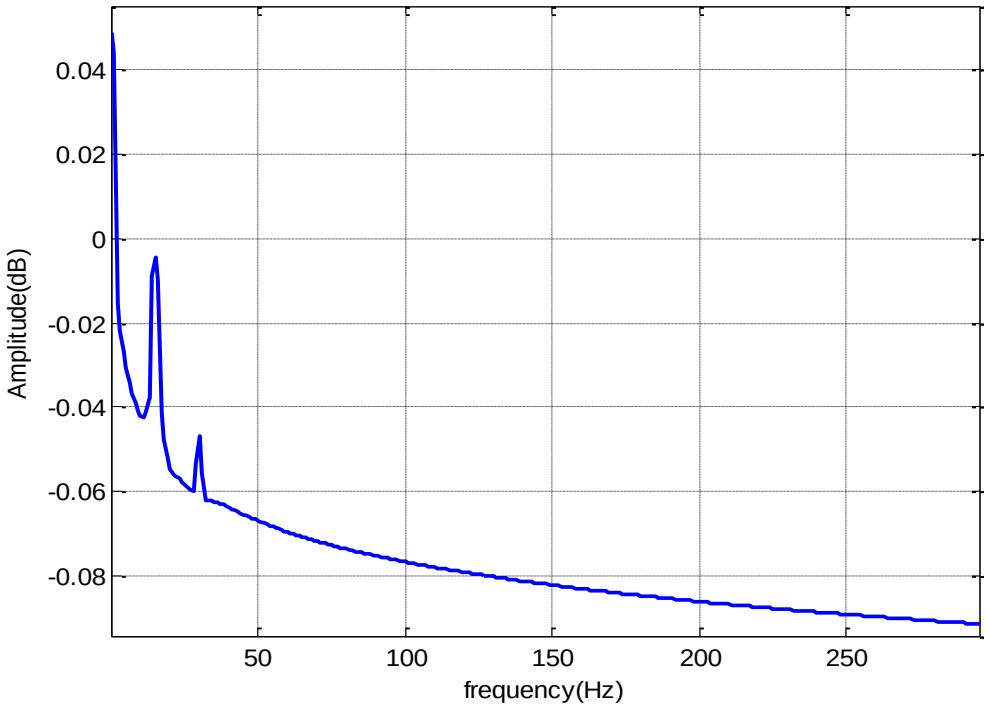

Figure 5.18: Spectral analysis of the rotor speed (RF=11 x Rb)

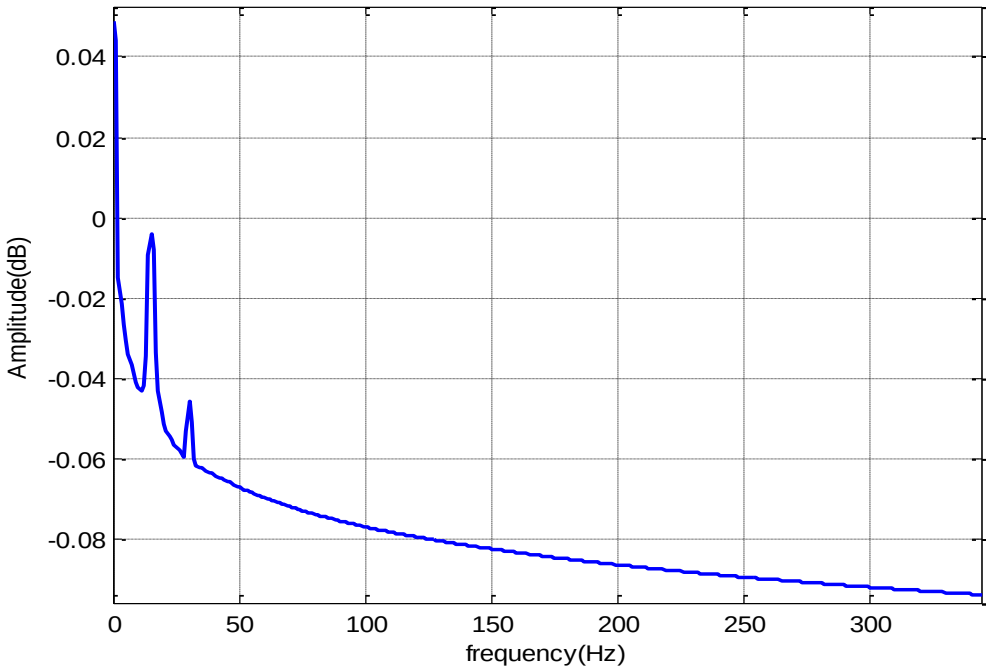

Figure 5.19: Spectral analysis of the rotor speed (RF=30 x Rb)

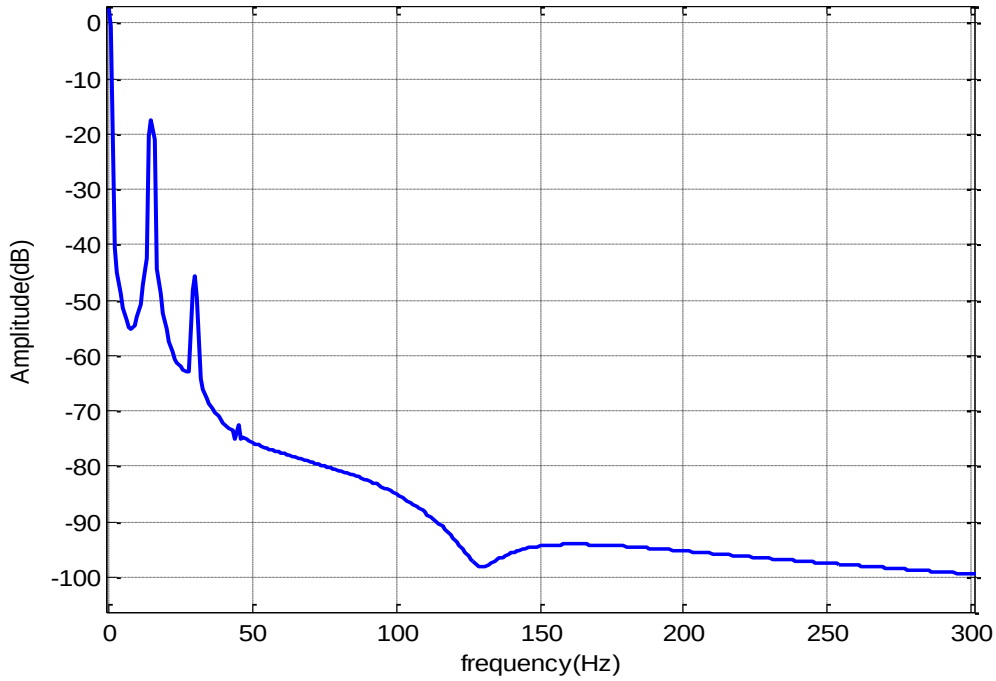

Figure 5.20: Spectral analysis of the electromagnetic torque (RF=11 x Rb)

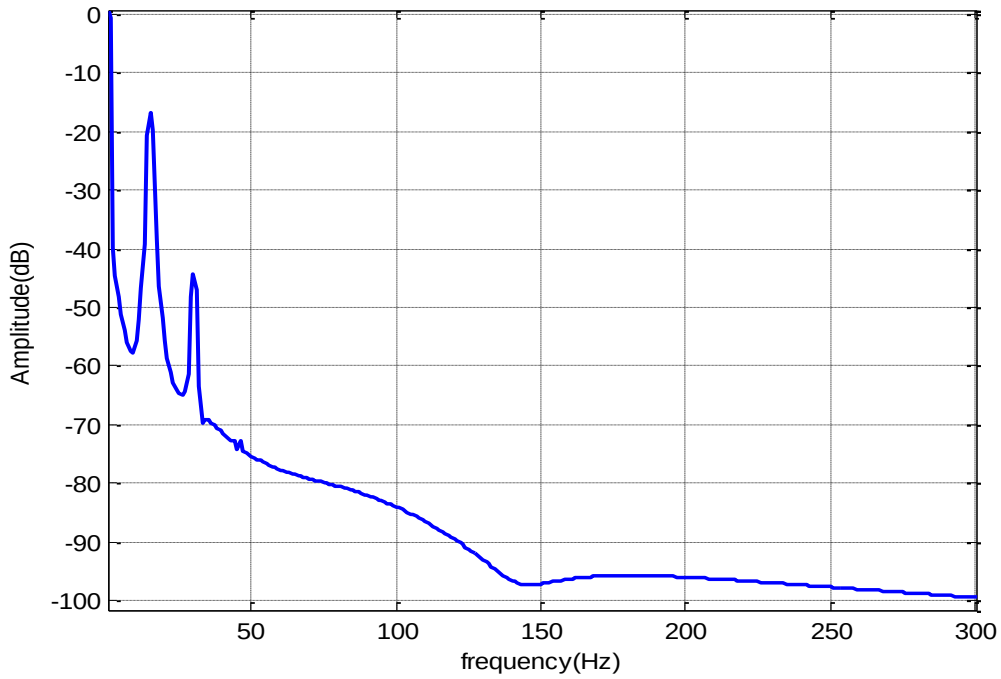

Figure 5.21: Spectral analysis of the electromagnetic torque (RF=30 x Rb)

5.3.5 Spectral analysis results of the induction motor with cracked end ring

Figure 5.22 show the spectral analysis of cracked end ring, the frequency content of the stator current is the same as in previous cases, however, the amplitudes are much higher compared to the previous cases (-42.95, -12.66, -72.5,35). This makes the cracked end rings the most severe fault compared with bar breakage.

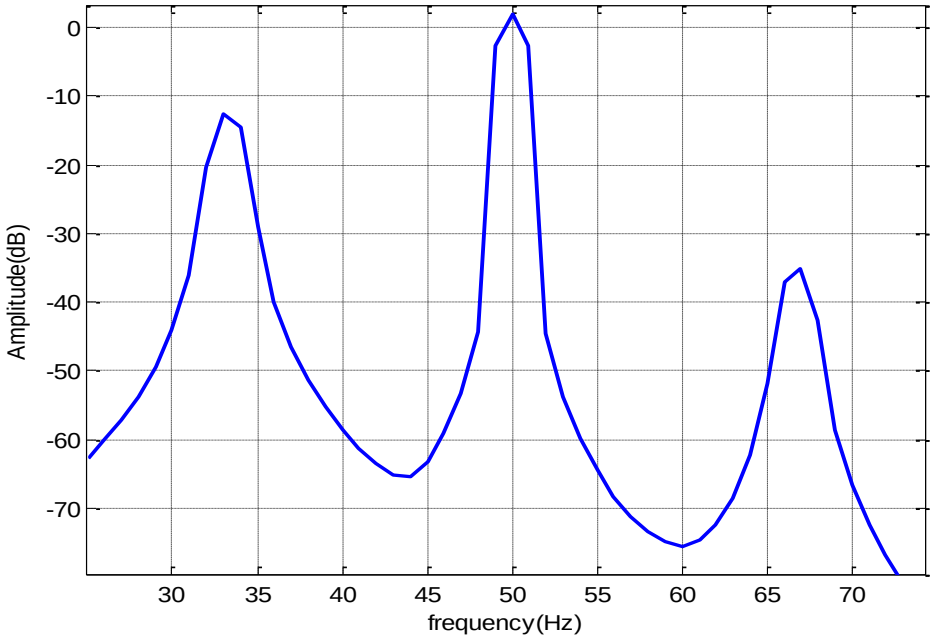

Figure 5.22.: Spectral analysis of the stator current

From the figures 5.23, 5.24 it is also noticed that both torque and speed underwent the same effect as the current. However, the expensive sensors needed to capture the speed and torque makes them less popular monitoring methods compared to current. Besides the oscillations seen in fault can be even of mechanical origin and that may lead to wrong diagnosis.

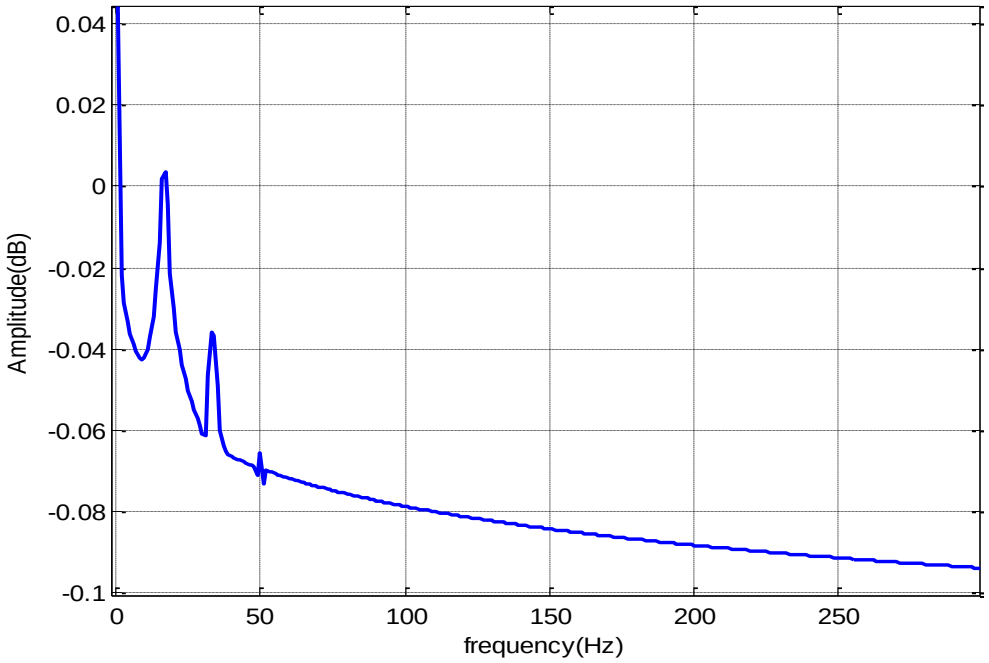

Figure 5.23: Spectral analysis of the rotor speed

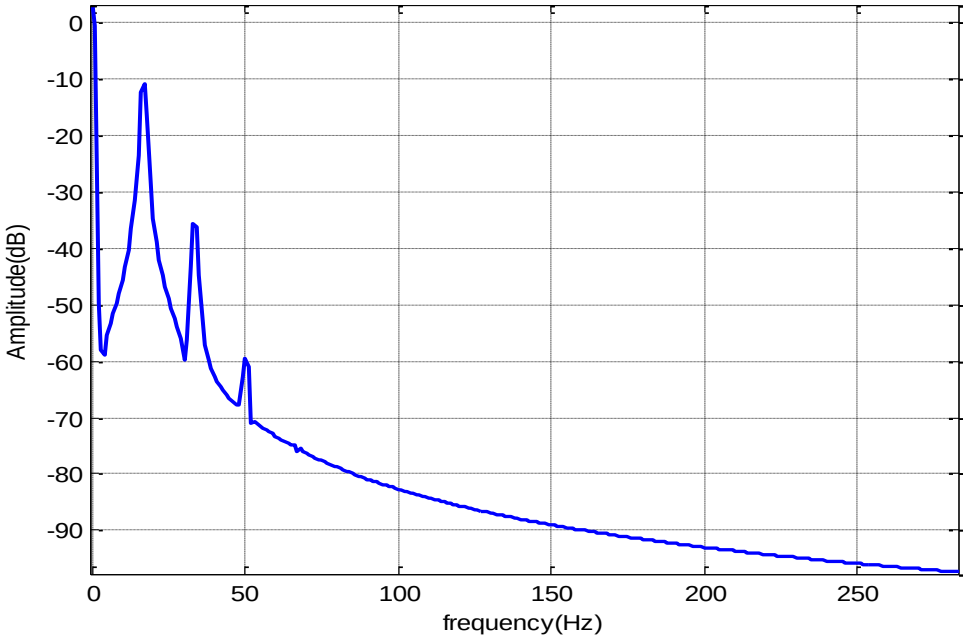

Figure 5.24: Spectral analysis of the electromagnetic torque

5.4 Processor in The Loop Based Rotor Fault Diagnosis

5.4.1 Implementation set up

The experiment conducted to test the performance of the STM32 in detecting bar breakage of an induction motor modelled in MATLAB software. This latter represents the PIL which consists of a microprocessor STM32F4 as a real chip and an induction machine as a digitalized model runs on an offline simulator. The procedure to implement PIL is as follows: First, simulate both healthy and faulty model of the IM in MATLAB, then extract the stator current and run it in the loop and print it to the USB to TTL module which is connected to the STM32. On the other hand, STM32 is programmed to receive the data of interest (Stator Current in this study) to be processed. This in turn will turn On the LEDs whenever a fault is detected based FFT analysis.

The following block diagram (Figure 5.25) illustrates the overall implementation process. The stator current data will ultimately be received form either simulation (From Matlab) or from an actual current sensor fed into the STM32.

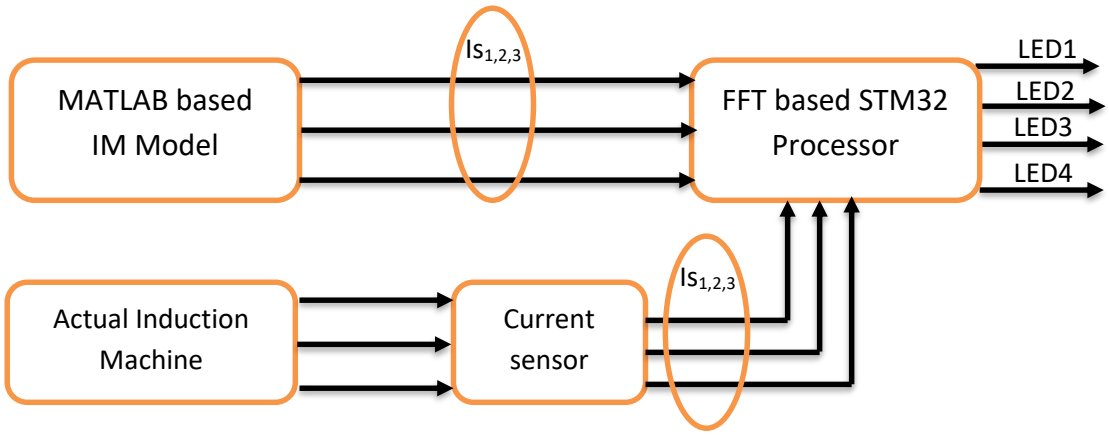

Figure 5.25: Block diagram for Hardware and Software in the loop based rotor fault diagnosis.

5.4.2 STM32F407 Discovery Board

STM32F407 Discovery Board (Figure 5.26) is a family of 32-bit microcontroller integrated circuits, based on the high-performance Arm® Cortex®-M4 32-bit RISC core. It operates at a frequency of up to 180 MHz. It is the first STM32 series to have DSP instructions and Floating point unit (FPU) single precision which makes it much faster to do floating-point calculations such as FFT analysis etc. It also incorporates high-speed embedded memories (Flash memory up to 512 Kbyte, up to 128 Kbytes of SRAM), up to 4 Kbytes of backup SRAM, and an extensive range of enhanced I/Os and peripherals. The STM32 board does not require any separate probe as it integrates the ST-LINK/2-1 debugger and programmer. Moreover, the board comes with the STM32 comprehensive software HAL library together with various packaged software examples. Also included is direct access to the Arm® Mbed™ online resource. Besides those peripherals STM32F4 series display more features such as, ART Accelerator™ enabling 0 wait state executing from internal Flash, Up to 2x USB2.0 OTG FS/HS, SDIO, USART, SPI, I²C, 16-bit and 32-bit timers, Up to 3x 12-bit ADC, Up to 2x 12-bit DAC, External memory controller, 1.7V to 3.6V low voltage.

5.4.3 USB to TTL

USB to TTL module (Figure 5.27) is essential for prototyping, it connects a microcontroller with a personal computer (PC). It is essentially used to send/receive data from PC to other devices and/or from external device to PC through USART hardware driver. This module has 5 pin breakout which includes:

- TXD = Transmit Output - Connect to Receive Pin(RXD) of Micro controller.
- RXD = Receive Input - Connect to Transmit Pin(TXD) of Micro controller.

- GND = Should be common to microcontroller ground.
- 3V3 = Optional output to power external circuit up to 50mA.

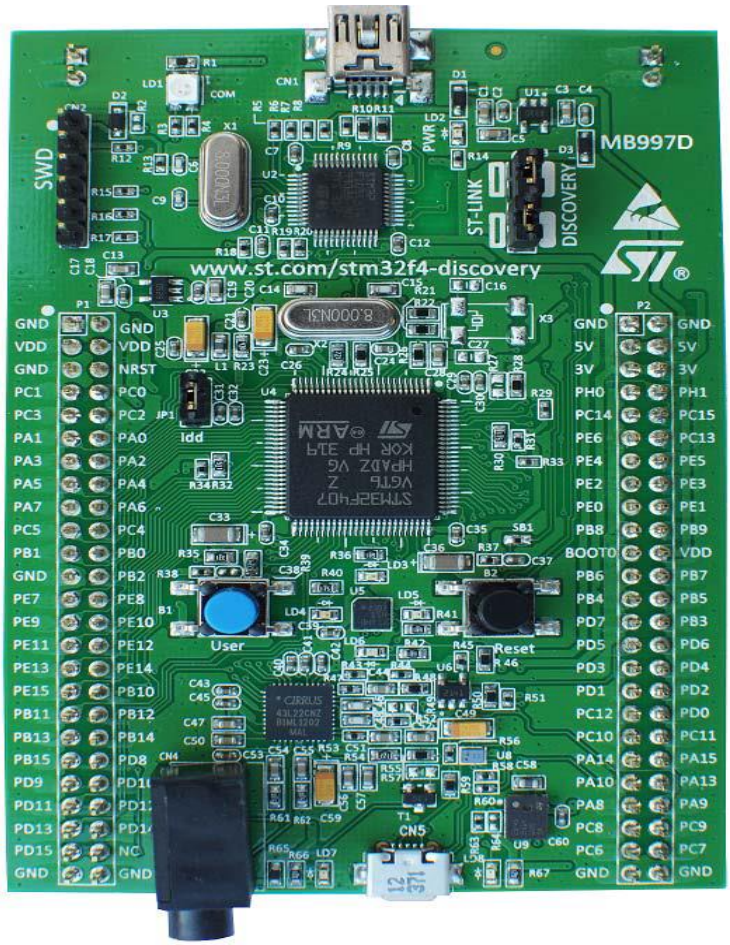

Figure 5.26: STM32 Development Board

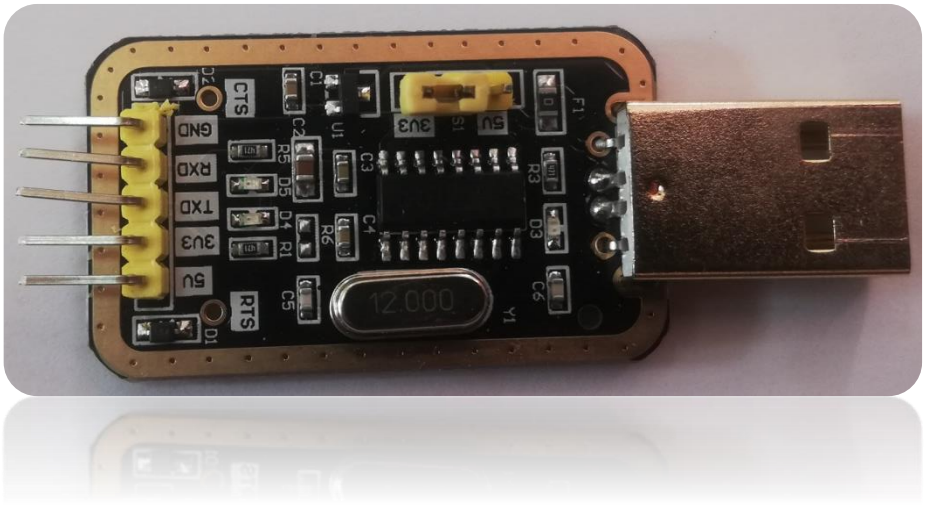

Figure 5.27: USB to TTL Module

5.4.4 Hardware setup and Pin assignments

To interface MATLAB with the STM32 board, a number of components need to be identified including the UART, LEDs pins out assignment on the STM32 board. For the LEDs pinout, the GPIO port D is assigned as a digital output which in turn is connected to the LEDs circuit. While, in this setup, USART2 on STM32 is assigned to perform the communication between MATLAB and STM32.

The following table summarizes the used pinout

Table 5.1: Pinout assignments

GPIOD	Definition	Purpose
PD15	LED1	LEDs
PD13	LED2	
PD11	LED3	
PD9	LED4	
PA2	RX Line	USART2
PA3	TX Line	

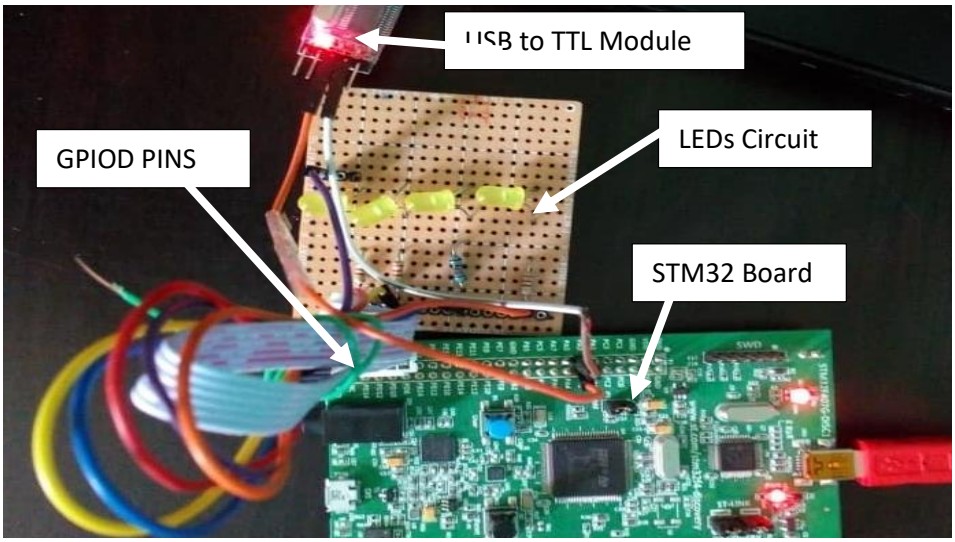

Figure 5.28: Hardware setup

5.4 Chapter Summary

This chapter presents the results of spectral analysis based on Fast Fourier Transform applied to induction machine signals (current, speed and electromagnetic torque) in both Cases: healthy and faulty. The results prove the effectiveness of the latter method in detecting faults by spotting abnormal frequencies with different amplitudes in faulty machine compared with a healthy one. In addition, the implementation has verified the proposed method.

CHAPTER FIVE

CONCLUSION AND RECOMMENDATION FOR FUTURE WORK

The main purpose of this work is to detect induction motor failures to prevent cost reduction and improve productivity.

In this dissertation, the machine is modelled in MATLAB software as a coupled magnetic circuit that consists on resistances and inductances. In order to visualize the behaviour of the machine when a fault occurs namely bar breakage and end ring fault, the resistance parameter is modified which leads to the modification of the operating characteristics compared to healthy motor characteristics that reveal eventually the condition of the motor (healthy or faulty). To unfold the severity of the later faults a diagnosis based signal processing method is used, the method is known as a Fast Fourier Transform that exposes the frequency content of the signal. Thus any abnormal frequencies in the signal are usually related to a certain type of faults for instance sideband frequencies in the stator current are related to the bar breakage, moreover, the more the number of broken bars increases the more amplitudes of those sidebands increases.

Besides an experiment conducted using the current signature analysis method to detect faults in the induction motor which operates online under constant load. The experiment consists of implementing the Fast Fourier Transform along with Hanning window on an electronic board (STM32), that detects the induction motor condition (healthy or faulty), as well as, the severity of fault (number of broken bars) when it analyses the stator current.

The overall finding of this work is that analysing steady-state current using current signature analysis based on FFT can show effectively the fault of the induction motor.

Based on the achieved methodology in this work, we suggest continuing this research by implementing advanced techniques such as artificial intelligence methods in which are more efficient in detecting faults. Besides, it is suggested to acquire more signals from the IM such as vibration, temperature, bearing vibration signals to get a full information on the machine and hence a complete diagnosis will be achieved.

REFERENCES

A Alwodai, F Gu and A D Ball. (2012). "A Comparison of Different Techniques for Induction Motor Rotor Fault Diagnosis", 25th International Congress on condition Monitoring and Diagnostic Engineering, *IOP Publishing, Journal of Physics*: Conference Series 364.

Abdelkrim, C., Meridjet, M. S., Boutasseta, N., & Boulanouar, L. (2019). Detection and classification of bearing faults in industrial geared motors using temporal features and adaptive neuro-fuzzy inference system. Heliyon, 5(8), e02046..2019. 02046 .

Ahmed K. Ibrahim Mostafa I. Marei Hamdy S. El-Gohary Somaya A. M. Shehata.(2010).Modeling of Induction Motor Based on Winding Function Theory to Study Motor under Stator/Rotor Internal Faults.Electrical power and Machine department Ain-Shams university Cairo, Egypt.

Amara, Y., Lucidarme, J., Gabsi, M., Lecrivain, M., Almed, A. H. B., & Akemakou, A. D. (2001). A new topology of hybrid synchronous machine. IEEE Transactions on Industry Applications, 37(5), 1273–1281. doi:10.1109/28.952502

Amirat, Y., Benbouzid, M., Wang, T., & Turri, S. (2014). Performance analysis of an EEMD-based Hilbert Huang transform as a bearing failure detector in wind turbines. 2014 First International Conference on Green Energy ICGE 2014.

Arkkio,Antero (1987).Analysis of Induction Motors Based on the Numerical Solution of the Magnetic Field and Circuit Equations.Helsinki University of Technology,Laboratoiry of Electromechanics.SF-02150 Espoo, Finland

Arvind Singh, Bevon Grant, Ronald DeFour, Chandrabhan Sharma, Sanjay Bahadoorsingh. (2016) A review of induction motor fault modeling. The University of the West Indies, Trinidad and Tobago.

BELHAMDI Saad (2005) « Prise en Compte D'un Défaut Rotorique Dans la Commande d'un Moteur Asynchrone. Thèse de Magister, Université Mohamed Khider Biskra, Soutenue 2005.

Bellini, A., Filippetti, F., Franceschini, G., Tassoni, C., Passaglia, R., Saottini, M., … Rossi, A. (2002). On-field experience with online diagnosis of large induction motors cage failures using MCSA. *IEEE Transactions on Industry Applications*, 38(4), 1045–1053.

Benbouzid, M. E. H., & Kliman, G. B. (2003). What stator current processing-based technique to use for induction motor rotor faults diagnosis? *IEEE Transactions on Energy Conversion*, 18(2), 238–244.

Cabal-Yepez, E., Osornio-Rios, R. A., Romero-Troncoso, R. J., Razo-Hernandez, J. R., & Lopez-Garcia, R. (2009). FPGA-Based Online Induction Motor Multiple-Fault Detection with Fused FFT and Wavelet Analysis. *2009 International Conference on Reconfigurable Computing and FPGAs*.

Chee-Muan Ong.(1998).Dynamic simulation of electric machinery using Matlab/Simulink.school of electrical and computer engineering.Purdue UniversityWest Lafayette,Indiana.

Choudhary, A., Shimi, S. ., & Akula, A. (2018). Bearing Fault Diagnosis of Induction Motor Using Thermal Imaging. 2018 International Conference on Computing, Power and Communication Technologies.

Dlamini, M., Barendse, P. S., & Khan, A. (2013). Autonomous detection of interturn stator faults in induction motors. *IEEE International Conference on Industrial Technology* (ICIT).

E.Ayaz,(2014).A Review Study onMathematical Methods for Fault Detection Problems inInduction Motor,BALKAN JOURNAL OF ELECTRICAL & COMPUTER ENGINEERING, 2014, Vol.2, No.3

Kliman G. B. and J. Stain,(1992) "Methods of motor current signature anal-ysis,"Elect. Mach. Power Syst., no. 20, pp. 463–474, 1992

Kliman G. B. and J. Stein. (1992). "Methods of motor current signature analysis" Electric Machines and Power Systems, Vol. 20, No. 5, pp. 463-474,.

Houdouin G., Barakat, G. Dakyo B., Destobbeleer,(2003).A Winding Function Theory Based Global Method for the Simulation of Faulty Induction Machines.GREAH, Universitk du-Havre, 25 rue Philippe Lebon, BP 540,76058 LE HAVRE Cedex, France.

Ghorbanian, V., & Faiz, J. (2015). A survey on time and frequency characteristics of induction motors with broken rotor bars in line-start and inverter-fed modes. *Mechanical Systems and Signal Processing*, 54-55, 427–456..2014.08.022

Gindy N, Al-Habaibeh A (1997) Condition monitoring of cutting tools using artificial neural networks. *Proceedings of the thirty-second international matador conference*, pp 299–304. Springer, Berlin.

Glowacz, A. (2018). Acoustic based fault diagnosis of three-phase induction motor. *Applied Acoustics*, vol (137), pp: 82–89 .

Harris, Tedric, (2001). *Rolling Bearing Analysis*. New York, NY, John Wiley and Sons, 2001. - 1104 p.

Immovilli, F., Bianchini, C., Cocconcelli, M., Bellini, A., & Rubini, R. (2013). Bearing Fault Model for Induction Motor With Externally Induced Vibration. *IEEE Transactions on Industrial Electronics*, 60(8), 3408–3418.

Izzet Yilmaz Onel and Mohamed El Hachemi Benbouzid. (2008.) "Induction Motor Bearing Failure Detection and Diagnosis: Park and Concordia Transform Approaches Comparative Study", *IEEE/ASME Transactions on Mechatronics*, vol. 13(2).

Jigyasu, R., Sharma, A., Mathew, L., & Chatterji, S. (2018). A Review of Condition Monitoring and Fault Diagnosis Methods for Induction Motor. 2018 Second *International Conference on Intelligent Computing and Control Systems (ICICCS).*

Jorge Carrera, Rafael Franceschi, and Guadalupe Gonzalez, (2018), "Induction Motor Fault Modeling Based on the Winding Function" in *6th Engineering, Science and Technology Conference, KnE Engineering.* pp: 758–767.

Lipo, T. A. (2017), Analysis of Synchronous Machines. *CRC press*. University of Wisconsin-Madison.

Liu, R., Yang, B., Zio, E., & Chen, X. (2018). Artificial intelligence for fault diagnosis of rotating machinery: A review. *Mechanical Systems and Signal Processing*, 108, pp: 33–47.

Lopez-Perez, D., & Antonino-Daviu, J. (2016). Application of infrared thermography to fault detection in industrial induction motors: Case stories. 2016 *XXII International Conference on Electrical Machines (ICEM)*. pp: 2172-2177.

Önel, I. Y., & Benbouzid, M. E. H. (2008). Induction Motor Bearing Failure Detection and Diagnosis: Park and Concordia Transform Approaches Comparative Study. *IEEE/ASME Transactions on Mechatronics*, 13(2), 257–262.

Ordaz-Moreno, A., de Jesus Romero-Troncoso, R., Vite-Frias, J. A., Rivera-Gillen, J. R., & Garcia-Perez, A. (2008). Automatic Online Diagnosis Algorithm for Broken-Bar Detection on Induction Motors Based on Discrete Wavelet Transform for FPGA Implementation. *IEEE Transactions on Industrial Electronics*, 55(5), 2193–2202.

Pandarakone, S. E., Gunasekaran, S., Mizuno, Y., & Nakamura, H. (2018). Application of Naive Bayes Classifier Theorem in Detecting Induction Motor Bearing Failure. *2018 XIII International Conference on Electrical Machines (ICEM)*. pp. 1761-1767

Partha Sarathee Bhowmik, SouravPradhanand Mangal Prakash.(2013). Fault Diagnostic and Monitoring Methods of Induction Motor: A Review .*International Journal of Applied Control, Electrical and Electronics Engineering(IJACEEE*). Vol(1), Number 1,May 2013.

Priteem Ranjan Beher, Somnath Sarang.(2016).Transient Modelling of Induction Machine using Winding Function Method under Stator Fault.IIT Patna, Bihta, India.

Pu. Shi, Zheng. Chen, Yuriy. Vagapov, Zoubir. Zouaoui.(2013).Winding Function Approach for Induction Machine Fault Detection.

R. Hirvonen.(1994). "On-line condition monitoring of defects in squirrel cage motors" *Int Conf. Electrical Machines*, Paris,France, vol. 2, pp. 267–272.

Sahraoui Mohamed (2003) Contribution aux Diagnostic des Machines Asynchrones Triphasées à cage. *Université Mohamed Khider Biskra*.

Sahraoui, M., Ghoggal, A., Zouzou, S. E., & Benbouzid, M. E. (2008). Dynamic eccentricity in squirrel cage induction motors – Simulation and analytical study of its spectral signatures on stator currents. *Simulation Modelling Practice and Theory*, 16(9), 1503–1513.

Salloum, K., &Wooi, H. (2011). *Wavelet Fault Diagnosis of Induction Motor. MATLAB for Engineers - Applications in Control, Electrical Engineering, IT and Robotics.* doi:10.5772/19584

Sanjay Kumar, Pabitra K. Guchhait,Ramashis Banerjee,A.K. Srivastava, D.N. Vishwakrma,Saket .(2020). Condition Based Prognostic Maintenance (CBPM) for Induction Machine – A Review ,Electrical Engineering Department, Indian Institute.

Schiferl, R. F., & Melfi, M. J. (2004). Bearing current remediation options. *IEEE Industry Applications Magazine,* 10(4), 40–50.

Schoen, R. R., Habetler, T. G., Kamran, F., & Bartfield, R. G. (1995). Motor bearing damage detection using stator current monitoring. *IEEE Transactions on Industry Applications,* 31(6), 1274–1279.

Seera, M., Lim, C. P., & Ishak, D. (2012). Detection and Diagnosis of Broken Rotor Bars in Induction Motors Using the Fuzzy Min-Max Neural Network. *International Journal of Natural Computing Research,* 3(1), 44–55.

Stephen J. Chapman. (2005). Electric Machinery Fundamentals, 4th edition Published by McGraw-Hill.

Thomson, W. T., & Fenger, M. (2001). Current signature analysis to detect induction motor faults. *IEEE Industry Applications Magazine,* 7(4), 26–34.

Yiqi,L & All Bazzl, A review and comparison of fault detection and diagnosis methods for squirrel-cage induction motors: State of the art. *ISA Transaction*, vol(70), pp:400-409

Zaabi, W., Bensalem, Y., & Trabelsi, H. (2014). Fault analysis of induction machine using finite element method (FEM). *15th International Conference on Sciences and Techniques of Automatic Control and Computer Engineering* (STA). pp. 388-393

Zhongming Ye, and Bin Wu, (2001). Simulation of Electrical Faults of Three Phase Induction Motor Drive System. *32nd Annual Power Electronics Specialists Conference.* Vol (1), pp: 75-80

APPENDICES

Appendix A

Table A.1: Selected Induction Machine Parameters

Notation	Definition	Unit
$R = 63.29 \times 10^{-3}$	Mean diameter of the machine	m
$l = 65 \times 10^{-3}$	Length of the slots in the stator	m
$g = 0.3 \times 10^{-3}$	Air gap between the stator and the rotor	m
$Nr = 16$	Number of the bars in the squirrel cage rotor	
$Ns = 90$	Number of turns in the stator winding	
$Rs = 7.828$	Single phase winding resistance	Ω
$Re = 72 \times 10^{-6}$	End ring resistance	Ω
$Le = 0.03 \times 10^{-6}$	End ring leakage inductance	H
$Lb = 0.1 \times 10^{-6}$	Rotor bar's leakage inductance	H
$Lls = 28 \times 10^{-3}$	Stator leakage inductance in each phase	H
$K_0 = 0$	Friction coefficient	
$J = 6 \times 10^{-3}$	Moment of Inertia	$Kg.m^2$

Appendix B

B.1 Resistance matrix of the rotor bars

$$
RH = \begin{bmatrix}
Rb0+2*Re+Rb15 & -Rb0 & 0 & 0 & 0 & 0 & 0 & 0 & 0 & 0 & 0 & 0 & 0 & 0 & 0 & -Rb15 & -Re \\
-Rb0 & Rb0+2*Re+Rb1 & -Rb1 & 0 & 0 & 0 & 0 & 0 & 0 & 0 & 0 & 0 & 0 & 0 & 0 & 0 & -Re \\
0 & -Rb1 & Rb1+2*Re+Rb2 & -Rb2 & 0 & 0 & 0 & 0 & 0 & 0 & 0 & 0 & 0 & 0 & 0 & 0 & -Re \\
0 & 0 & -Rb2 & Rb2+2*Re+Rb3 & -Rb3 & 0 & 0 & 0 & 0 & 0 & 0 & 0 & 0 & 0 & 0 & 0 & -Re \\
0 & 0 & 0 & -Rb3 & Rb3+2*Re+Rb4 & -Rb4 & 0 & 0 & 0 & 0 & 0 & 0 & 0 & 0 & 0 & 0 & -Re \\
0 & 0 & 0 & 0 & -Rb4 & Rb4+2*Re+Rb5 & -Rb5 & 0 & 0 & 0 & 0 & 0 & 0 & 0 & 0 & 0 & -Re \\
0 & 0 & 0 & 0 & 0 & -Rb5 & Rb5+2*Re+Rb6 & -Rb6 & 0 & 0 & 0 & 0 & 0 & 0 & 0 & 0 & -Re \\
0 & 0 & 0 & 0 & 0 & 0 & -Rb6 & Rb6+2*Re+Rb7 & -Rb7 & 0 & 0 & 0 & 0 & 0 & 0 & 0 & -Re \\
0 & 0 & 0 & 0 & 0 & 0 & 0 & -Rb7 & Rb7+2*Re+Rb8 & -Rb8 & 0 & 0 & 0 & 0 & 0 & 0 & -Re \\
0 & 0 & 0 & 0 & 0 & 0 & 0 & 0 & -Rb8 & Rb8+2*Re+Rb9 & -Rb9 & 0 & 0 & 0 & 0 & 0 & -Re \\
0 & 0 & 0 & 0 & 0 & 0 & 0 & 0 & 0 & -Rb9 & Rb9+2*Re+Rb10 & -Rb10 & 0 & 0 & 0 & 0 & -Re \\
0 & 0 & 0 & 0 & 0 & 0 & 0 & 0 & 0 & 0 & -Rb10 & Rb10+2*Re+Rb11 & -Rb11 & 0 & 0 & 0 & -Re \\
0 & 0 & 0 & 0 & 0 & 0 & 0 & 0 & 0 & 0 & 0 & -Rb11 & Rb11+2*Re+Rb12 & -Rb12 & 0 & 0 & -Re \\
0 & 0 & 0 & 0 & 0 & 0 & 0 & 0 & 0 & 0 & 0 & 0 & -Rb12 & Rb12+2*Re+Rb13 & -Rb13 & 0 & -Re \\
0 & 0 & 0 & 0 & 0 & 0 & 0 & 0 & 0 & 0 & 0 & 0 & 0 & -Rb13 & Rb13+2*Re+Rb14 & -Rb14 & -Re \\
-Rb15 & 0 & 0 & 0 & 0 & 0 & 0 & 0 & 0 & 0 & 0 & 0 & 0 & 0 & -Rb14 & Rb14+2*Re+Rb15 & -Re \\
-Re & -Re & -Re & -Re & -Re & -Re & -Re & -Re & -Re & -Re & -Re & -Re & -Re & -Re & -Re & -Re & -Nr*Re
\end{bmatrix}
$$

B.2 Breakage of bar one Resistance matrix

$$
Rb1 = \begin{bmatrix}
10 \times Rb0 & -10 \times Rb0 & 0 & 0 & 0 & 0 & 0 & 0 & 0 & 0 & 0 & 0 & 0 & 0 & 0 & 0 & 0 \\
-10 \times Rb0 & 10 \times Rb0 & 0 & 0 & 0 & 0 & 0 & 0 & 0 & 0 & 0 & 0 & 0 & 0 & 0 & 0 & 0 \\
0 & 0 & 0 & 0 & 0 & 0 & 0 & 0 & 0 & 0 & 0 & 0 & 0 & 0 & 0 & 0 & 0 \\
0 & 0 & 0 & 0 & 0 & 0 & 0 & 0 & 0 & 0 & 0 & 0 & 0 & 0 & 0 & 0 & 0 \\
0 & 0 & 0 & 0 & 0 & 0 & 0 & 0 & 0 & 0 & 0 & 0 & 0 & 0 & 0 & 0 & 0 \\
0 & 0 & 0 & 0 & 0 & 0 & 0 & 0 & 0 & 0 & 0 & 0 & 0 & 0 & 0 & 0 & 0 \\
0 & 0 & 0 & 0 & 0 & 0 & 0 & 0 & 0 & 0 & 0 & 0 & 0 & 0 & 0 & 0 & 0 \\
0 & 0 & 0 & 0 & 0 & 0 & 0 & 0 & 0 & 0 & 0 & 0 & 0 & 0 & 0 & 0 & 0 \\
0 & 0 & 0 & 0 & 0 & 0 & 0 & 0 & 0 & 0 & 0 & 0 & 0 & 0 & 0 & 0 & 0 \\
0 & 0 & 0 & 0 & 0 & 0 & 0 & 0 & 0 & 0 & 0 & 0 & 0 & 0 & 0 & 0 & 0 \\
0 & 0 & 0 & 0 & 0 & 0 & 0 & 0 & 0 & 0 & 0 & 0 & 0 & 0 & 0 & 0 & 0 \\
0 & 0 & 0 & 0 & 0 & 0 & 0 & 0 & 0 & 0 & 0 & 0 & 0 & 0 & 0 & 0 & 0 \\
0 & 0 & 0 & 0 & 0 & 0 & 0 & 0 & 0 & 0 & 0 & 0 & 0 & 0 & 0 & 0 & 0 \\
0 & 0 & 0 & 0 & 0 & 0 & 0 & 0 & 0 & 0 & 0 & 0 & 0 & 0 & 0 & 0 & 0 \\
0 & 0 & 0 & 0 & 0 & 0 & 0 & 0 & 0 & 0 & 0 & 0 & 0 & 0 & 0 & 0 & 0 \\
0 & 0 & 0 & 0 & 0 & 0 & 0 & 0 & 0 & 0 & 0 & 0 & 0 & 0 & 0 & 0 & 0 \\
0 & 0 & 0 & 0 & 0 & 0 & 0 & 0 & 0 & 0 & 0 & 0 & 0 & 0 & 0 & 0 & 0
\end{bmatrix}
$$

B.3 Breakage of bar two Resistance matrix

$$
Rb\,2 = \begin{bmatrix}
0 & 0 & 0 & 0 & 0 & 0 & 0 & 0 & 0 & 0 & 0 & 0 & 0 & 0 & 0 & 0 & 0 \\
0 & 10 \times Rb1 & -10 \times Rb1 & 0 & 0 & 0 & 0 & 0 & 0 & 0 & 0 & 0 & 0 & 0 & 0 & 0 & 0 \\
0 & -10 \times Rb1 & 10 \times Rb1 & 0 & 0 & 0 & 0 & 0 & 0 & 0 & 0 & 0 & 0 & 0 & 0 & 0 & 0 \\
0 & 0 & 0 & 0 & 0 & 0 & 0 & 0 & 0 & 0 & 0 & 0 & 0 & 0 & 0 & 0 & 0 \\
0 & 0 & 0 & 0 & 0 & 0 & 0 & 0 & 0 & 0 & 0 & 0 & 0 & 0 & 0 & 0 & 0 \\
0 & 0 & 0 & 0 & 0 & 0 & 0 & 0 & 0 & 0 & 0 & 0 & 0 & 0 & 0 & 0 & 0 \\
0 & 0 & 0 & 0 & 0 & 0 & 0 & 0 & 0 & 0 & 0 & 0 & 0 & 0 & 0 & 0 & 0 \\
0 & 0 & 0 & 0 & 0 & 0 & 0 & 0 & 0 & 0 & 0 & 0 & 0 & 0 & 0 & 0 & 0 \\
0 & 0 & 0 & 0 & 0 & 0 & 0 & 0 & 0 & 0 & 0 & 0 & 0 & 0 & 0 & 0 & 0 \\
0 & 0 & 0 & 0 & 0 & 0 & 0 & 0 & 0 & 0 & 0 & 0 & 0 & 0 & 0 & 0 & 0 \\
0 & 0 & 0 & 0 & 0 & 0 & 0 & 0 & 0 & 0 & 0 & 0 & 0 & 0 & 0 & 0 & 0 \\
0 & 0 & 0 & 0 & 0 & 0 & 0 & 0 & 0 & 0 & 0 & 0 & 0 & 0 & 0 & 0 & 0 \\
0 & 0 & 0 & 0 & 0 & 0 & 0 & 0 & 0 & 0 & 0 & 0 & 0 & 0 & 0 & 0 & 0 \\
0 & 0 & 0 & 0 & 0 & 0 & 0 & 0 & 0 & 0 & 0 & 0 & 0 & 0 & 0 & 0 & 0 \\
0 & 0 & 0 & 0 & 0 & 0 & 0 & 0 & 0 & 0 & 0 & 0 & 0 & 0 & 0 & 0 & 0 \\
0 & 0 & 0 & 0 & 0 & 0 & 0 & 0 & 0 & 0 & 0 & 0 & 0 & 0 & 0 & 0 & 0 \\
0 & 0 & 0 & 0 & 0 & 0 & 0 & 0 & 0 & 0 & 0 & 0 & 0 & 0 & 0 & 0 & 0
\end{bmatrix}
$$

B.4 Breakage of bar eight Resistance matrix

$$
Rd\,8 = \begin{bmatrix}
0 & 0 & 0 & 0 & 0 & 0 & 0 & 0 & 0 & 0 & 0 & 0 & 0 & 0 & 0 & 0 & 0 \\
0 & 0 & 0 & 0 & 0 & 0 & 0 & 0 & 0 & 0 & 0 & 0 & 0 & 0 & 0 & 0 & 0 \\
0 & 0 & 0 & 0 & 0 & 0 & 0 & 0 & 0 & 0 & 0 & 0 & 0 & 0 & 0 & 0 & 0 \\
0 & 0 & 0 & 0 & 0 & 0 & 0 & 0 & 0 & 0 & 0 & 0 & 0 & 0 & 0 & 0 & 0 \\
0 & 0 & 0 & 0 & 0 & 0 & 0 & 0 & 0 & 0 & 0 & 0 & 0 & 0 & 0 & 0 & 0 \\
0 & 0 & 0 & 0 & 0 & 0 & 0 & 0 & 0 & 0 & 0 & 0 & 0 & 0 & 0 & 0 & 0 \\
0 & 0 & 0 & 0 & 0 & 0 & 0 & 0 & 0 & 0 & 0 & 0 & 0 & 0 & 0 & 0 & 0 \\
0 & 0 & 0 & 0 & 0 & 0 & 0 & 10 \times Rb7 & -10 \times Rb7 & 0 & 0 & 0 & 0 & 0 & 0 & 0 & 0 \\
0 & 0 & 0 & 0 & 0 & 0 & 0 & -10 \times Rb7 & 10 \times Rb7 & 0 & 0 & 0 & 0 & 0 & 0 & 0 & 0 \\
0 & 0 & 0 & 0 & 0 & 0 & 0 & 0 & 0 & 0 & 0 & 0 & 0 & 0 & 0 & 0 & 0 \\
0 & 0 & 0 & 0 & 0 & 0 & 0 & 0 & 0 & 0 & 0 & 0 & 0 & 0 & 0 & 0 & 0 \\
0 & 0 & 0 & 0 & 0 & 0 & 0 & 0 & 0 & 0 & 0 & 0 & 0 & 0 & 0 & 0 & 0 \\
0 & 0 & 0 & 0 & 0 & 0 & 0 & 0 & 0 & 0 & 0 & 0 & 0 & 0 & 0 & 0 & 0 \\
0 & 0 & 0 & 0 & 0 & 0 & 0 & 0 & 0 & 0 & 0 & 0 & 0 & 0 & 0 & 0 & 0 \\
0 & 0 & 0 & 0 & 0 & 0 & 0 & 0 & 0 & 0 & 0 & 0 & 0 & 0 & 0 & 0 & 0 \\
0 & 0 & 0 & 0 & 0 & 0 & 0 & 0 & 0 & 0 & 0 & 0 & 0 & 0 & 0 & 0 & 0 \\
0 & 0 & 0 & 0 & 0 & 0 & 0 & 0 & 0 & 0 & 0 & 0 & 0 & 0 & 0 & 0 & 0
\end{bmatrix}
$$

B.5 Breakage of end ring Resistance matrix

$$
R_{end} = \begin{bmatrix}
10 \times Re & 0 & 0 & 0 & 0 & 0 & 0 & 0 & 0 & 0 & 0 & 0 & 0 & 0 & 0 & 0 & -10 \times Re \\
0 & 0 & 0 & 0 & 0 & 0 & 0 & 0 & 0 & 0 & 0 & 0 & 0 & 0 & 0 & 0 & 0 \\
0 & 0 & 0 & 0 & 0 & 0 & 0 & 0 & 0 & 0 & 0 & 0 & 0 & 0 & 0 & 0 & 0 \\
0 & 0 & 0 & 0 & 0 & 0 & 0 & 0 & 0 & 0 & 0 & 0 & 0 & 0 & 0 & 0 & 0 \\
0 & 0 & 0 & 0 & 0 & 0 & 0 & 0 & 0 & 0 & 0 & 0 & 0 & 0 & 0 & 0 & 0 \\
0 & 0 & 0 & 0 & 0 & 0 & 0 & 0 & 0 & 0 & 0 & 0 & 0 & 0 & 0 & 0 & 0 \\
0 & 0 & 0 & 0 & 0 & 0 & 0 & 0 & 0 & 0 & 0 & 0 & 0 & 0 & 0 & 0 & 0 \\
0 & 0 & 0 & 0 & 0 & 0 & 0 & 0 & 0 & 0 & 0 & 0 & 0 & 0 & 0 & 0 & 0 \\
0 & 0 & 0 & 0 & 0 & 0 & 0 & 0 & 0 & 0 & 0 & 0 & 0 & 0 & 0 & 0 & 0 \\
0 & 0 & 0 & 0 & 0 & 0 & 0 & 0 & 0 & 0 & 0 & 0 & 0 & 0 & 0 & 0 & 0 \\
0 & 0 & 0 & 0 & 0 & 0 & 0 & 0 & 0 & 0 & 0 & 0 & 0 & 0 & 0 & 0 & 0 \\
0 & 0 & 0 & 0 & 0 & 0 & 0 & 0 & 0 & 0 & 0 & 0 & 0 & 0 & 0 & 0 & 0 \\
0 & 0 & 0 & 0 & 0 & 0 & 0 & 0 & 0 & 0 & 0 & 0 & 0 & 0 & 0 & 0 & 0 \\
0 & 0 & 0 & 0 & 0 & 0 & 0 & 0 & 0 & 0 & 0 & 0 & 0 & 0 & 0 & 0 & 0 \\
0 & 0 & 0 & 0 & 0 & 0 & 0 & 0 & 0 & 0 & 0 & 0 & 0 & 0 & 0 & 0 & 0 \\
0 & 0 & 0 & 0 & 0 & 0 & 0 & 0 & 0 & 0 & 0 & 0 & 0 & 0 & 0 & 0 & 0 \\
-10 \times Re & 0 & 0 & 0 & 0 & 0 & 0 & 0 & 0 & 0 & 0 & 0 & 0 & 0 & 0 & 0 & -10 \times Nr \times Re
\end{bmatrix}
$$